박 사 학 위 논 문

Ph.D. Dissertation

변형에너지 변분을 이용한 국부 구조의 실용적인 안정성 평가 방법

A practical method for evaluating stability of local structures using strain energy variation

2020

오 민 한 (吳 珉 漢 Oh, Min-Han)

한 국 과 학 기 술 원

Korea Advanced Institute of Science and Technology

박 사 학 위 논 문

변형에너지 변분을 이용한 국부 구조의 실용적인 안정성 평가 방법

2020

오 민 한

한 국 과 학 기 술 원

기계항공공학부/기계공학과

변형에너지 변분을 이용한 국부 구조의 실용적인 안정성 평가 방법

오 민 한

위 논문은 한국과학기술원 박사학위논문으로
학위논문 심사위원회의 심사를 통과하였음

2019년 11월 21일

심사위원장 이 필 승 (인)

심 사 위 원 오 일 권 (인)

심 사 위 원 김 성 수 (인)

심 사 위 원 부 승 환 (인)

심 사 위 원 김 을 년 (인)

A practical method for evaluating stability of local structures using strain energy variation

Min-Han Oh

Advisor: Phill-Seung Lee

A dissertation/thesis submitted to the faculty of
Korea Advanced Institute of Science and Technology in
partial fulfillment of the requirements for the degree of
Doctor of Philosophy in Mechanical Engineering

Daejeon, Korea
November 21, 2019

Approved by

Phill-Seung Lee,
Professor of Mechanical Engineering

The study was conducted in accordance with Code of Research Ethics[1].

1) Declaration of Ethical Conduct in Research: I, as a graduate student of Korea Advanced Institute of Science and Technology, hereby declare that I have not committed any act that may damage the credibility of my research. This includes, but is not limited to, falsification, thesis written by someone else, distortion of research findings, and plagiarism. I confirm that my dissertation contains honest conclusions based on my own careful research under the guidance of my advisor.

DME
20135177

오민한. 변형에너지 변분을 이용한 국부 구조의 실용적인 안정성 평가 방법. 기계공학과. 2020년. 101+ix 쪽. 지도교수: 이필승. (영문 논문)

Min-Han Oh. A practical method for evaluating stability of local structures using strain energy variation. Department of Mechanical Engineering. 2020. 101+ix pages. Advisor: Phill-Seung Lee. (Text in English)

초 록

본 논문에서는 대형 구조물의 국부 안정성을 평가하기 위한 실용적인 방법을 제안한다. 전체 비선형 유한요소(FE) 해석을 통해 계산된 국부 변형 에너지의 2차 변분값을 조사하여 국부 안정성을 평가한다. 이전의 방법들과 달리, 국부 구조와 전체 구조 간의 복잡한 상호 작용을 완벽히 고려할 수 있으며 별도의 국부 FE 해석을 필요로 하지 않는다. FE 모델이 많은 수의 자유도를 가지는 경우, 모델 축소법을 적용하여 계산 효율성을 크게 향상시킬 수 있다. 가장 큰 장점은 제안된 방법이 단순하고 일반적인 구조의 임의 형상 부분에 적용 가능하다는 것이다. 산업계 엔지니어가 적은 노력으로 실용적으로 사용할 수 있다. 몇 가지 수치 예제들을 통해 제안한 평가 방법론의 실효성을 입증하였다.

핵 심 낱 말 국부 안정성, 변형에너지 변분, 비선형 유한요소해석, 모델 축소법, 좌굴

Abstract

In this thesis, we propose a practical method to evaluate the local stability of large size structures. Local stability is assessed by investigating the second variation of the local strain energy calculated through global nonlinear finite element (FE) analysis. Unlike previous methods, complicated interactions between local and global structures are fully considered and the local FE analysis is not necessary. The computational efficiency is greatly improved by applying the model reduction method to the FE model with a large number of degrees of freedom. A great advantage is that the proposed method is simple and applicable to arbitrary parts of general structures. That is, it can be practically used by engineers in industries without much effort. The evaluation methodology is proposed and its practical effectiveness is demonstrated through several numerical examples.

Keywords Local stability, Strain energy variation, Nonlinear finite element analysis, Model reduction, Buckling

Contents

List of Tables

List of Figures

Nomenclature

Π	potential energy
U	strain energy
W	work of load
q_i	i-th general displacement variable
E	Young's modulus of truss beam
ε	strain of truss beam
L	length of truss beam
A	area of truss beam
α	initial angle of truss beam
θ	applied angle of truss beam
P	applied load of truss beam
q	applied vertical displacement of truss beam
$\mathbf{f}_i$	i-th step applied load vector
$\mathbf{f}_r$	reference load vector
$\mathbf{u}$	displacement vector
λ	displacement factor
λ_s, λ_c	displacement factor at service load and critical load
η	usage factor
$\tilde{\eta}$	usage factor for proposed method
$\tilde{\lambda}$	local load ratio by approximated load method
$\tilde{\lambda}_s, \tilde{\lambda}_c$	local load ratio by approximated load method at service load and critical load
$\bar{\lambda}$	local load ratio by norm value method
φ_i	i-th step error function
x_i	i-th step displacement index
EPSP	error tolerance for load (P) criterion
EPSW	error tolerance for work (W) criterion
LSF	local safety factor

Chapter 1. Introduction

Steels are commonly used in civil, ship and offshore structures. Since the steels are characterized by high strength and high toughness, and tensile and compressive strengths are almost the same, steel structures can be designed to be thin-walled. However, this characteristic is likely to cause local structural failures mainly due to buckling. The structural instability due to buckling is a very dangerous phenomenon in terms of structural safety.

In the past, a Mississippi bridge collapse occurred in 2007 as shown in Fig. 1 [1]. The primary cause of the collapse was due to the poor structural stability (buckling) evaluation of the small gusset plate, which did not account for the increased load. The concrete had been added to the road surface over the years, and the extraordinary weight of construction equipment and material rested on the bridge just above its weakest point at the time of the collapse. This unexpected load increase caused lateral buckling of the load-carrying local gusset structure, followed by a sudden collapse of the entire structure. It is recorded as a major disaster that caused the whole structure collapse due to poor evaluation of the structural stability of the local structure.

(a) (b)

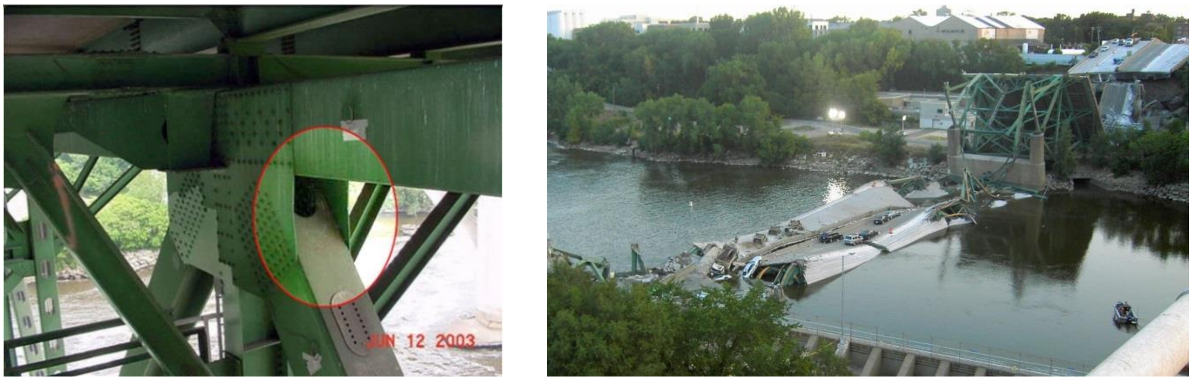

Fig. 1. Mississippi bridge collapse [1]: (a) bowed gusset plates (June 2003) and (b) overall view after collapse (August 1, 2007).

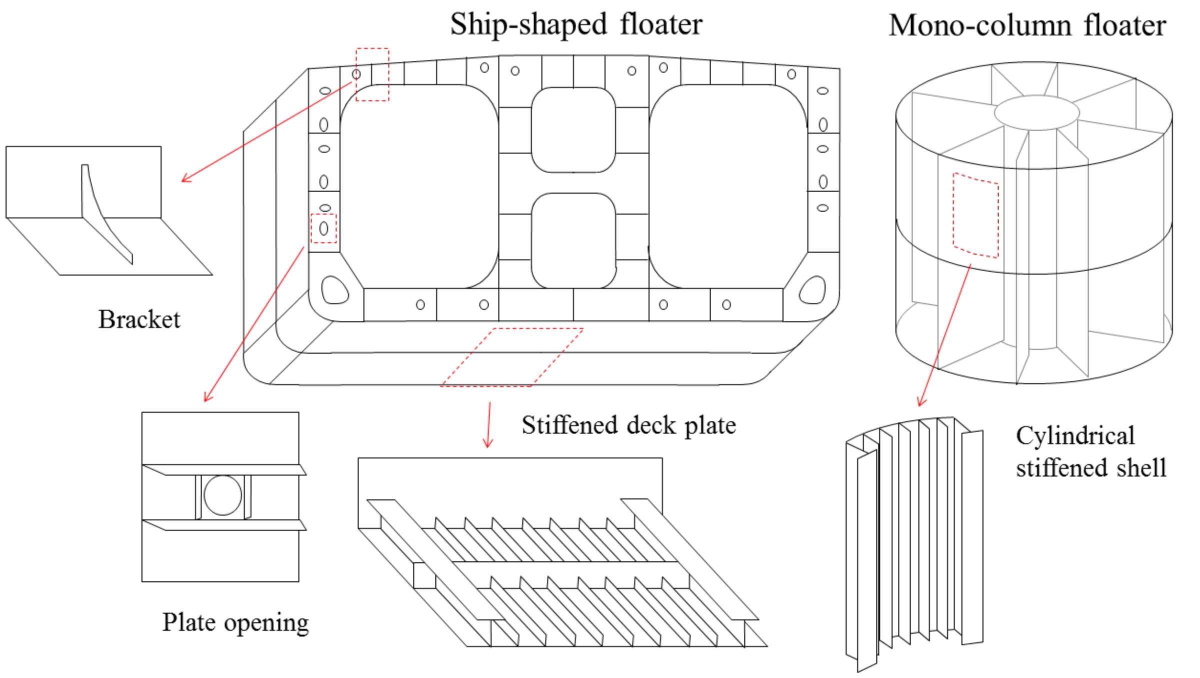

Fig. 2. Typical local structures in thin-walled ship and offshore structures: stiffened panels, cylindrical shells, brackets, and opening structures.

The buckling refers to the loss of stability of a component structure. The buckling strength is to be checked on the local strength level [2]. Fig. 2 shows various local parts of structures (or local structures), for which local buckling is considered in structural design. Fig. 3 illustrates permanent damages due to the local buckling [3]. When a local buckling happens, excessive local deformation occurs and the entire load resistance can be significantly reduced. The progressive local buckling would lead to a global failure of the structure. To maintain robust structural systems with desired capacity, it is important to ensure that local structures still contribute to the entire resistance. If necessary, local reinforcement should be applied. For such purposes, the accurate evaluation of the local stability is essential. However, local and global structures are complexly connected. This fact makes the stability evaluation very difficult, especially, for structures with complicated geometry.

(a)

(b)

(c)

Fig. 3. Illustrations of permanent damages due to local buckling in ship structures [3]: (a) buckling of stiffened plate, (b) bucking and rupture around plate opening and (c) buckling of web plate.

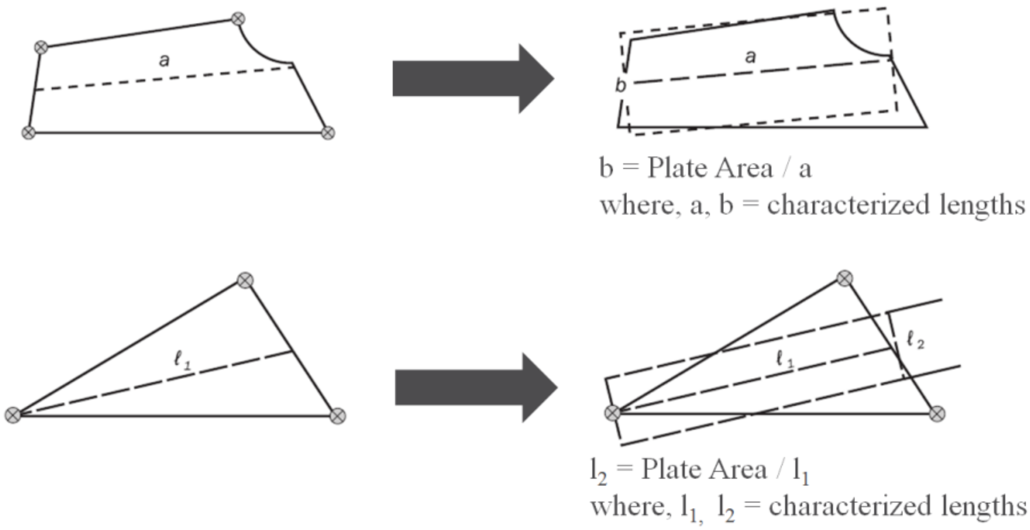

Fig. 4. Idealization of plate length and width for non-typical shaped local structures [4, 5].

The design standards for determining the resistance capacity of local structures involve using the design formula for the buckling and ultimate strengths, which are specified in Codes and Rules [3-10] and widely reviewed by Yao and Fujikubo (2016) and Paik (2018) [11,12]. However, these design formulas are only applicable to the structures with typical shapes such as beam-columns, rectangular stiffened plates, and cylindrical shells. Problems arise when the local structure is a non-typical shape that is not predefined in the formula. In this case, the geometry shape and load pattern of the local structure are idealized to be applied to a pre-defined evaluation category in the design formula as shown in Fig. 4 [4, 5]. However, this approach could significantly deteriorate the reliability of the formula. Further investigations for the arbitrary shape of the local structures are essential to predict accurate critical load of local buckling.

There were attempts to evaluate buckling of various shapes of local structures for assessing their resistance capacity. The theoretical studies were performed for evaluating the buckling of triangular plates [13-17]. Lee et al. (2015) conducted the ultimate strength assessment on the bracket structure designed in a ship hull structure by performing a series of local nonlinear finite element (FE) analyses [18]. Furthermore, the studies for the various shapes of plates, girders and arbitrarily stiffened plates were also performed [19-28]. To analyze the buckling and ultimate strengths of perforated plates, several numerical and experimental studies were carried out [29-34]. However, previous studies have focused on several specific geometric shapes and there is a need for a method for evaluating any arbitrary geometric shapes. For the purpose, a numerical evaluation method using the nonlinear finite element method (FEM), which can be applied to any shape without limitation, is commonly recommended [35].

The basic difficulty is that the resistance capacity of local structures is hard to distinguish because the local structures are included in a global structure with complicated couplings. That is, the local behavior is not independent from the global one. To overcome these limitations, Zi et al. (2017) separated the local and global behaviors and employed nonlinear finite element analysis for a local bracket girder structure [36]. The reference displacement vector on the boundary of the local bracket girder was extracted from the linear global finite element analysis, and then the local finite element analysis was performed linearly-incrementing the prescribed reference displacement. The method was successful for the local stability evaluation of an arbitrarily shaped bracket girder in an offshore structure. However, the coupling between local and global structures was not considered.

In this thesis, an adoptable evaluation method of local stability of structures by using nonlinear finite element analysis is proposed. Of course, the coupling between local and global structures is fully considered. The energy criterion of the local structure is investigated to evaluate the structural stability as the extension of the energy method developed by Zi et al. [36]. The accuracy and efficiency of the evaluation procedure are improved in the practical structural design aspect. For this, we define the local load of the considered local structure and the representative local load ratio for the quantitative safety factor assessment. In this step, the local load distribution is approximately fitted to the reference value with a scalar factor. A displacement index is introduced to show the physical quantities representing the equivalent displacement level. For a large number of degrees of freedom problem, the analysis time can be significantly reduced by applying the model reduction method. The proposed method is simple and applicable to arbitrary parts of general global structures. We illustrate the usefulness of the proposed method through four examples: a stiffened rectangular plate structure in a ship-shaped structure, a cylindrical shell structure with radial bulkheads, a horizontally stiffened cylindrical shell structure with radial bulkheads, and a bracket girder in the column-pontoon connection structure of tension leg platform. The evaluation procedure uses the nonlinear finite element analysis by the Newton-Raphson method or the arc-length method [37].

The proposed method can be used for following practical purposes:

- We can identify whether the target local structure is buckled. When the target local structure loses its stability, the corresponding magnitude of the external force acting on the global structure can be calculated.
- We can identify areas where local buckling occurs in the global structure. That is, damaged areas can be identified.
- The residual strength of the damaged areas can be calculated.
- When we locally reinforce the damaged areas, the effectiveness of the local reinforcement can be measured.
- We reduce analysis time economically through the model reduction technique for finite element models with a large number of degrees of freedom.

In Chapter 2 of this paper, the structural stability is reviewed in brief. The proposed evaluation method is presented in Chapter 3. In Chapter 4, we verify the performance of the proposed method through several simplified numerical examples and actual large scale problems. Chapter 5 examines the computational efficiency of the model reduction, and finally, conclusions are presented in Chapter 6.

Chapter 2. Structural stability

In this chapter, we review the definition and formulation for the structural stability and investigate how incremental nonlinear finite element analysis can be applied to stability evaluation.

2.1 Variation criterion for stable state

Structural stability refers to the phenomenon in which a structure returns to an equilibrium state when an external displacement disturbance is applied to the structure under this equilibrium state. To maintain a structurally stable state, the potential energy at the equilibrium state must be the minimum value [38]. Fig. 5 shows the ball in the gravity field. Fig. 5(a) shows a case where the potential gravitational energy is minimal and this state is stable.

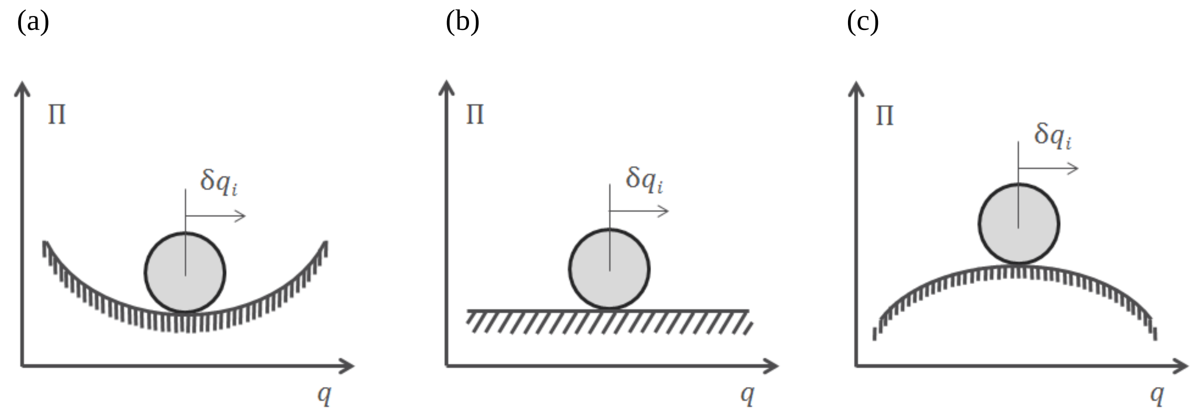

Fig. 5. Ball in different gravity field conditions [38]: (a) stable, (b) unstable (neutral equilibrium) and (c) unstable.

To introduce structural stability, we construct a simple model, derive evaluation equations, and perform stability assessments. In particular, we choose an example of a sudden snap-buckling as shown in Fig. 6(a). We see how the overall behavior would change if an additional structure is attached. Fig. 6(b) illustrates the problem of structural stability of the truss beam with a spring which simplifies adjacent structures.

(a) (b)

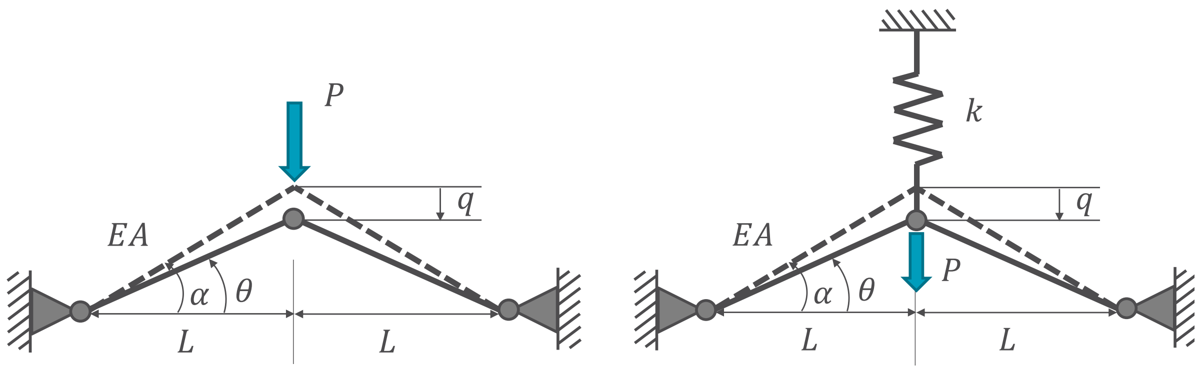

Fig. 6. Schematic models of truss beam structure: (a) a truss alone and (b) a truss with vertical spring.

The potential energy Π is defined as

$$\Pi = U - W\,, \tag{1}$$

where U is the strain energy and W is the work of loads.

According to the law of conservation of energy, the equilibrium state of a structure with respect to a given change in load or displacement means that the change in potential energy is zero as below:

$$\Delta\Pi = \Delta U - \Delta W = 0\,. \tag{2}$$

That is, in the equilibrium state, the value of Π is always a constant. If the Π is continuous derivatives, the function Π may be expanded into a Taylor series with second-order variations about the equilibrium state:

$$\Delta\Pi = \Pi\left(q_1 + \delta q_1, \ldots, q_n + \delta q_n\right) - \Pi\left(q_1, \ldots., q_n\right) \approx \delta\Pi + \delta^2\Pi \tag{3}$$

with $\delta\Pi = \sum_{i=1}^{n} \frac{\partial \Pi}{\partial q_i}\delta q_i$ and $\delta^2\Pi = \frac{1}{2}\sum_{i=1}^{n}\sum_{j=1}^{n} \frac{\partial^2 \Pi}{\partial q_i \partial q_j}\delta q_i \delta q_j$,

in which δq_i is small variations in the *i*-th generalized displacements from the equilibrium state at constant load, and $\delta\Pi$ and $\delta^2\Pi$ are the first and second variations of the potential energy, respectively.

The conditions of equilibrium are

$$\delta\Pi = 0 \quad \text{for any} \quad \delta q_i , \tag{4a}$$

$$\text{or} \quad \frac{\partial \Pi}{\partial q_i} = 0 \quad \text{for each} \quad i . \tag{4b}$$

According to the Lagrange-Dirichlet theorem, the equilibrium state is stable for those values of the constant load for which

$$\delta^2\Pi > 0 \quad \text{for any} \quad \delta q_i , \ \ \delta q_j . \tag{5}$$

To obtain the variation criterion for satisfying the stable state for the snap-through problem in Fig. 7(a), we find the potential energy:

$$\Pi = U - W = 2\int \frac{1}{2} E\varepsilon^2 dV - Pq = \frac{EAL}{\cos\alpha}\left(\frac{\cos\alpha}{\cos\theta} - 1\right)^2 - Pq \tag{6}$$

with $\theta = \tan^{-1}\left(\tan\alpha - \dfrac{q}{L}\right)$,

where E, ε, L, and A are the Young's modulus, strain, length and section area of the truss member, respectively, and α is the initial angle, θ is the applied angle, P is the applied load, and q is the applied vertical displacement.

To decide the question of stability of equilibrium states, we need to calculate the second-order derivative of Π:

$$\frac{\partial^2 \Pi}{\partial q^2} = \frac{2EA}{L}\left(\cos\alpha - \cos^3\theta\right) = \frac{2EA}{L}\left(\cos\alpha - \cos^3\left(\tan^{-1}\left(\tan\alpha - \frac{q}{L}\right)\right)\right). \tag{7}$$

The truss is stable if this expression is positive as $\dfrac{\partial^2 \Pi}{\partial q^2} > 0$.

This yields the condition that

$$\cos\alpha - \cos^3\theta > 0 \text{, or} \tag{8a}$$

$$\cos\alpha - \cos^3\left(\tan^{-1}\left(\tan\alpha - \frac{q}{L}\right)\right) > 0 . \tag{8b}$$

We examine how snap-through phenomena change if we add additional stiffness in addition to the structure in which snap-through occurs. Fig. 6(b) shows the case where the grounded spring is added to the load application point in Fig. 6(a). Considering the case of a spring in the direction of load, we find the potential energy with a vertical stiffness:

$$\Pi = 2\int \frac{1}{2} E\varepsilon^2 dV + \frac{1}{2} Kq^2 - Pq = \frac{EAL}{\cos\alpha}\left(\frac{\cos\alpha}{\cos\theta} - 1\right)^2 + \frac{1}{2} Kq^2 - Pq , \tag{9}$$

where K is additional grounded spring stiffness.

To decide the question of stability of equilibrium states, we need to calculate the second-order derivative of Π.

$$\frac{\partial^2 \Pi}{\partial q^2} = \frac{2EA}{L}\left(\cos\alpha - \cos^3\theta\right) + K = \frac{2EA}{L}\left(\cos\alpha - \cos^3\left(\tan^{-1}\left(\tan\alpha - \frac{q}{L}\right)\right)\right) + K . \tag{10}$$

The truss is stable if this expression is positive as $\frac{\partial^2 \Pi}{\partial q^2} > 0$.

This yields the condition that

$$\frac{2EA}{L}\left(\cos\alpha - \cos^3\theta\right) + K > 0 \text{, or} \tag{11a}$$

$$\frac{2EA}{L}\left(\cos\alpha - \cos^3\left(\tan^{-1}\left(\tan\alpha - \frac{q}{L}\right)\right)\right) + K > 0 . \tag{11b}$$

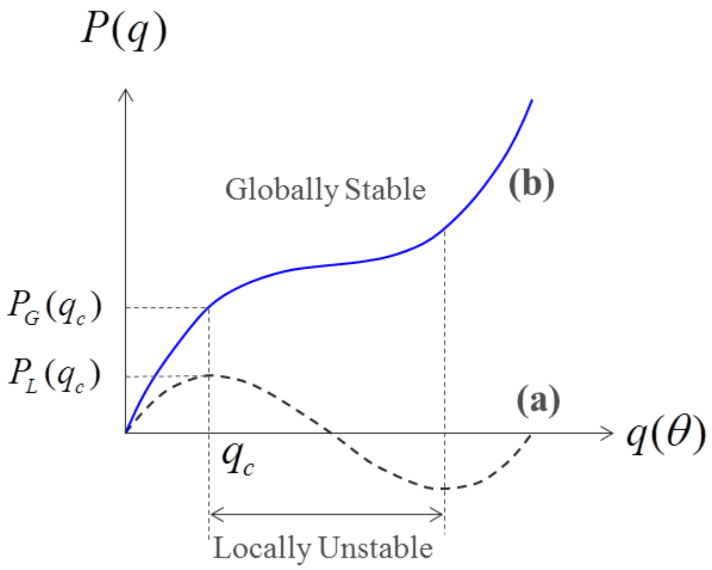

Fig. 7. Load - displacement curve for truss beam structure with vertical spring.

Whether the entire structure may be stable is depending on the spring stiffness value attached to the truss structure as shown in Fig. 7. The global load $P_G(q_i)$ is applied when the displacement is at q_i and the local load $P_L(q_i)$ of a part of the local structure works. It can be seen that the global load and displacement are nonlinear relationships. The truss structure itself with zero spring stiffness unstably behaves like the snap buckling after the load reaches the critical load $P_L(q_c)$ as the curve (a). However, the entire structure may be the stable state when the adjacent structure is relatively stiff as the curve (b). In other words, it means that even if the entire structure is stable, the local structure itself may already be in a state of losing its stability. The instability of the local structure makes it not to have the resistance to the external load. If additional external loads are applied, local deformation may increase rapidly. For the robust and cost-effective design, the own resistance capacity of the local structure has to be evaluated reliably and quantitatively. As can be seen in the truss beam model, it can be precisely identified when the local structure itself loses stability by investigating the second variation of the potential energy of the local structure.

2.2 Incremental strain energy criterion using nonlinear FE method

When the load has a constant value, the formulation of the second variation of the potential energy can be simplified to a second variation of the strain energy [36, 38]. For practical purposes, it can be assumed that there is no load change due to small external displacement disturbances. When this assumption is applied, we can see that the term of the second-order work regarding the constant load (P) is absent in Eqs. (7) and (10). Therefore, when the second variation of the strain energy stored in structures is from positive to negative, the structure loses stability. This is the energy criterion for evaluating the stability of structures. The structural resistance can be defined as the maximum load level within the stable load range obtained from the stability evaluation.

The stability of the structure can be easily evaluated using a nonlinear finite element analysis. We apply the energy criterion to the target structure using the incremental strain energy value at each analysis step while incrementing the load or displacement [36, 38]. If the analysis is performed at sufficiently small intervals, we can precisely find the instant losing stability. In the equilibrium state, the second variation of the strain energy becomes the second-order term of the incremental external work according to the law of conservation of energy. Depending on the preference, an evaluation of the second-order term of the incremental external work can be applied as an energy criterion for the stability evaluation.

Therefore, if $\delta^2 W_i > 0$, it becomes a stable state as

$$0.5\delta\mathbf{f}_i \cdot \delta\mathbf{u}_i \approx 0.5\Delta\mathbf{f}_i \cdot \Delta\mathbf{u}_i > 0, \tag{12}$$

where $\mathbf{f}_i$ is the load vector and $\mathbf{u}_i$ is the displacement vector, and $\mathbf{f}_i$ and $\mathbf{u}_i$ are directly obtained from results of the nonlinear FE analysis, where the subscript *i* refers to the *i*-th analysis step.

This method is effective for evaluating the stability of elastic structures, and it is also applicable to inelastic structures on the approximation that they are considered as the tangentially equivalent elastic structures during each small loading step [38]. That is, the structural stability in consideration of the plasticity of the material can be evaluated.

The method applies initial fabrication imperfections to the target structure in the form of an elastic buckling mode that easily occurs in the considered load configuration. By applying the initial imperfections, incremental displacement disturbances corresponding to intended specific load paths induce the predominant instability for the structure. The method is efficient in terms of calculation time because it does not consider all possible displacement disturbances and only reflects the displacement disturbances corresponding to a specific load.

Chapter 3. Evaluation of local stability

In this Chapter, we briefly review the method to evaluate the local stability of structures through sequential FE analysis of a local structure proposed by Zi et al. (2017) [36]. We then newly propose a method to directly evaluate the local stability of structures through the global FE analysis.

3.1 Evaluation through the local FE analysis

Recently, Zi et al. proposed an index (usage factor) to measure the safety from the local buckling failure for the local structures of non-typical geometry. Doing so, linear FE analysis of a global structure is performed first and nonlinear incremental analysis of a local structure is performed using the calculated displacement field on the boundary of the local structure included in the global structure. Then, the critical buckling load can be evaluated by finding the load level which the second variation of the strain energy of the local structure becomes zero [38].

Considering a target local structure as shown in Fig 8, we here summarize the method proposed by Zi et al. in the following four steps.

(Step 1) The linear finite element analysis is performed for the global structure, see Fig. 8(a). We then find the displacement distribution along the interface between the local and global structures (or the boundary of the local structure). The distribution is represented by a nodal displacement vector $\mathbf{u}$.

(Step 2) We construct the finite element model only for the local structure and apply the prescribed displacement $\lambda\mathbf{u}$ with a factor λ. Note that the displacement distribution is varying depending on load level in the global structure but we assume that the distribution does not change. Increasing the displacement factor representing the magnitude of the prescribed displacement, we perform nonlinear incremental finite element analysis, see Fig. 8(b).

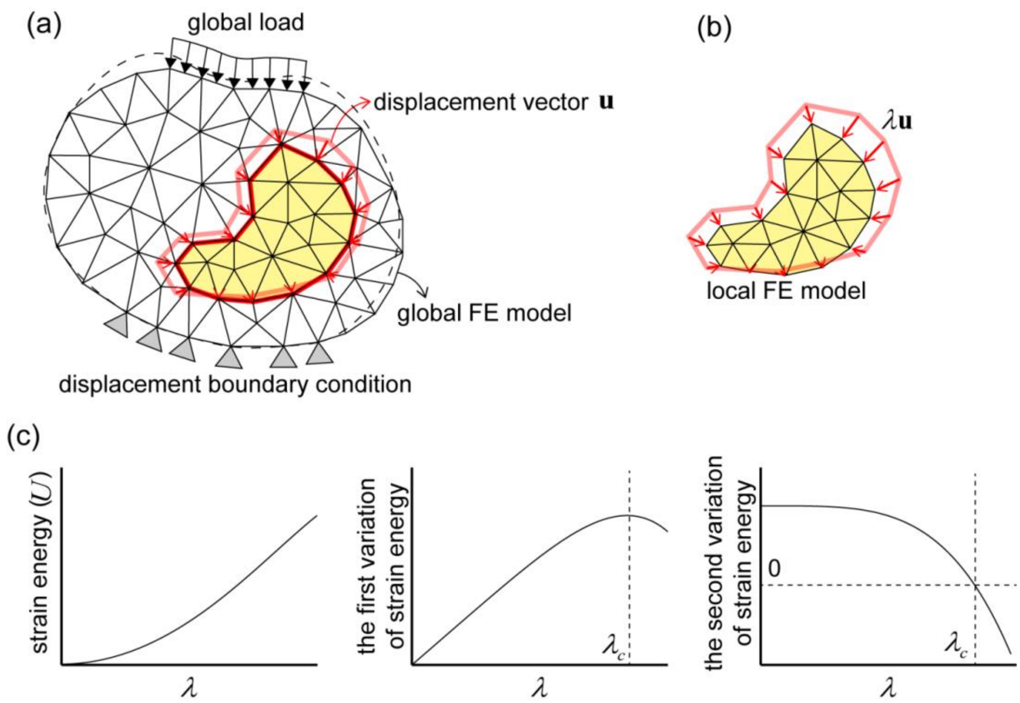

Fig. 8. Finite element models and strain energy: (a) FE model of a global structure, (b) FE model of a local structure with prescribed nodal displacements and (c) strain energy and its variations.

(Step 3) The displacement factor (λ) – strain energy curve (U) is plotted as shown in Fig. 8(c). The first and second variations of the strain energy with respect to λ is plotted. The buckling occurs when the second variation of the strain energy becomes zero first and the corresponding prescribed displacement is represented by λ_c.

(Step 4) The usage factor (η) is calculated by

$$\eta = \sqrt{\frac{U(\lambda_s)}{U(\lambda_c)}} \quad \text{with} \quad 0 \le \eta \le 1, \tag{13}$$

in which λ_s is the displacement factor corresponding to the service load. When the factor is smaller, the local structure is safer. That is, the local structure has larger residual buckling strength. The local structure is buckled when $\eta = 1$.

The factor is useful to evaluate the residual buckling strength of the local structure. However, this method has limitations to calculate the magnitude of the external force acting on the global structure when the target local structure has buckled and to identify the areas damaged due to buckling.

3.2 Direct evaluation through the global FE analysis

In this newly proposed method, the buckling failure of a local structure is directly evaluated from solutions of the global nonlinear FE analysis. The second variation of the strain energy stored in the local structure is considered. This method is to perform a nonlinear FE analysis of the global structure with increments of external global load, evaluate the stability with the strain energy generated in the local structure, and calculate the local safety factor by measuring the local load distribution of the local structure.

Let us consider a global structure with a target local structure as shown in Fig 9. The proposed method can be summarized in the following four steps.

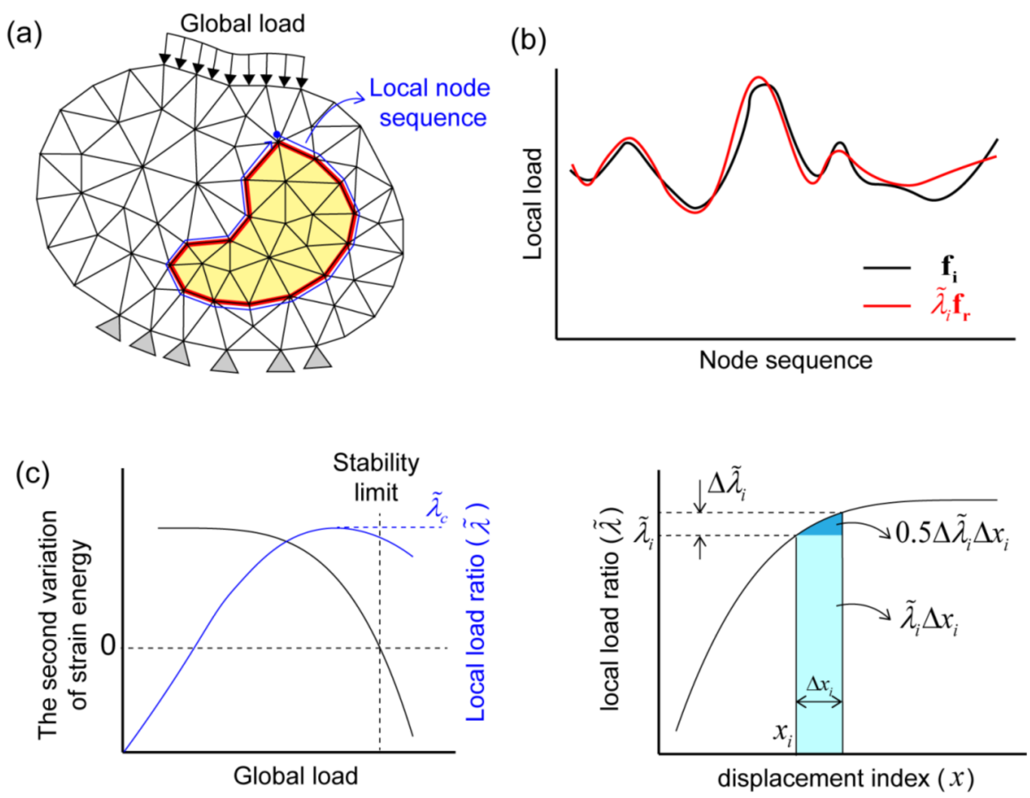

Fig. 9. Finite element models and local load ratio: (a) FE model of a global structure, (b) local load distribution and its approximation and (c) second variation of the strain energy, local load ratio and displacement index.

(Step 1) A finite element model for the global structure is constructed, see Fig. 9(a). The nonlinear incremental finite element analysis is performed for the global structure. The external load is incrementally imposed with load step i =1, 2, 3, …… We first obtain the reference interface force distribution $\mathbf{f}_r$ (i.e., force distribution along the boundary of the local structure), which is chosen from results of the early load step within linear response stage. We then find the interface force $\mathbf{f}_i$ at each load step, see Fig. 9(b).

(Step 2) In this step, we find a single scalar value which represents the interface force level. Since the force distribution varies depending on the external load level, we approximate the interface force $\mathbf{f}_i$ at load step i using the reference force distribution $\mathbf{f}_r$ ($\mathbf{f}_i \approx \tilde{\lambda}_i \mathbf{f}_r$ with a local load ratio $\tilde{\lambda}_i$).

For the typical shapes of local structures, the applied and reference load distributions on the loaded area are commonly converted into single scalar loads by averaging or integrating the load distributions and then the ratio of these scalar loads is calculated as the local load ratio. However, this method is not effective for an arbitrarily shaped local structure, because the averaged or summed value might be zero even if significant loads exist when the signs of the nodal loads are different.

The present approximation method is proposed to overcome this problem in the arbitrarily shaped local structures. The local load ratio ($\tilde{\lambda}_i$) is derived by the least squares fitting method. The sum squared error function (φ_i) of the local load is as follows:

$$\varphi_i = \left(\mathbf{f}_i - \tilde{\lambda}_i \mathbf{f}_r\right) \cdot \left(\mathbf{f}_i - \tilde{\lambda}_i \mathbf{f}_r\right). \tag{14}$$

The local load ratio ($\tilde{\lambda}_i$) is calculated so that the error function (φ_i) has a minimum value as follows; this is called the approximated load method:

$$\tilde{\lambda}_i = \frac{\mathbf{f}_i \cdot \mathbf{f}_r}{\mathbf{f}_r \cdot \mathbf{f}_r}. \tag{15}$$

For comparison, another measure can be considered. The local load ratio ($\bar{\lambda}_i$) is defined as a ratio of the norm values (magnitudes) of the critical local load and reference local load as follows; this is called the norm value method:

$$\bar{\lambda}_i = \sqrt{\frac{\mathbf{f}_i \cdot \mathbf{f}_i}{\mathbf{f}_r \cdot \mathbf{f}_r}} . \tag{16}$$

Note that both methods only consider the translational degrees of freedom of the nodal load component to calculate the local load ratio. The contribution of the rotational degrees of freedom to strain energy is not considered, as they can be ignored in most numerical problems.

(Step 3) We then find the critical state, i.e., the stability limit. The stability limit is determined by the load level at which the sign of the second variation of the strain energy shifts from positive to negative at each analysis step, see Fig. 9(c). The largest local load ratio within a stable load range is selected as the critical local load ratio $\tilde{\lambda}_c$. The stability of the structure can be evaluated by the second variation of the strain energy which is obtained from the second-order term of the incremental external work $(0.5\Delta\mathbf{f}_i \cdot \Delta\mathbf{u}_i)$ as mentioned in section 2.2.

The displacement index is introduced to investigate tendencies such as the severity of deformation at a specific load step. The correlation curve between the local load ratio and displacement index is derived from the strain energy at each step. The scalar value of the incremental displacement index (Δx_i) is calculated as follows:

$$\frac{\Delta W_i}{|\mathbf{f}_r|} = \tilde{\lambda}_i \Delta x_i + 0.5\Delta\tilde{\lambda}_i \Delta x_i , \tag{17a}$$

$$\Delta x_i = \frac{\Delta W_i}{|\mathbf{f}_r|\left(\tilde{\lambda}_i + 0.5\Delta\tilde{\lambda}_i\right)} , \tag{17b}$$

in which $\Delta\tilde{\lambda}_i$ is the incremental local load ratio.

(Step 4) The usage factor ($\tilde{\eta}$) is calculated by

$$\tilde{\eta} = \frac{\tilde{\lambda}_s}{\tilde{\lambda}_c} \quad \text{with} \quad 0 \le \tilde{\eta} \le 1, \tag{18}$$

in which $\tilde{\lambda}_s$ is the load factor corresponding to the service load. The local safety factor (LSF) is proposed with an inversed form of the usage factor as the measure of the safety in the structural design. When the safety factor is larger, the local structure is safer:

$$LSF = \frac{1}{\tilde{\eta}} = \frac{\tilde{\lambda}_c}{\tilde{\lambda}_s}. \tag{19}$$

The safety factor characterized by the ratio of the load levels is used to be more rational and useful to accurately evaluate the residual buckling strength of the local structure. Since the proposed method can fully consider complicated interactions between local and global structures.

The method can be easily used to define vulnerable areas by changing the local extents without additional finite element analysis. Fig. 10 shows how to identify damaged areas. We first find an unstable element (blue color) that is no longer, and then evaluate the stability of that area (red borderline) extending to adjacent elements. When the sign of the sum of the second variation of strain energy in an extended area is negative, then this area is identified as a probable damaged area. At this stage, the identified local structure loses its stability and no longer contributes to the overall resistance. When we remedy the presence of extensive damage, it is cost-effective to intensively reinforce the identified damaged area.

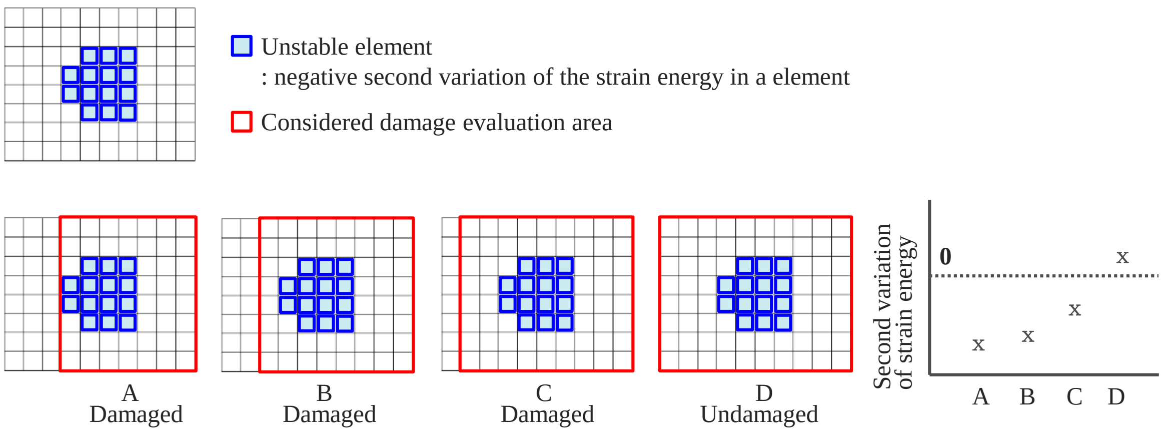

Fig. 10. Identification of damaged area along to the range of the evaluated area.

Chapter 4. Numerical examples

In this Chapter, to verify the performance of the proposed method, we solve four practical engineering problems involving stiffened plate structure in ship-shaped floating structure, cylindrical shell and stringer structures in mono-column FPSO (floating production storage and offloading) and local bracket girder structure in TLP (tension leg platform).

4.1 Stiffened rectangular plate structure in ship-shaped structure

This section shows a detailed step-by-step procedure for applying the proposed methodology to the first example for stability evaluation. We evaluate typical rectangular plates in the stiffened plate structure in ship and offshore floating structure. The stiffened side shell structure in ship structure is considered under uniformly varying loads representing hull girder bending as shown in Fig. 11.

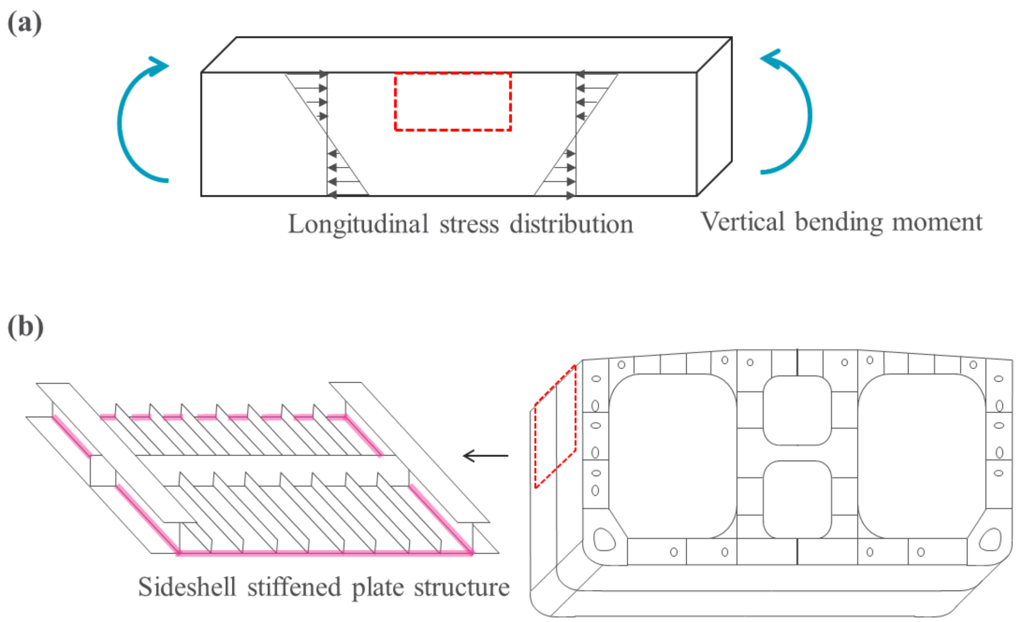

Fig. 11. Floating structure and stiffened plate: (a) overview of ship-shaped floating structure under vertical bending moment and (b) stiffened rectangular local plate structure at the upper sideshell of the floating structure.

To represent the bending condition, uniformly varying distributed load of $y \times 630/8300$ MPa are applied to the edges, where y is the vertical coordinate (unit: mm) from the bottom of the stiffened plate structure in Fig. 13(a). The reference global load is selected as one-tenth of the applied load. The structural stability of the local plate structure is evaluated through the incremental finite element analysis with intervals of 1/20 of the applied loads to investigate the safety margin. Simply supported boundary conditions are applied to all the edges of the stiffened plate structure and a straight constraint is added. The initial imperfection is applied as the form of five half waves in longitudinal direction and the maximum deflection of 5.73 mm is applied [39]. The structure is discretized by using 31,100 four node shell elements. We used the material properties of high-tensile steel (yield stress = 315 MPa, Young's modulus = 205.8 GPa, and Poisson's ratio = 0.3). Material nonlinearity is considered as a perfectly plastic stress-strain relationship without strain hardening.

Fig. 12 shows the strain energy composition of force and moment components. We can see that the portion of the force component is dominant in the local strain energy. The von Mises stress plot and deformed shape for a representative analysis results (10th analysis step) is displayed in Fig. 13(b) and the most compressive plate in corner of entire structure is selected as the local structure to be evaluated. The local loads are obtained for all analysis steps of nonlinear global FE analysis. As an example, the result of 10th analysis step is plotted in Fig. 13(c).

The local load of 2nd analysis step is used as the reference local load in Fig. 14(a) and the local load (10th analysis step) is approximated with a factor $\tilde{\lambda}_{10} = 3.96$ in Fig. 14(b), which is calculated by the least-squares fitting method in Fig. 14(c). For all applied loads, the calculated local load ratios by the approximated load method and norm value method are plotted in Fig. 14(d).

As shown in Fig. 15(a), the plate is stable up to the normalized global load of 5.0 (10th analysis step) because the sign of the second variation of the strain energy is positive. In approximated load method, the critical load is the normalized global load of 4.5 (9th analysis step) and the corresponding local safety factor is 4.0 as shown in Fig. 15(b). The first unstable local load ratio from the norm value method is 4.19 (4.8% higher than the approximated load method). The applied and approximated local loads are plotted in Fig. 15(c). A difference exists between the critical load and approximated load after nonlinear behavior occurs.

When the service load is the reference load (i.e., normalized load = 1), the usage factor ($\tilde{\eta}$) is 0.25 in Fig. 16(a) and local safety factors (LSF) is 4.0 in Fig. 16(b). Fig. 16(c) shows the local load ratio - displacement index curve for both present and previous methods [36]. The local safety factor is calculated as 4.26 by the design formula [9] as shown in Fig.17. As shown in Table 1, local safety factor calculated by the proposed method is 6% smaller than the design formula, but the local safety factor of the previous method through local FE analysis is 56.6% higher than the design formula.

Table 1. Local safety factors for a stiffened rectangular plate structure in ship-shaped structure.

	Direct evaluation through global FE analysis (Proposed)	Evaluation method through local FE analysis (Zi et al. 2017 [36])	Design formula (DNV, 2010 [9])
No. 1 plate	4.00	6.67	4.26

Fig. 18 shows the von Mises stress distribution and deformed shape at the normalized global loads of 4.0, 4.5 and 5.0. It can be seen that a large shear load is applied to the corner of the plate and high stresses occur. Fig. 19 shows the distribution of the second variation of the strain energy at the normalized global loads of 4.0, 4.5 and 5.0. The stability of local structure is lost when the summed values for the elements in the local extent becomes zero. The partly damaged area occurs in the considered No. 1 plate at the normalized global load of 4.5, and fully damaged one is at 5.25.

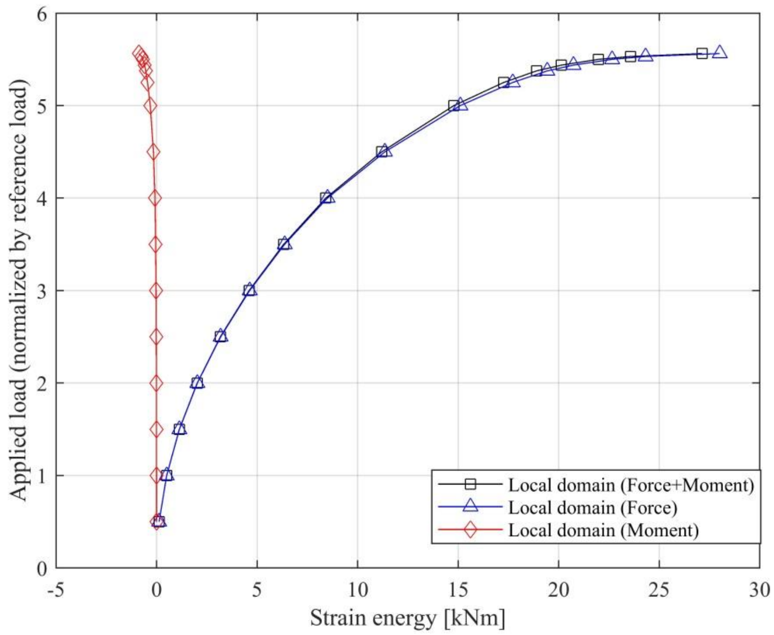

Fig. 12. Strain energy composition of force and moment components for local structural domain of a stiffened rectangular plate structure in ship-shaped structure

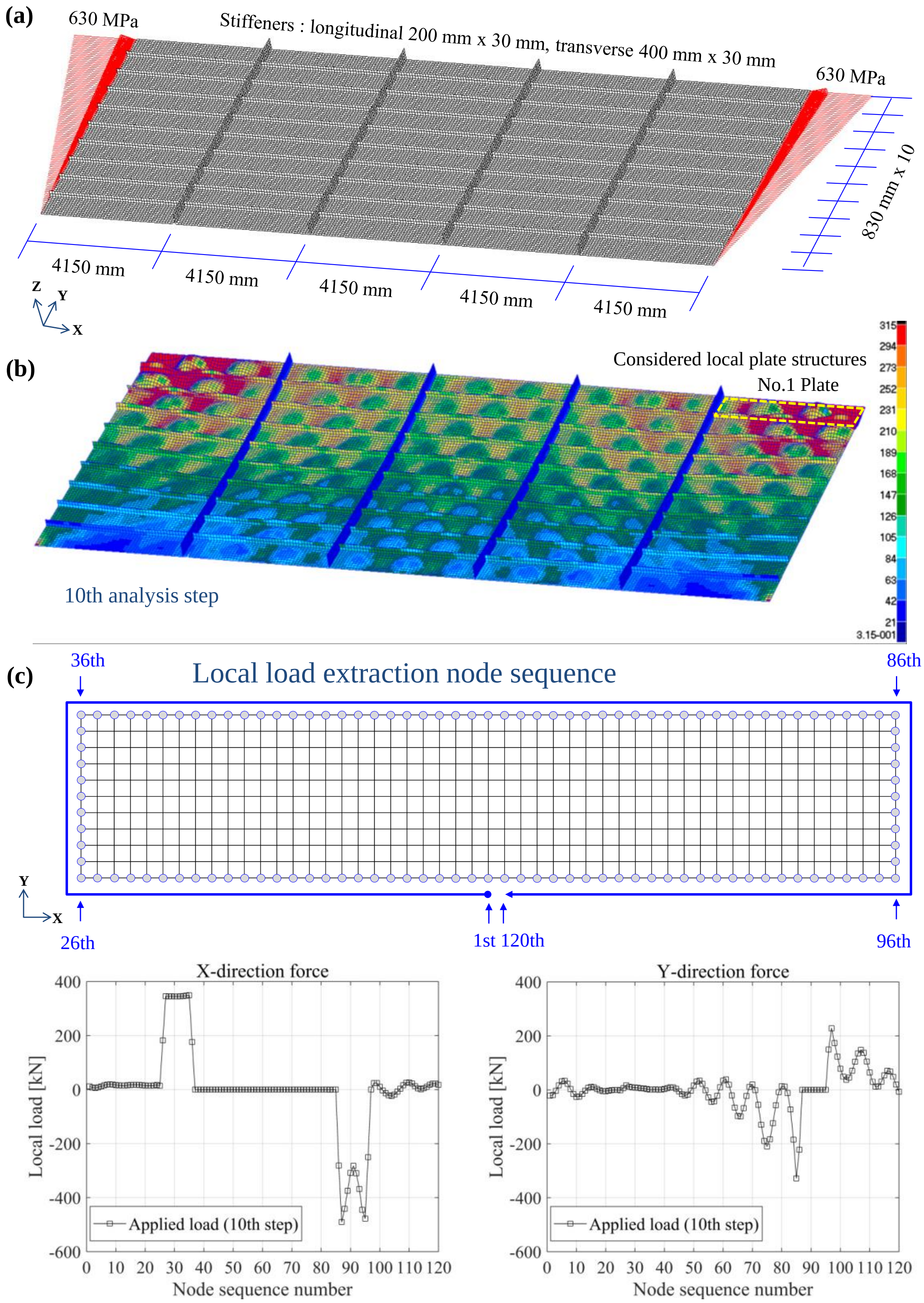

Fig. 13. Finite element model, applied global loads and local loads of a stiffened rectangular plate structure in ship-shaped structure: (a) finite element model, (b) von Mises stress distribution and (c) local loads at 10th analysis step.

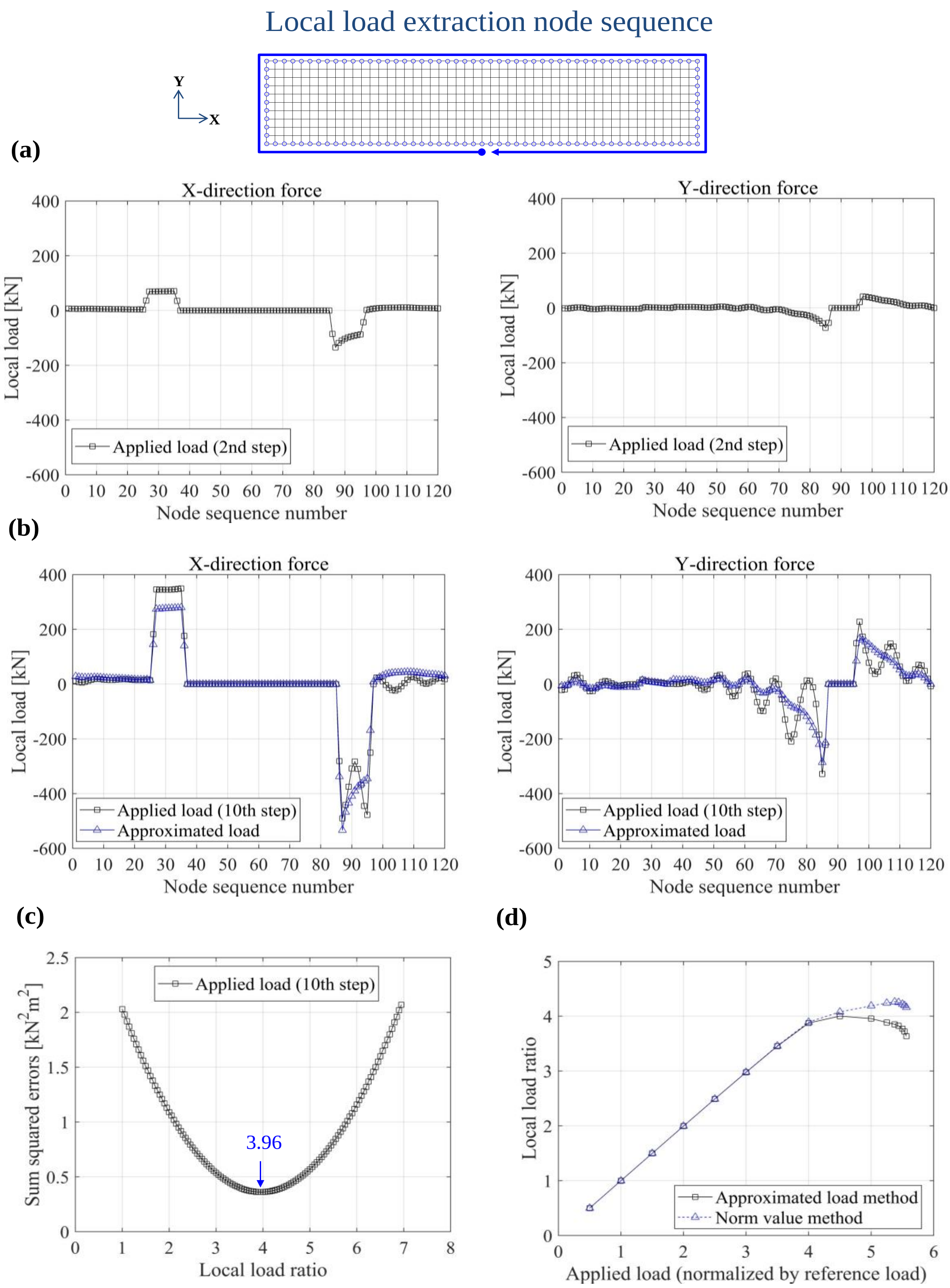

Fig. 14. The reference local load and calculated local load ratios of a stiffened rectangular plate structure in ship-shaped structure: (a) reference local load (2nd step), (b) applied and approximated local loads (10th step), (c) error function of local load (10th step) and (d) calculated local load ratios along the applied loads.

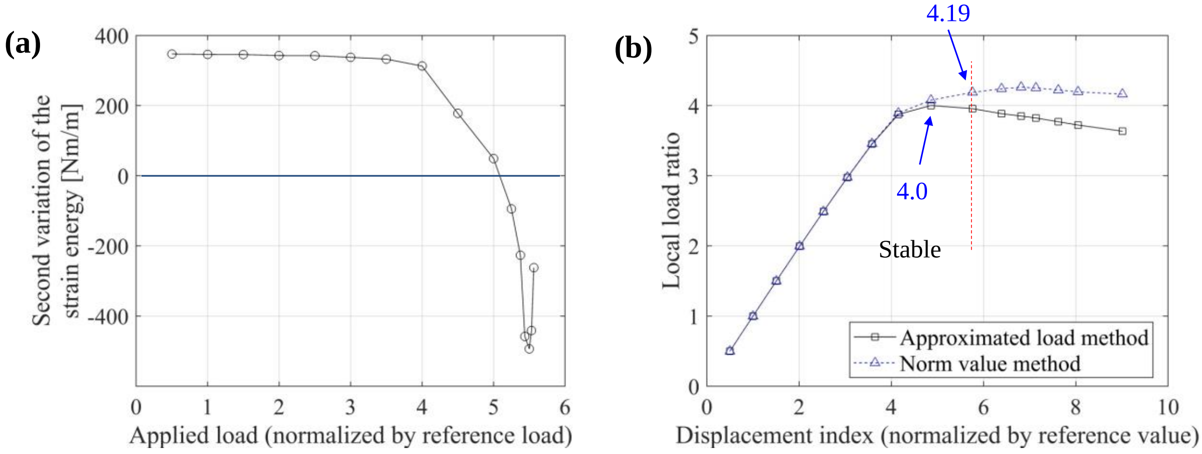

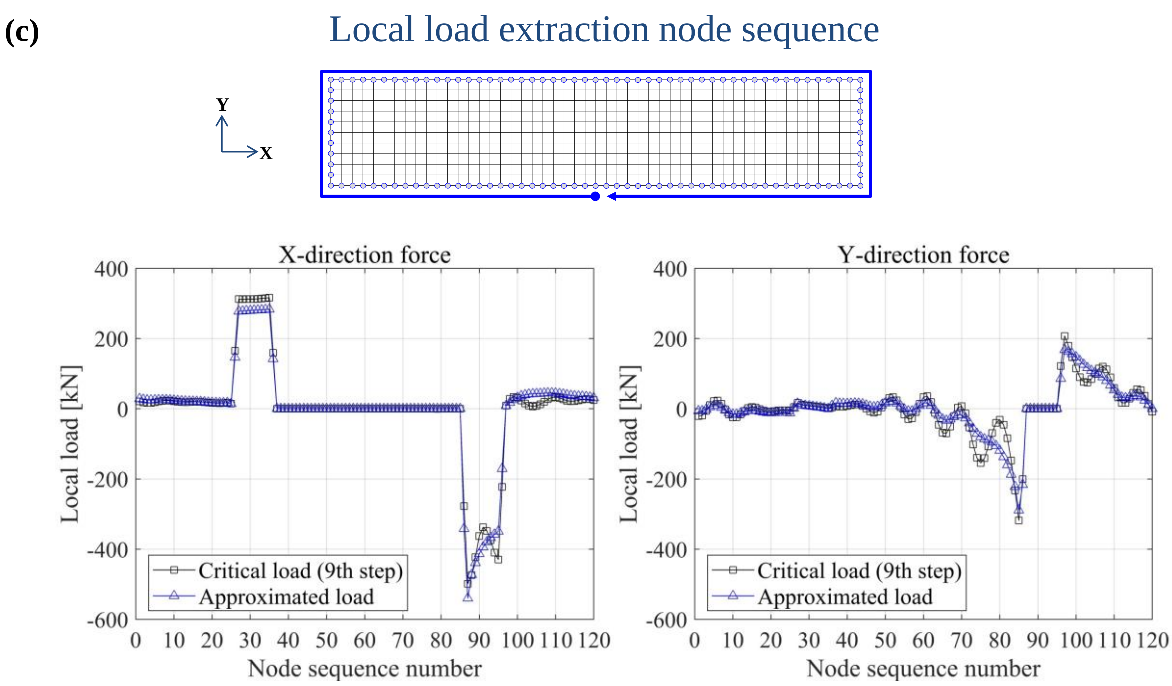

Fig. 15. Stability evaluation with the second variation of the local strain energy, local load ratios and selected critical local load of a stiffened rectangular plate structure in ship-shaped: (a) second variation of the local strain energy, (b) local load ratio and displacement index and (c) critical local load selected from the stability evaluation.

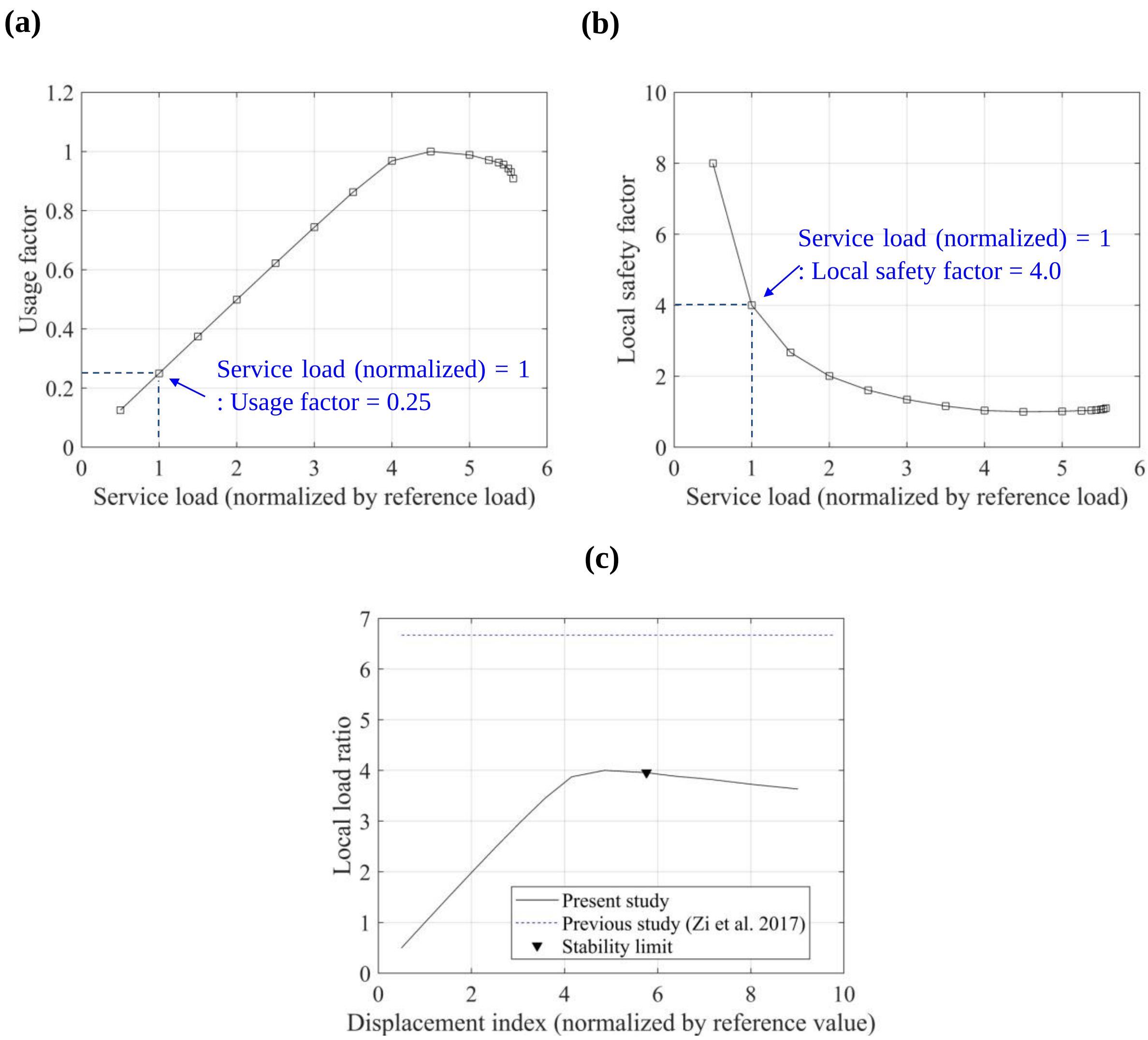

Fig. 16. Calculation of usage factors and local safety factors of a stiffened rectangular plate structure in ship-shaped structure: (a) usage factors along to service load levels, (b) local safety factors along to service load levels and (c) comparison of local load ratios with previous study (Zi et al. 2017).

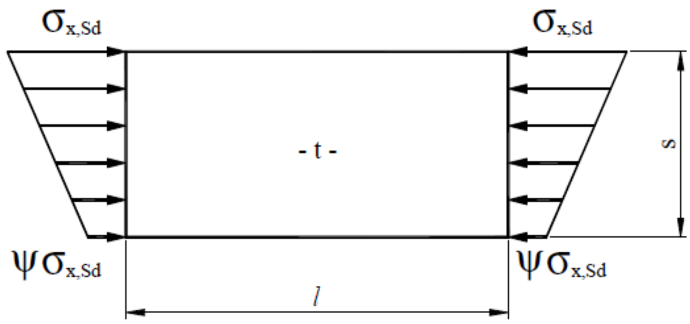

Parameter	Value	Unit
$\sigma_{x,Sd}$	63	MPa
t	18.5	mm
f_y	315	MPa
ε	0.86	
ψ	0.9	
k_σ	4.21	
$\bar{\lambda}_p$	0.89	
C_x	0.85	
$\sigma_{x,Rd}$	268.24	MPa
$\sigma_{x,Rd} / \sigma_{x,Sd}$	4.26	

Fig. 17. Calculation of the safety factor of the Plate No. 1 in a stiffened rectangular plate structure in ship-shaped structure by the design formula of DNV-RP-C201 [9].

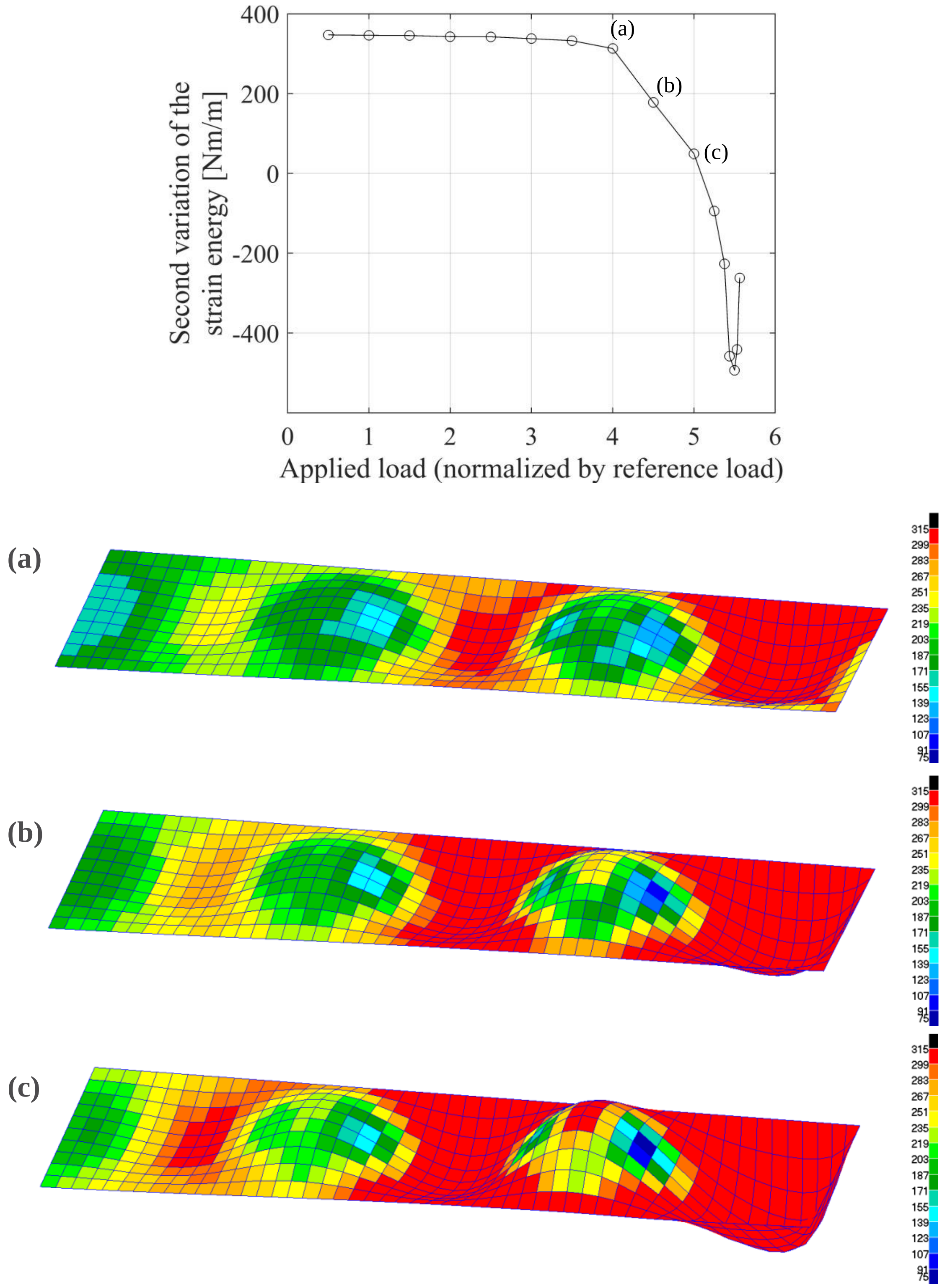

Fig. 18. von Mises stress plots (unit: MPa) and deformed shapes (30-time scale) of the Plate No. 1 in a stiffened rectangular plate structure in ship-shaped structure. The normalized global loads are (a) 4.0, (b) 4.5 and (c) 5.0.

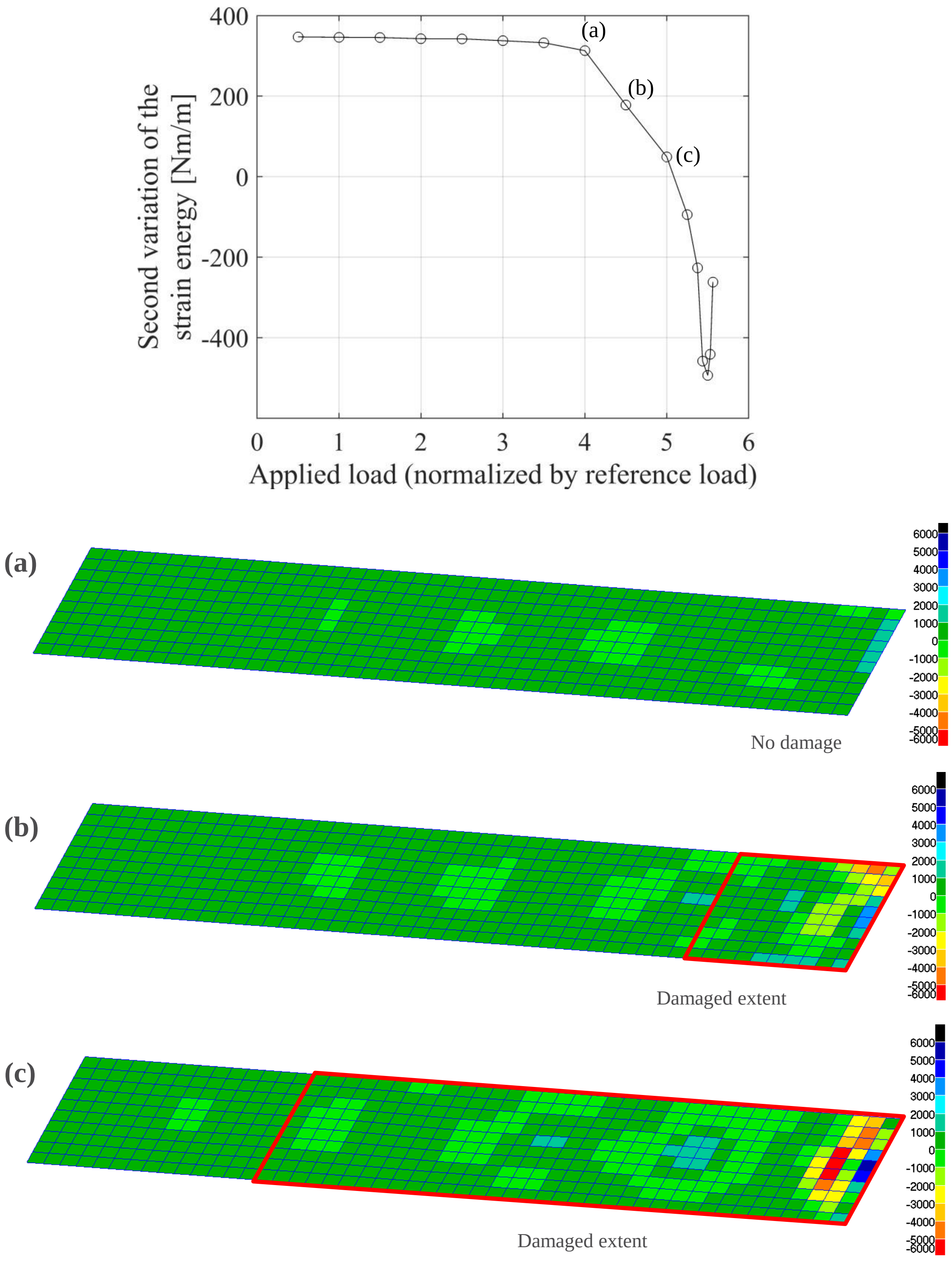

Fig. 19. Second variation of the strain energy plots (unit: Nmm) and damaged areas of the Plate No. 1 in a stiffened rectangular plate structure in ship-shaped structure. The normalized global loads are (a) 4.0, (b) 4.5 and (c) 5.0.

4.2 Cylindrical shell structure with radial bulkheads

Mono-column FPSO (floating production storage and offloading) unit is selected as the second example in which snap-through buckling could occur in offshore structures. Fig. 20(a) shows a typical mono-column FPSO [40] in the North Sea. The overall structure includes top and bottom horizontal circular decks, outer cylinder shell, inner radial bulkheads, and horizontal stringers. To evaluate characteristics of the local structural stability, we simplify the actual circular FPSO as shown in Fig. 20(b) and 20(c).

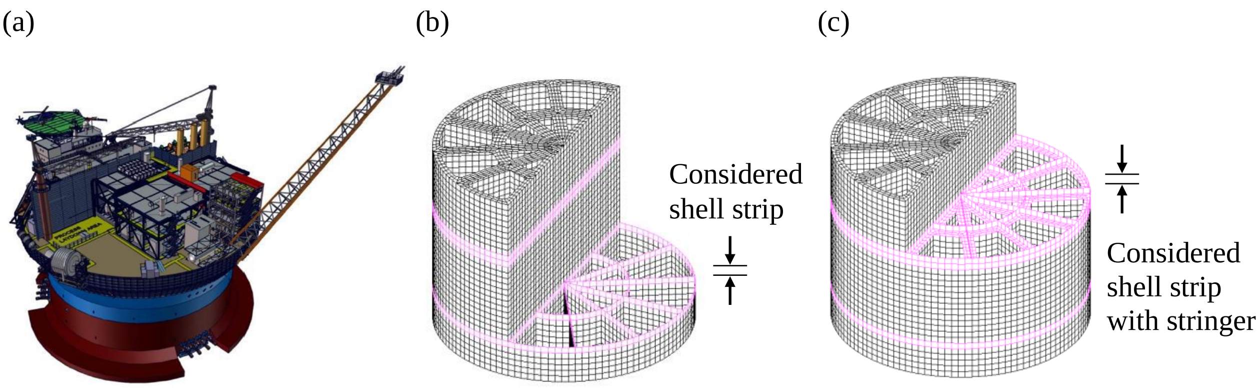

Fig. 20. Monocolumn FPSO for North Sea field: (a) overview of monocolumn FPSO [40], (b) inner view of cylindrical shell and radial bulkhead in a simplified model, and (c) inner view of cylindrical shell and radial bulkhead with horizontal stringer in a simplified model.

We make an example corresponding to a representative strip section of the outer shell where snap-through failure can occur first under lateral loads as shown in Fig. 21. The area of interest is selected as the shell plating between two bulkheads as shown in the figure.

The large and small diameters of cylinder are 2.0 m and 1.0 m, respectively. The height and thicknesses of strip are 0.05 m and 0.01 m, respectively. A 0.05 m × 0.05 m mesh of shell finite elements is used. The reference (service) load is defined as 500 N and the applied load is 50,000 N as hundred times the reference load with a load increment step of 500 N. The boundary conditions are applied somewhere away from the region of interest to avoid a rigid body motion.

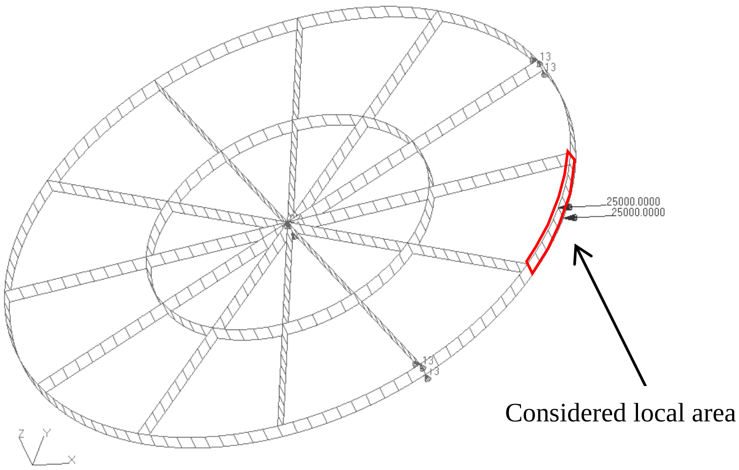

Fig. 21. Simplified structural strip model of a cylindrical shell structure with radial bulkheads in monocolumn FPSO.

Four node-shell elements are used for the FE models. The material properties of high-tensile steel are used (yield stress = 355 MPa, Young's modulus = 210 GPa, and Poisson's ratio = 0.3). Material nonlinearity is considered as a perfectly plastic stress-strain relationship without stress hardening.

Fig. 22 shows the increase in strain energy of the entire structure and the local structure of interest by the external load increment. The snap-through phenomenon occurs at 9.38 kN, after which the strain energy increases significantly. Since the external load acts only on the member to be evaluated, most of the total strain energy is the strain energy of the considered local strip until the snap-through occurs. Fig. 23 shows the strain energy composition of force and moment components. We can see that the portion of the force component is dominant in the local strain energy.

As shown in Fig. 24, it is stable until the external load of 9.38 kN since the sign of the second variation of the strain energy is positive. Also, after 9.95 kN, the local structure becomes stable again. Fig. 25 shows the magnitude of the displacement at the loading point as the external global load increases. It can be seen that the load point is abruptly displaced and there is no significant decrease in load. Fig. 26 shows the deformation contour (unit: mm) and true-scaled deformed shapes for four applied load levels: 0.5 kN, 5 kN, 9.38 kN and 9.59 kN. The first yield stress occurs at a load of 5 kN.

Fig. 27 shows the displacement index corresponding to the local load ratio of the local structure by the approximated load method. The displacement index is also normalized by the displacement index value at the reference load of 500 N. The local structure itself is no longer resisted at 19.06 times the reference local load. So-called local snap-buckling occurs, so that the local load is reduced and the reduced amount of load is shifted to the adjacent structures. The local load ratio by norm value method also be plotted, and the first instability local load ratio is 19.76 which is 3.7% higher than the one by the approximated load method.

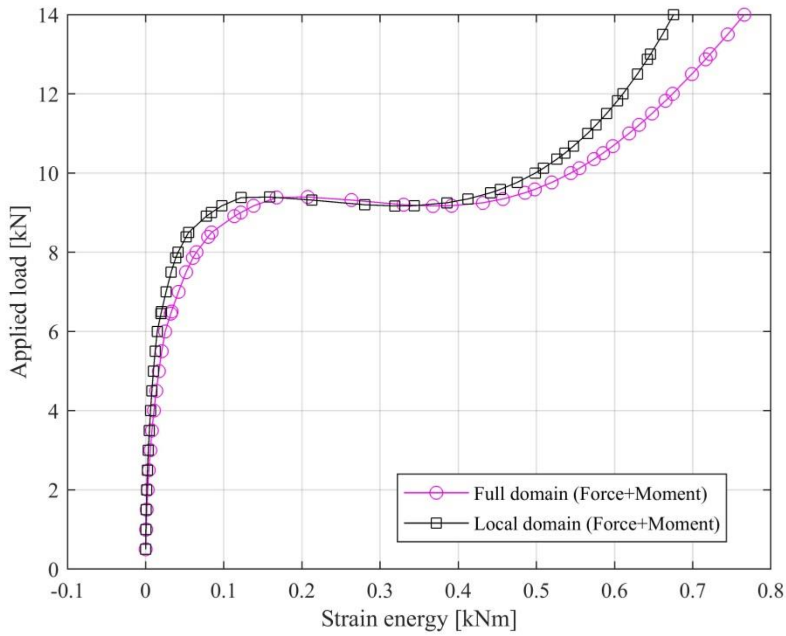

Fig. 22. Strain energy of full and local structural domains of a cylindrical shell structure with radial bulkheads.

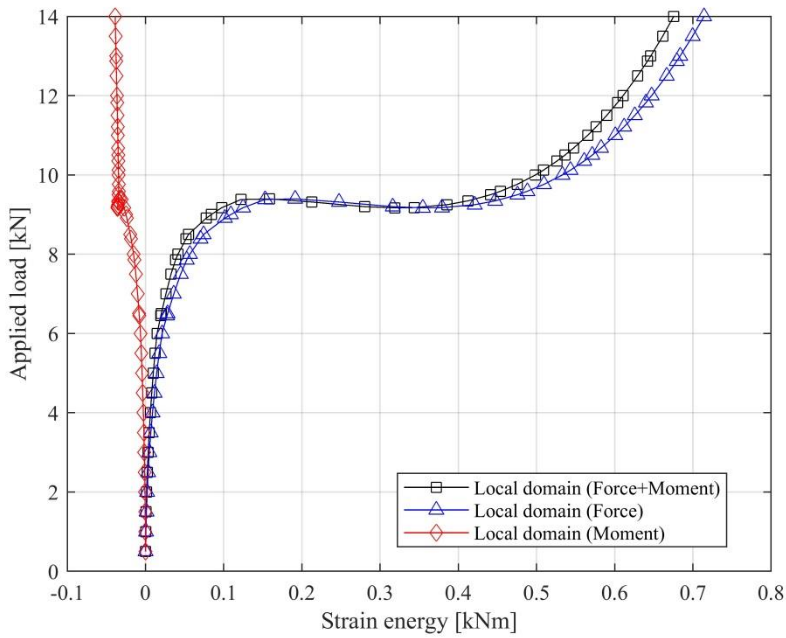

Fig. 23. Strain energy composition of force and moment components for local structural domain of a cylindrical shell structure with radial bulkheads.

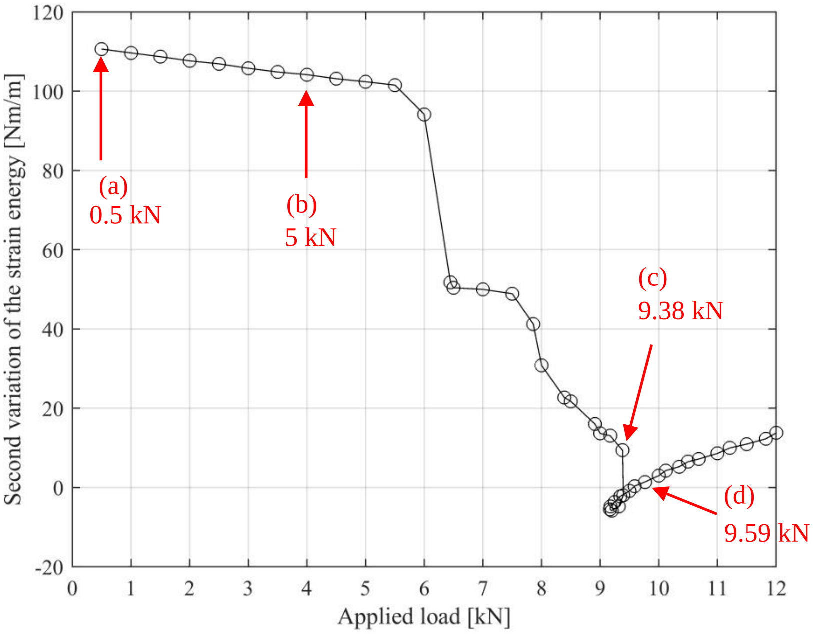

Fig. 24. Second variation of strain energy in local domain of a cylindrical shell structure with radial bulkheads.

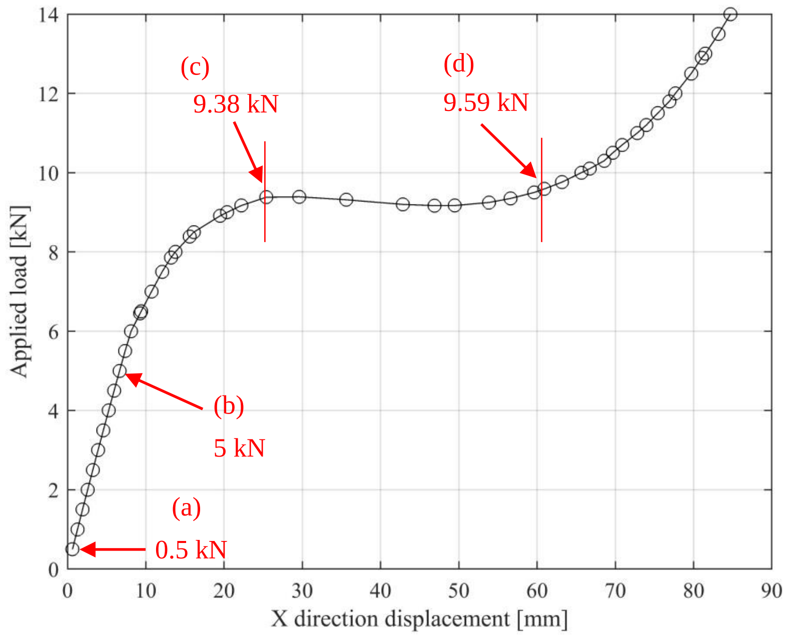

Fig. 25. Applied global load versus displacement on load points of a cylindrical shell structure with radial bulkheads.

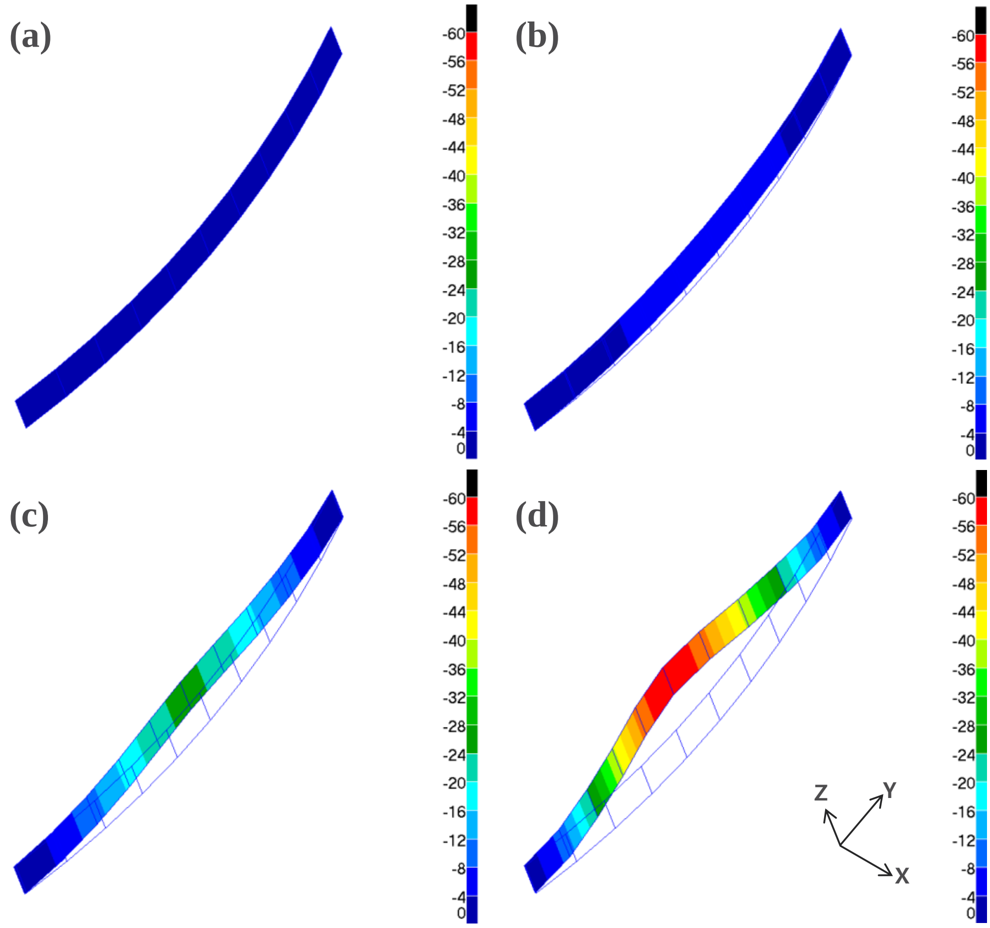

Fig. 26. X–directional deformation contour (unit: mm) and true-scaled deformed shapes of the simplified structural-strip model in a cylindrical shell structure with radial bulkheads for the evaluation of snap-through behavior. The applied loads are (a) 0.5 kN, (b) 5 kN, (c) 9.38 kN, and (d) 9.59 kN.

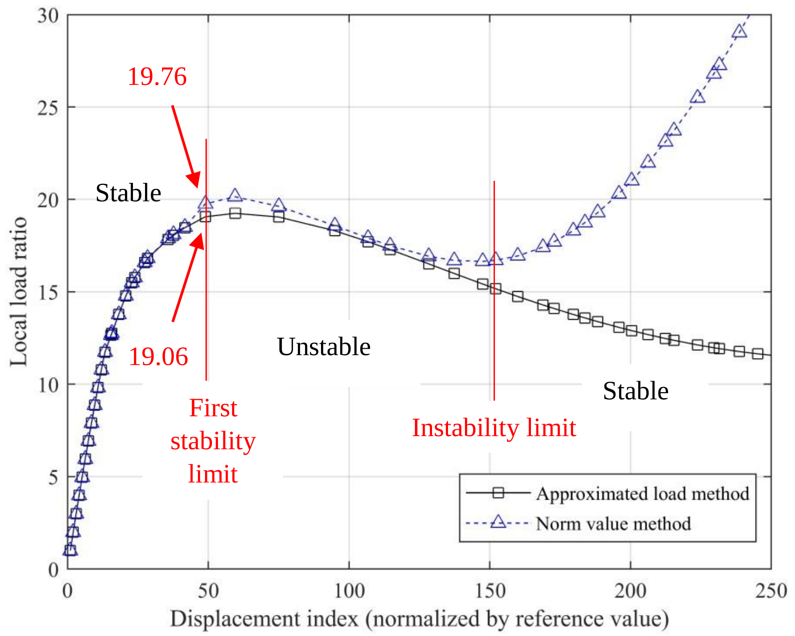

Fig. 27. Local load ratio - displacement index curve of a cylindrical shell structure with radial bulkheads.

4.3 Horizontally stiffened cylindrical structure with radial bulkheads

In the mono-column type structure, a stringer structure is designed between the radial bulkhead and cylindrical shell to resist the external pressure load. We use the FE model with horizontal stringers in Fig. 20(c). Fig. 28 shows the simplified model with the considered local stringer area.

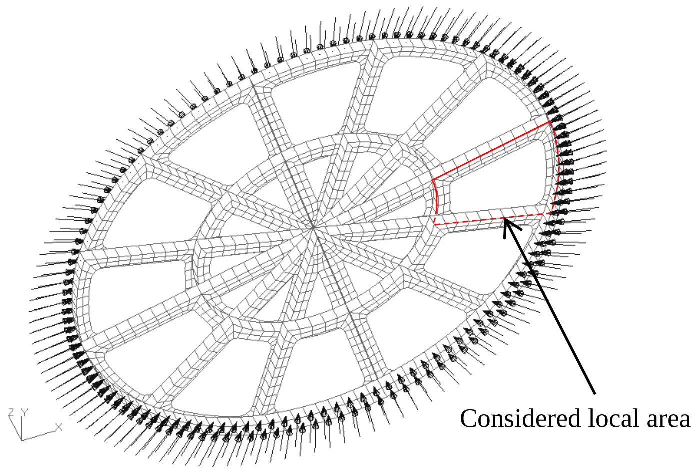

Fig. 28. Simplified stringer model of a horizontally stiffened cylindrical structure with radial bulkheads in monocolumn FPSO.

A stringer of a width of about 0.5 m is considered in the finite element model. The buckling mode analysis is performed to apply an initial imperfection. The model geometry is modified to fit the first mode shape with maximum imperfection of 2.5mm. The main loads are external uniform pressure loads. The reference (service) load is defined as 1 MPa and the applied load is 100 MPa, corresponding to 100 times the reference load, with a load increment step of 1 MPa. Because of the problem of force equilibrium as a whole, the boundary conditions are taken to avoid rigid body motion. Four node-shell elements are used for the FE models. The material properties of high-tensile steel are used (yield stress = 355 MPa, Young’s modulus = 210 GPa, and Poisson’s ratio = 0.3). Material nonlinearity is considered as a perfectly plastic stress-strain relationship without stress hardening.

Fig. 29 shows the strain energy composition of force and moment components. We can see that the portion of the force component is dominant in the local strain energy.

The nonlinear analysis solution is converged within the load of 10.76 MPa, which is 10.76 times the reference load of 1 MPa as shown in Fig. 30. The structure is stable until the global load of 10.76 MPa because the sign of the second variation of the strain energy is positive. Fig. 31 shows the elastic and plastic deformations for four applied load levels: 1 MPa, 7 MPa, 10.59 MPa, and 10.76 MPa. The first yield stress occurs at a load of 7 MPa. This example shows typical material plasticity-driven failure because the members directly subject to external loads become fully plastic at critical state.

Fig. 32 shows the maximum local load ratio of 10.23 times the local load for the approximated load method in the stable range. In the norm value method, however, the local load ratio steadily increases, and is overestimated compared to the approximated load method after the local load ratio of 9.0.

Fig. 33 shows the local load ratio - displacement index curve for both the present and previous methods [36], and the local safety factors are presented in Table 2. The evaluation through local FE analysis as the previous study shows much higher safety factor as 2.89 times present method because this problem is very ductile due to material plasticity.

Fig. 34 shows the local load extraction numbering sequence for the stringer structure. Fig. 35 shows the local load component plots for the critical load and approximated load at critical step. As the nonlinearity increases, it can be seen that there is a difference between the critical load and the approximated load due to the nonlinear behavior, especially in the edge from P13 to P23 which is directly subject to the external pressure.

Table 2. Local safety factors for a horizontally stiffened cylindrical structure with radial bulkheads.

	Direct evaluation through global FE analysis (Proposed)	Evaluation method through local FE analysis (Zi et al. 2017 [36])
Horizontal stringer	10.22	29.59

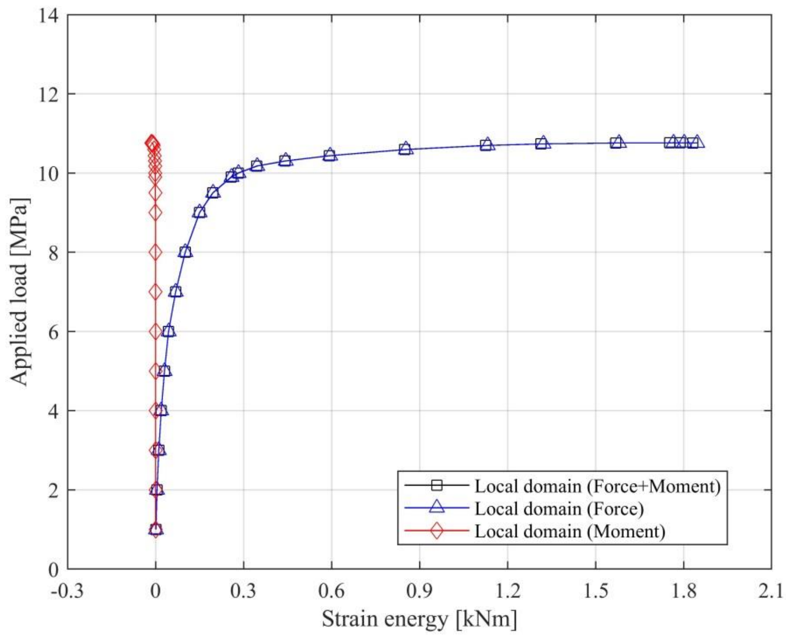

Fig. 29. Strain energy composition of force and moment components for local structural domain of a horizontally stiffened cylindrical structure with radial bulkheads.

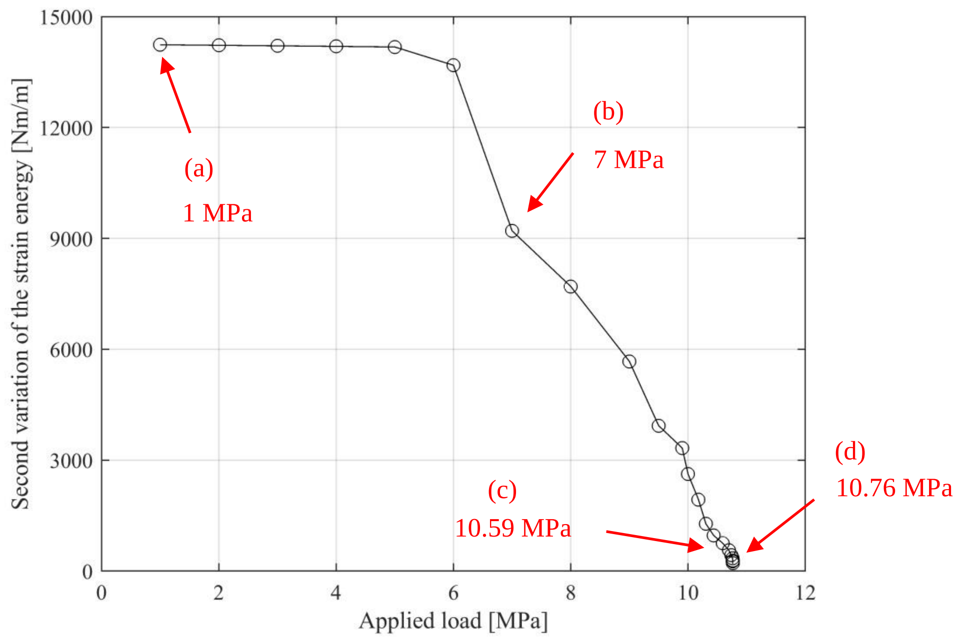

Fig. 30. Second variation of strain energy in local domain of a horizontally stiffened cylindrical structure with radial bulkheads.

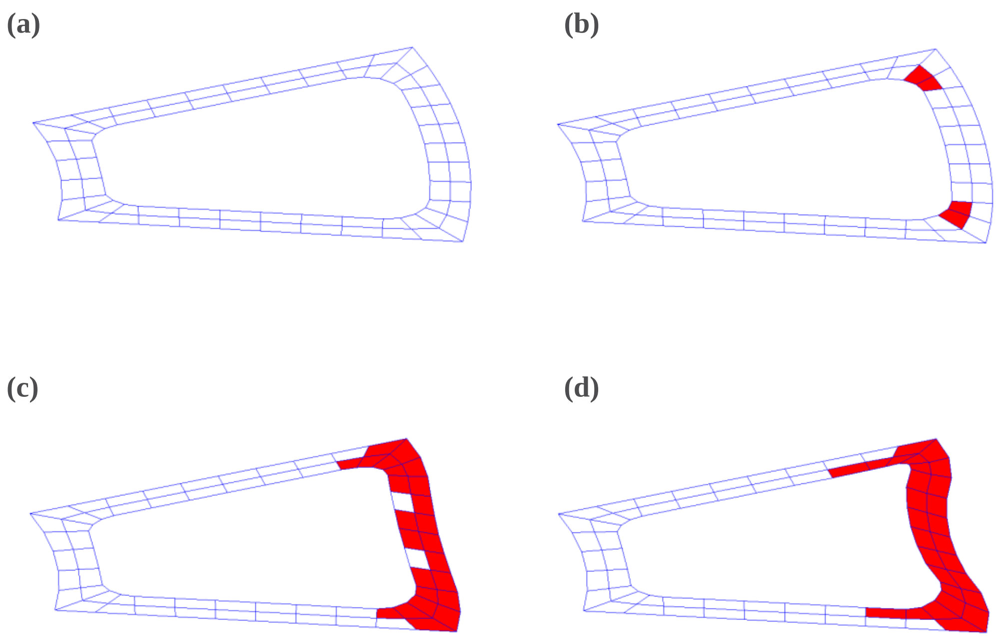

Fig. 31. Elastic and plastic deformations (five-time scale) of a stiffened cylindrical shell structure with radial bulkheads. The applied loads are (a) 1 MPa, (b) 7 MPa, (c) 10.59 MPa, and (d) 10.76 MPa. The red color indicates that the element has reached the material yield stress.

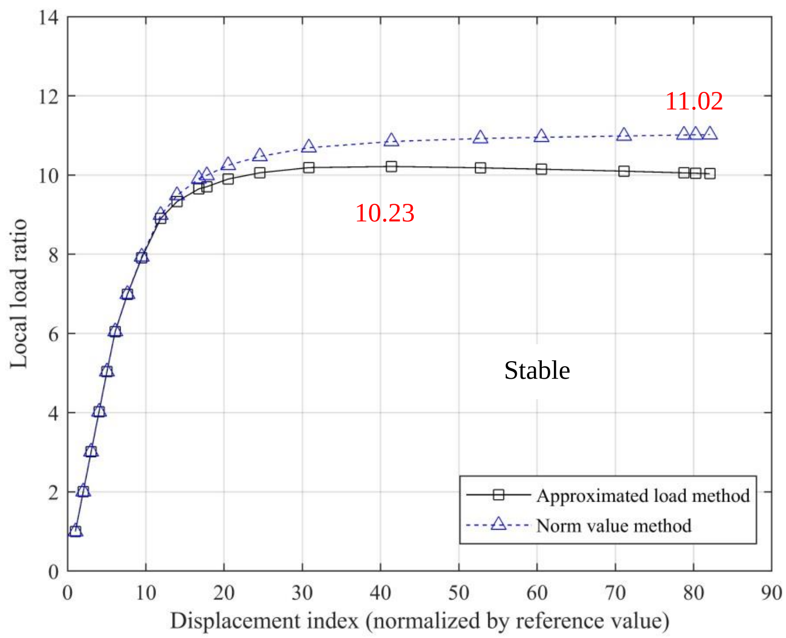

Fig. 32. Local load ratio - displacement index curve of a horizontally stiffened cylindrical structure with radial bulkheads.

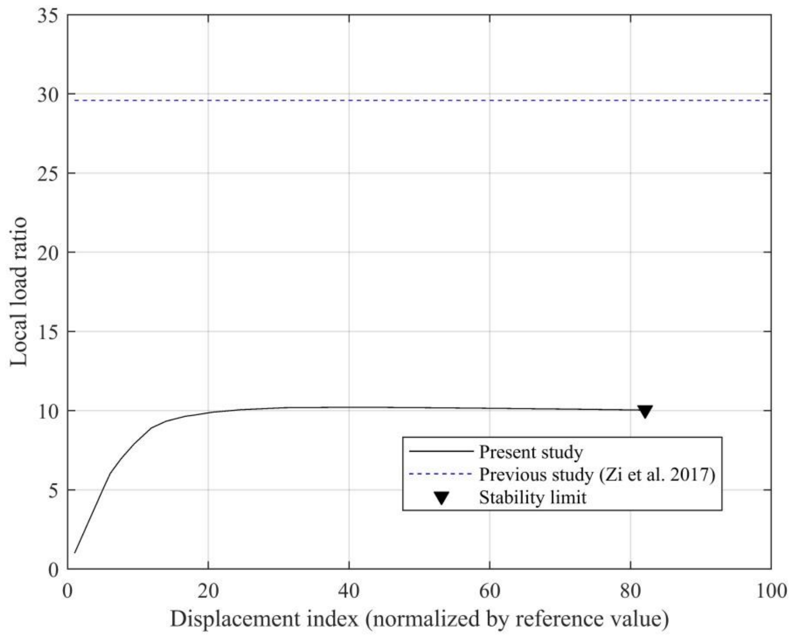

Fig. 33. Local load ratios of a stiffened cylindrical shell structure with radial bulkheads with previous study (Zi et al. 2017).

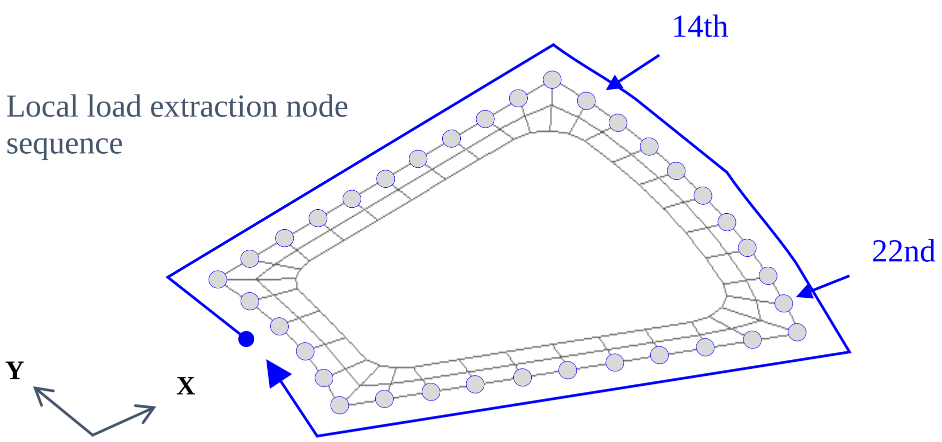

Fig. 34. Local load extraction numbering sequence for horizontal stringers structure of a horizontally stiffened cylindrical structure with radial bulkheads.

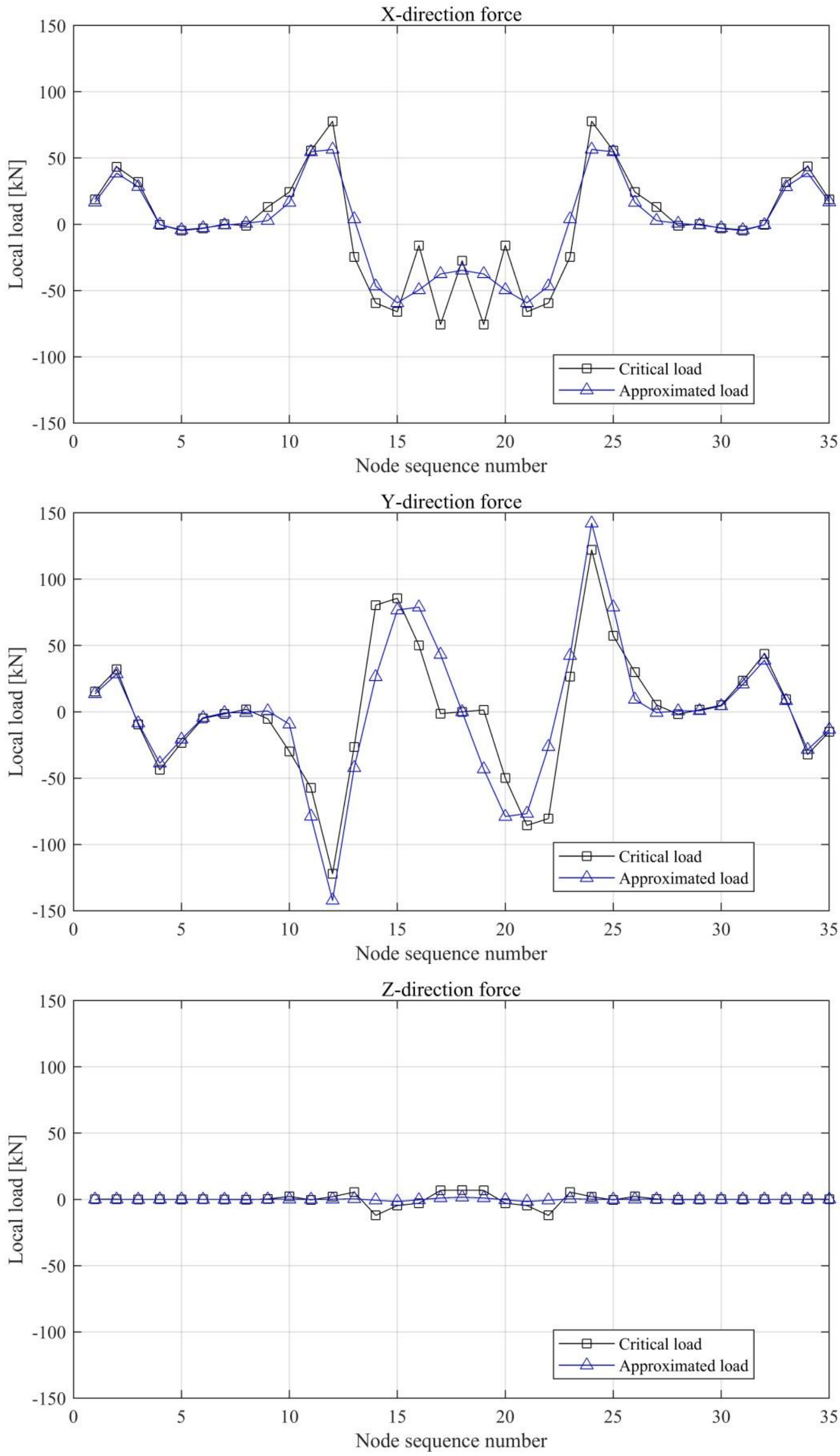

Fig. 35. Local load component plots (unit: MPa) for the critical load and approximated load at critical step of a horizontally stiffened cylindrical structure with radial bulkheads.

4.4 Bracket girder in the column-pontoon connection structure of tension leg platform

The local bracket girder structure in TLP (tension leg platform) hull is selected as the last example, which has a non-typical geometry not to be applied to the conventional design formula. TLP is a vertically moored floating structure for deep water as shown in Fig. 36 [41]. The horizontal pontoon structure is usually connected to the vertical column, which is locally reinforced by a stiffener and a bracket girder as shown in Fig. 37. Due to the connection geometry between cylindrical column and box type pontoon, irregular shaped bracket girder structure is attached on the connection area. Since it is difficult to intuitively estimate a typical deformed shape and stress distribution under the subjected load, a direct structural response should be analyzed in consideration of the global structural stiffness through the nonlinear finite element analysis.

(a) (b) (c)

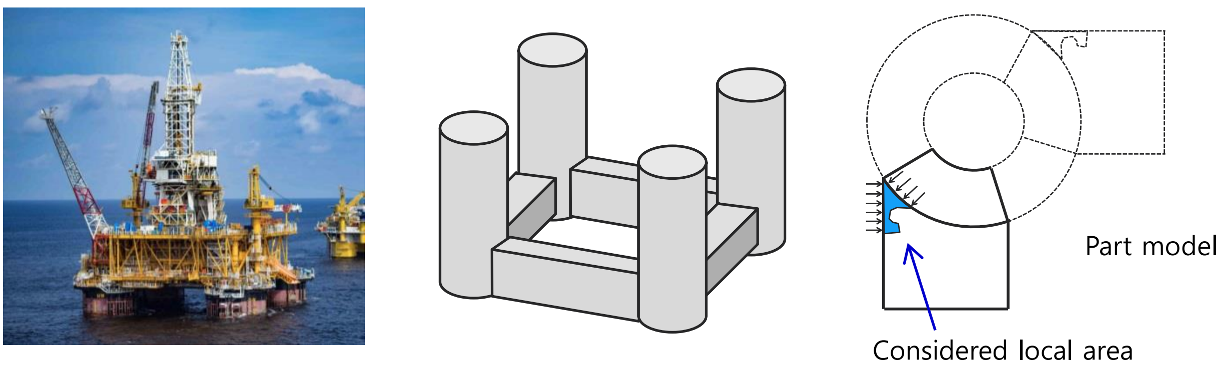

Fig. 36. TLP installed in West Africa field: (a) Photo of TLP [41], (b) schematic of TLP hull with column and pontoon structures, and (c) plan view of the bracket girder between column and pontoons.

In the tension leg platform problem, the part of column with adjacent pontoon structure is considered as the full domain of the finite element analysis as shown in Fig. 37. The local bracket girder structure of interest is the horizontally irregular-shaped plate between the cylindrical shell plating of the column and the horizontal girder in the pontoon. The zoomed view of the bracket girder is shown in Fig. 38.

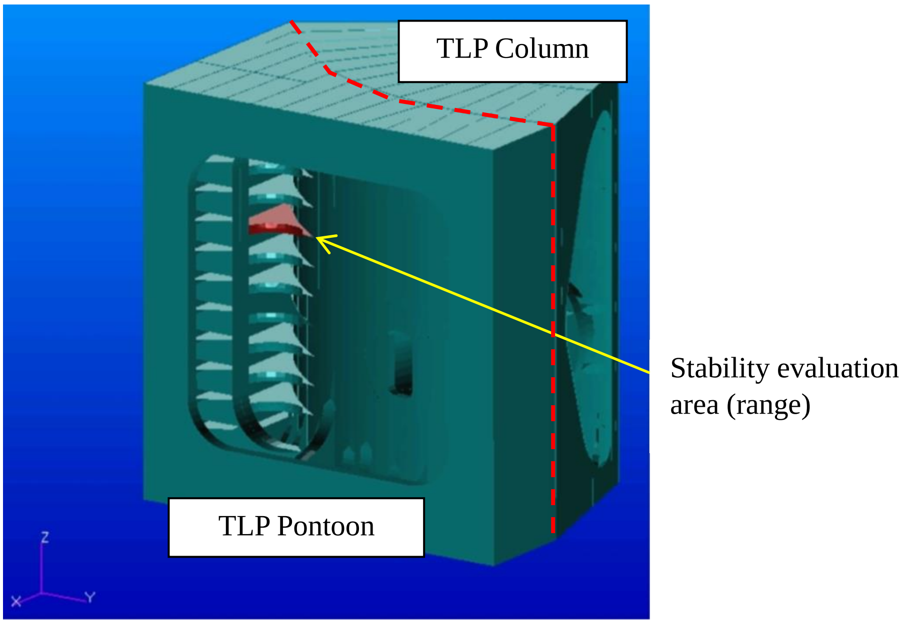

Fig. 37. Finite element model of a column-pontoon connection structure of tension leg platform.

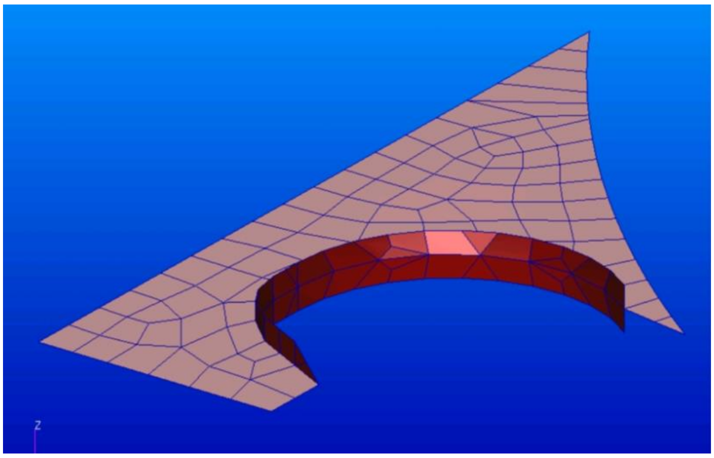

Fig. 38. Finite element model of a bracket girder of interest in the column-pontoon connection structure of tension leg platform.

As shown in Fig. 39, the bracket girders are located in vertically as a same design detail, and the concerned position is selected to the vertically medium level where the local load on bracket girder boundary is most generated. The initial imperfection of the bracket girder is assumed to be 3.5 mm in the vertical direction, and the geometry of the finite element model is modified as the lowest local mode shape. In order to prevent the occurrence of unbalance forces in the considered area, boundary conditions are specified far away from the target bracket girder. This tension leg platform mainly experiences the external and internal water head pressure because it is installed at calm sea of West Africa. Therefore, the inner tank and the external water head pressure are defined as the global reference (service) load. To investigate the design safety margin, the structural stability of the local bracket girder structure is evaluated by linearly increasing the global reference load on the column-pontoon connection structure.

Three and four node-shell elements are used for the FE models. The material properties of high-tensile steel are used (yield stress = 355 MPa, Young's modulus = 210 GPa, and Poisson's ratio = 0.3). Material nonlinearity is considered as a perfectly plastic stress-strain relationship without stress hardening.

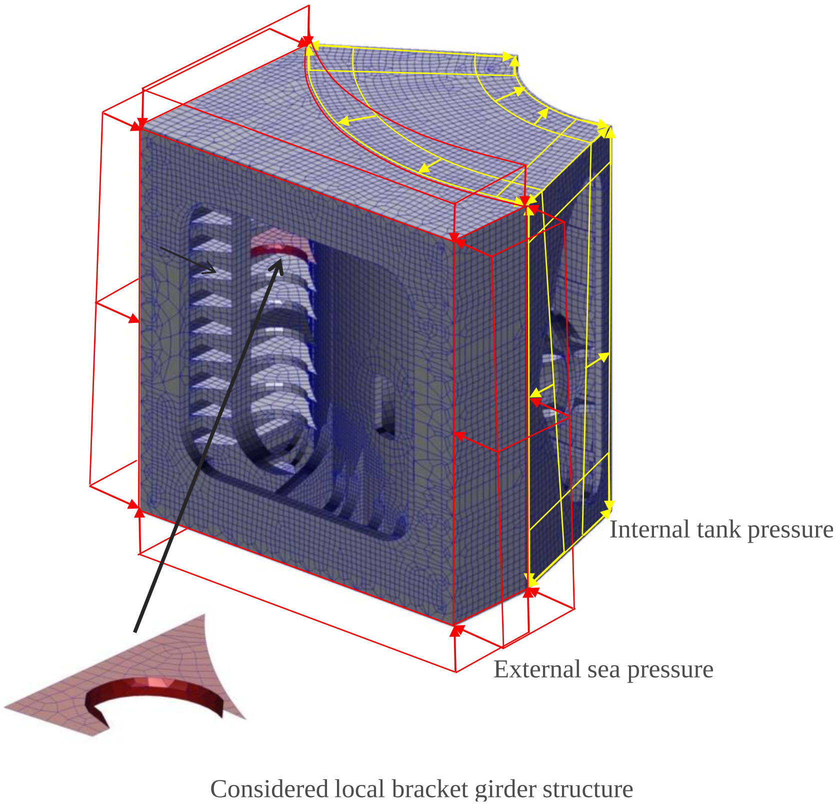

Fig. 39. Finite element model and applied loads of a bracket girder in the column-pontoon connection structure of tension leg platform.

Fig. 40 shows the strain energy composition of force and moment components. We can see that the portion of the force component is dominant in the local strain energy. As shown in Fig. 41, it is stable until the external load of 3.5 times reference (service) load since the sign of the second variation of the strain energy is positive. Fig. 42 shows the elastic and plastic deformations for normalized global loads of 1.0, 2.0, 3.1, 3.5, 3.8, and 4.0. The first yield occurs at a normalized global load of 2.0 and most of the area is plastic at a normalized global load of 4.0. This example shows failure that is driven by combined geometric and material nonlinearities.

At the critical limit state, the bracket girder flange edge is deformed in the lateral direction as shown in Fig. 43(a). The vertical (z-direction) displacement of the point, at which the maximum displacement occurs, is plotted along with the external load as shown in Fig. 43(b). In this figure, as the displacement increases, the external load also continues to increase, and it is not known at what load step the resistance of the local structure has been reached.

Fig. 44 shows the local load extraction numbering sequence. Fig. 45 shows local load component plots for the critical load and approximated load at critical step. As the nonlinearity increases, it can be seen that there is a difference between the critical load and the approximated load due to the nonlinear behavior

From the local load ratio - displacement index curve, we can find the analysis step with the highest local load ratio of 3.25 by the approximated load method as shown in Fig. 46. However, from the result of stability check, the local load ratio of 3.22 is the stable state limit, which is the representative critical local load ratio. The first instability local load ratio by norm value method is 3.31 which is 2.8% higher than the one by the approximated load method. After the stable state limit, the local load ratio by the norm value method doesn’t significantly decrease as a different tendency compared to approximated method.

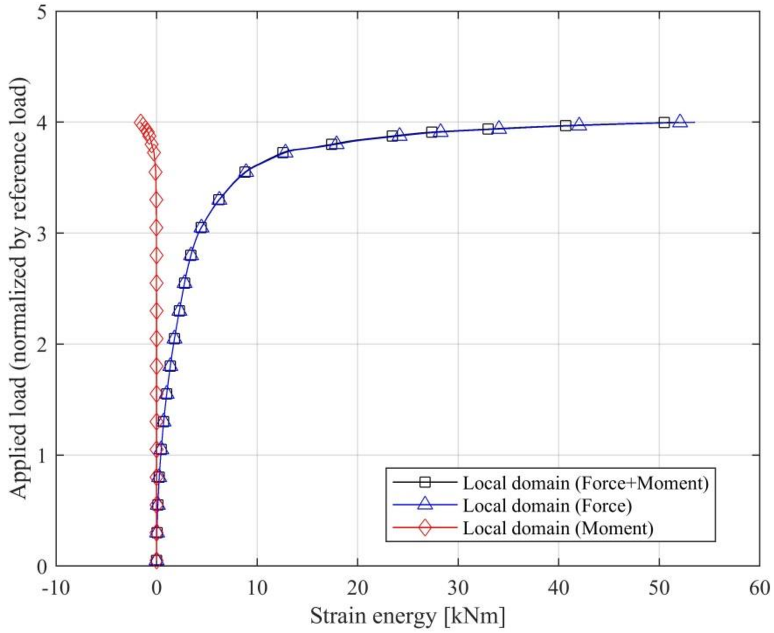

Fig. 40. Strain energy composition of force and moment components for local structural domain of a bracket girder in the column-pontoon connection structure of tension leg platform.

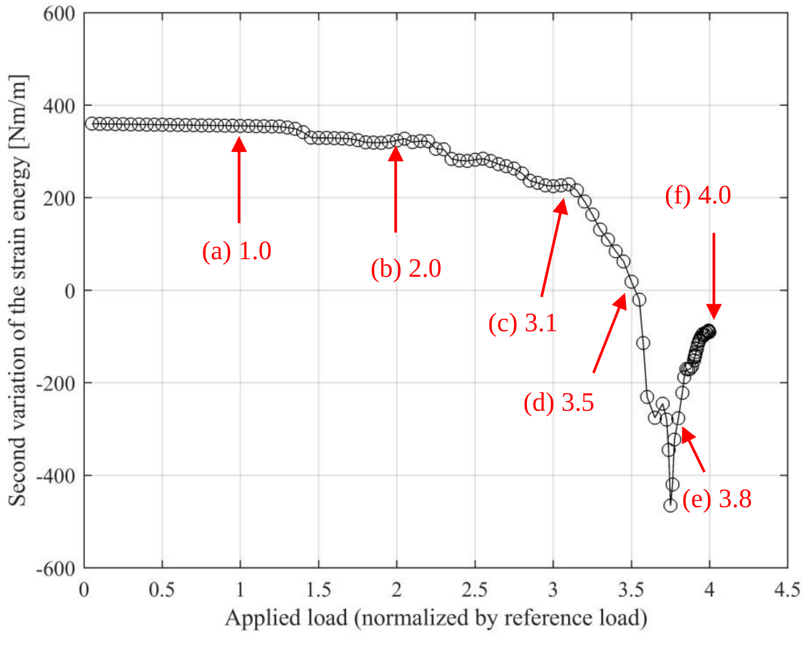

Fig. 41. Second variation of strain energy in local domain of a bracket girder in the column-pontoon connection structure of tension leg platform.

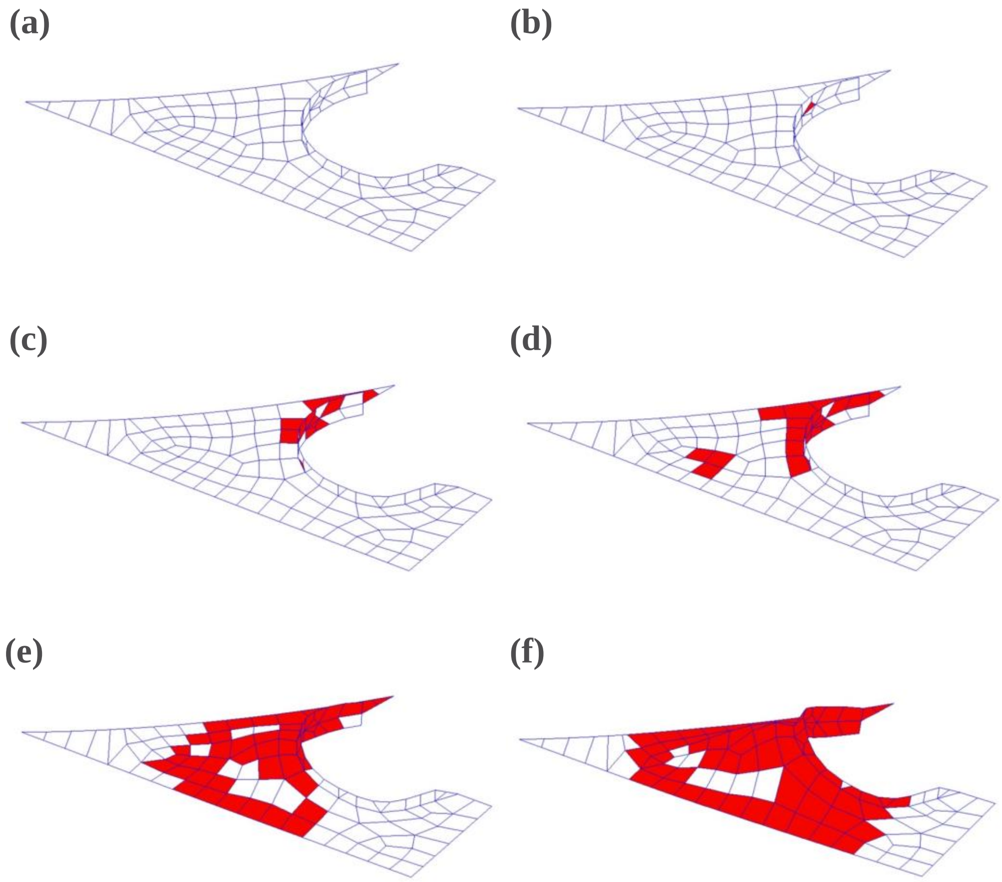

Fig. 42. Elastic and plastic deformations (three-time scale) of a bracket girder in the column-pontoon connection structure of tension leg platform. Applied normalized global loads are (a) 1.0, (b) 2.0, (c) 3.1, (d) 3.5, (e) 3.8, and (f) 4.0. The red color indicates that the element has reached the material yield stress.

(a)

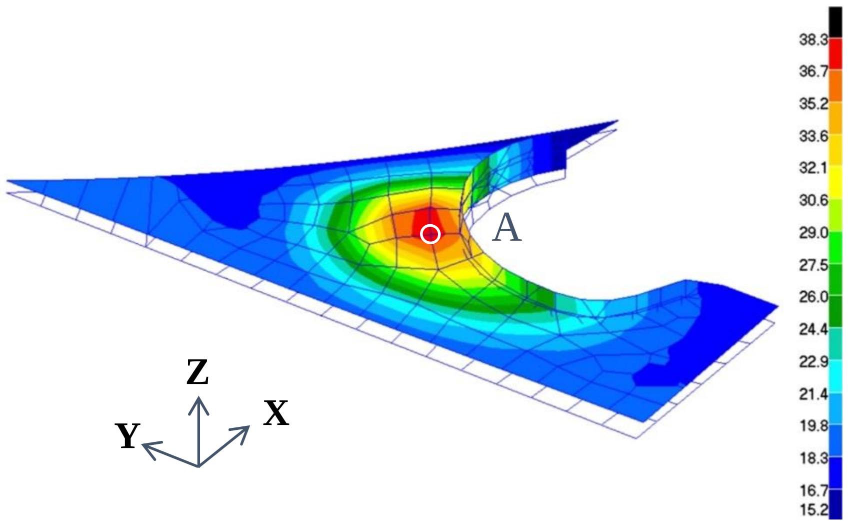

(b)

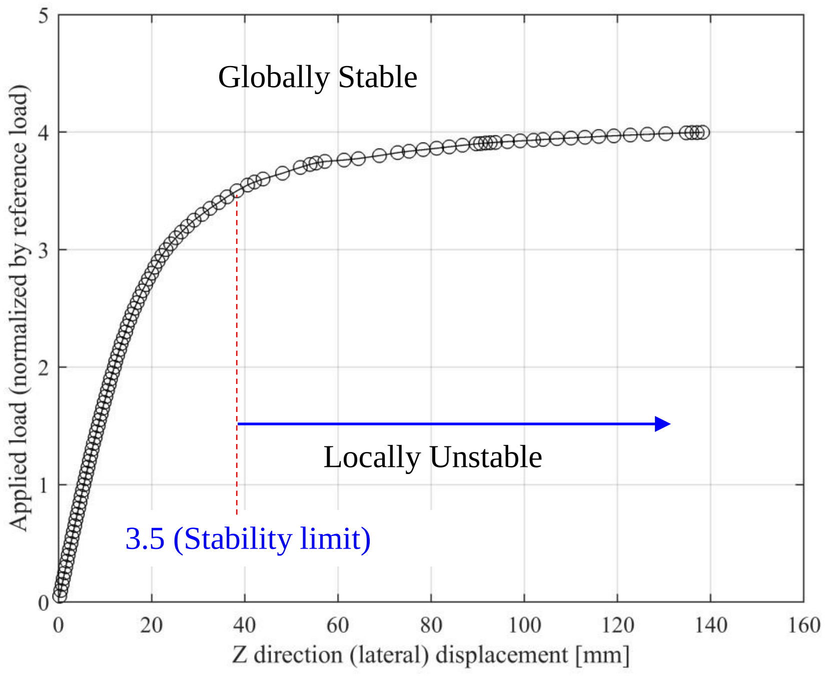

Fig. 43. Deformation of a bracket girder in the column-pontoon connection structure of tension leg platform: (a) vertical (z-) direction displacement contour (unit: mm) at critical state and (b) vertical (z-) direction displacement on point A under the various applied loads.

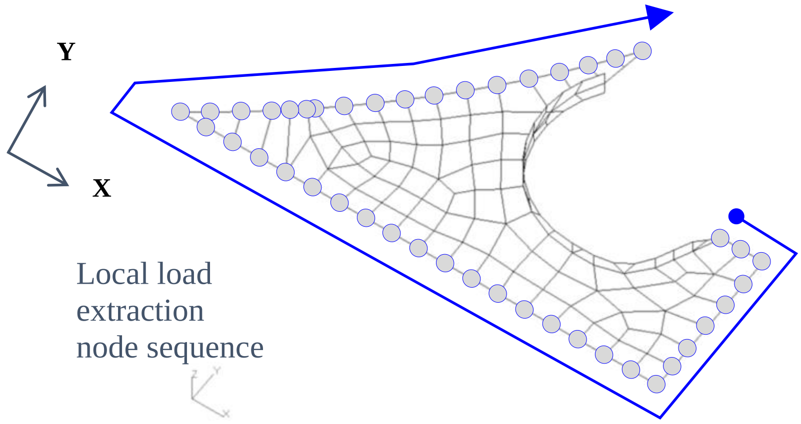

Fig. 44. Local load extraction numbering sequence of a bracket girder in the column-pontoon connection structure of tension leg platform.

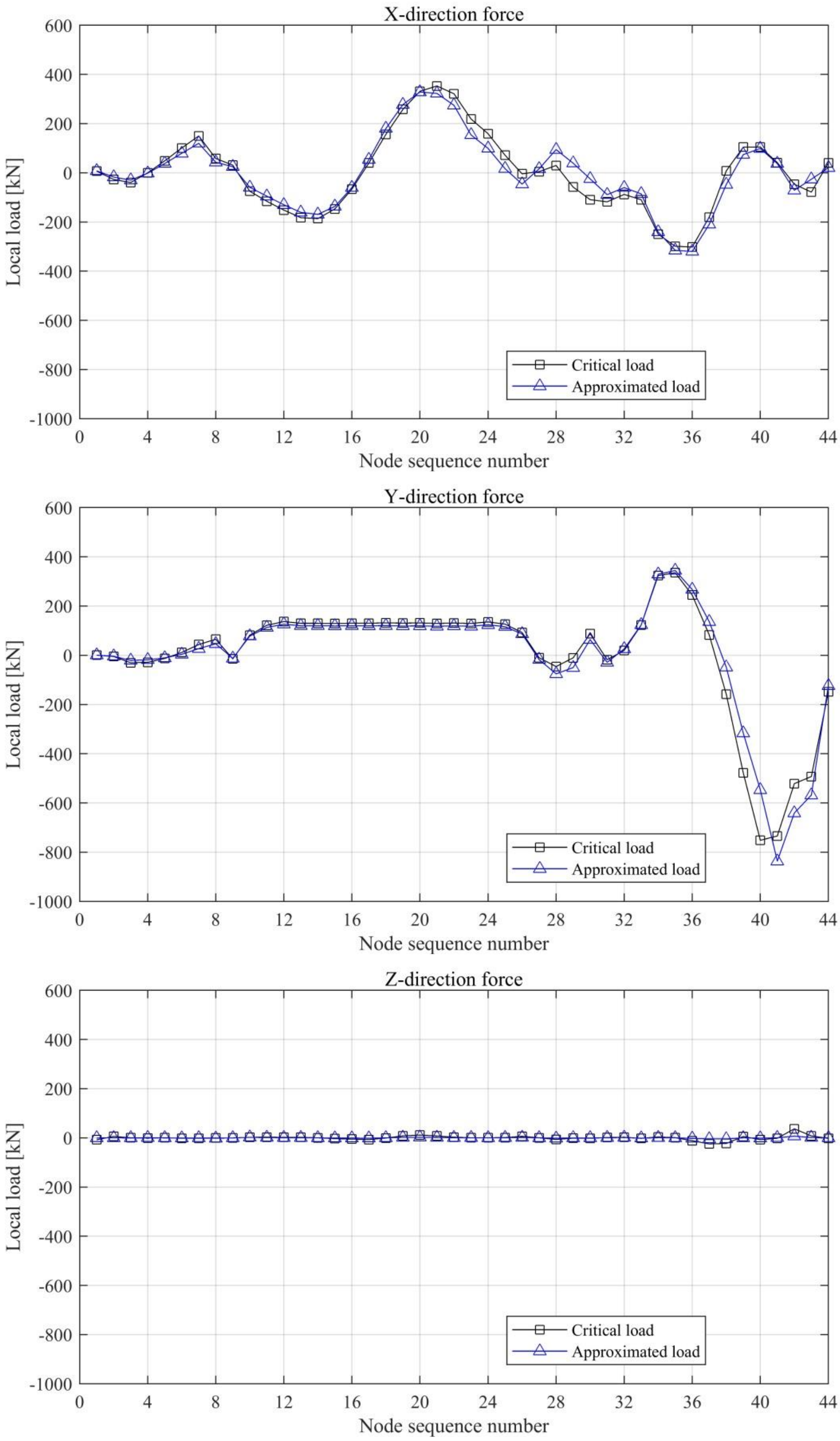

Fig. 45. Local load component plots for the critical load and approximated load at critical step of a bracket girder in the column-pontoon connection structure of tension leg platform.

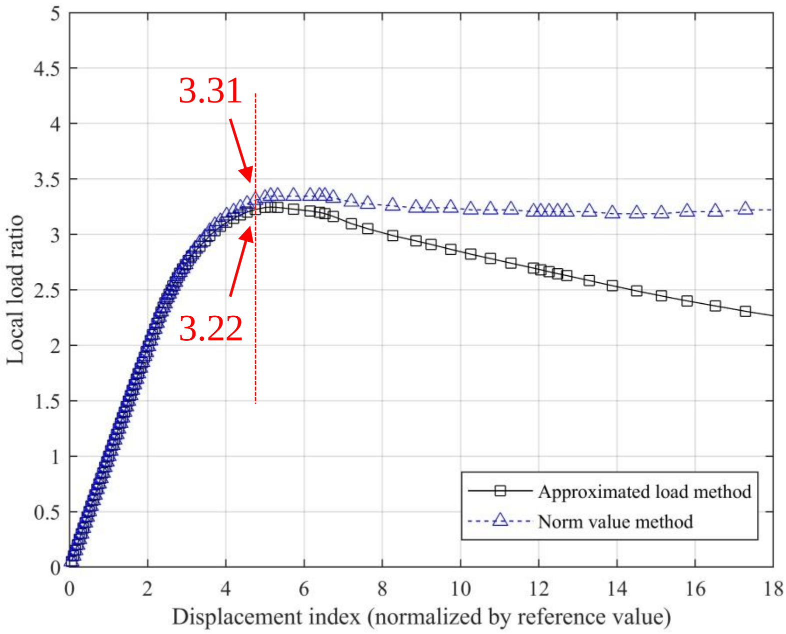

Fig. 46. Local load - displacement index curve of a bracket girder in the column-pontoon connection structure of tension leg platform.

Chapter 5. Computational efficiency

In this Chapter, the nonlinear analysis results for the full domain and reduced domain FE models are reviewed to validate the reliability and applicability of model reduction method. We then apply the model reduction method to evaluating the stability of local structures for two numerical examples. Finally, we check the computation efficiency improvement.

5.1 Reliability and applicability of model reduction method

In general, the finite element model of the global structure has many degrees of freedom, but the local structure may have a relatively a few degree of freedom. In this case, in a computational cost point of view, it is very useful to condense the stiffness for the degrees of freedom except the region of interest using the model reduction method [42], and proceed to perform the nonlinear analysis only for the region of interest as shown in Fig. 47. A condensed stiffness is linear and does not require nonlinear iterations every time, so the computational cost can be greatly reduced.

The static condensation technique is briefly illustrated in the following derivations. The relationship between displacements and loads is shown as the static equilibrium equation;

$$\begin{bmatrix} \mathbf{K}_{11} & \mathbf{K}_{12} \\ \mathbf{K}_{21} & \mathbf{K}_{22} \end{bmatrix} \begin{Bmatrix} \mathbf{U}_1 \\ \mathbf{U}_2 \end{Bmatrix} = \begin{Bmatrix} \mathbf{R}_1 \\ \mathbf{R}_2 \end{Bmatrix}, \tag{20}$$

where $[\mathbf{K}]$ is the stiffness matrix, $\{\mathbf{U}\}$ is the displacement vector, $\{\mathbf{R}\}$ is the load vector, and their subscripts 1 and 2 denote slave (removed) and master (residual) degrees of freedom, respectively.

When the formulation for $\{\mathbf{U}_2\}$ can be derived as

$$\left[-\mathbf{K}_{21}\mathbf{K}_{11}^{-1}\mathbf{K}_{12} + \mathbf{K}_{22}\right]\{\mathbf{U}_2\} = \left\{-\mathbf{K}_{21}\mathbf{K}_{11}^{-1}\mathbf{R}_1 + \mathbf{R}_2\right\}. \tag{21}$$

We can finally derive the stiffness matrix $\left[\bar{\mathbf{K}}\right]$ and load vector $\left\{\bar{\mathbf{R}}\right\}$ regarding residual degrees of freedom of $\left\{\mathbf{U}_2\right\}$;

$$\left[\bar{\mathbf{K}}\right]=\left[-\mathbf{K}_{21}\mathbf{K}_{11}^{-1}\mathbf{K}_{12}+\mathbf{K}_{22}\right], \tag{22a}$$

$$\left\{\bar{\mathbf{R}}\right\}=\left\{-\mathbf{K}_{21}\mathbf{K}_{11}^{-1}\mathbf{R}_{1}+\mathbf{R}_{2}\right\}. \tag{22b}$$

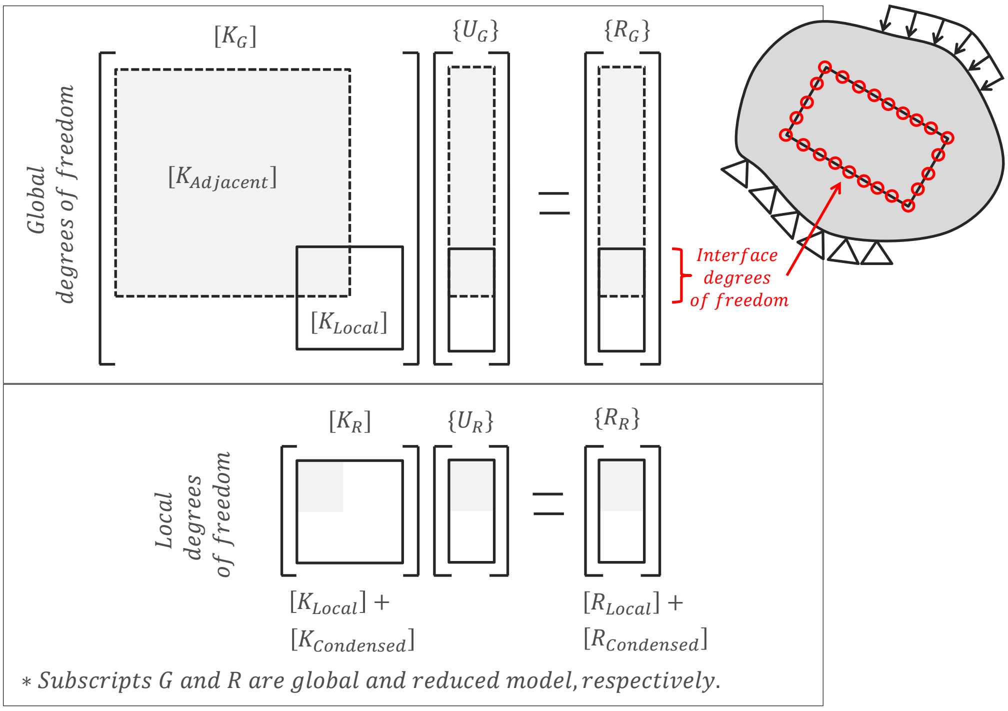

Fig. 47. Schematic of the model reduction method with static condensation for local structural stability evaluation.

The analysis results for load-carrying structures with nonlinear contact and frictional behaviors between large floating offshore structures are reviewed to validate the reliability and applicability of the model reduction method. The evaluation of contact and friction forces on the interface local connections is conducted by performing nonlinear contact analysis considering the local stiffness and geometry. The method is applied to the nonlinear behaviors of following interfaces;

- Vertical and anti-pitch/roll support interfaces between the FLNG hull and independent tank, and
- Stopper-type sea-fastening interfaces between cargo and transportation barge.

The proposed analysis method is a superelement method with a static condensation technique. A superelement is a group of finite elements in which part of the DOF is condensed out. Guyan reduction [43] can be used for the static condensation. The condensation of a large stiffness matrix can also be performed very quickly by applying an automated static condensation algorithm [44].

Verification of the superelement method using gap elements in MSC/NASTRAN [37] is performed. Fig. 48 shows a simple FE model used for verification. Yellow beams are modeled as gap elements. The DOFs in the stiffness matrix of the lower steel box are condensed to the DOF of the gap elements on the lower and external sides, denoted as superelement No. 10. The DOF of the upper steel box are condensed to the DOF of the gap elements on the upper and inner sides, denoted as superelement No. 20. A vertical boundary condition is applied on the lower face of the lower box using a vertical spring to represent restoring behavior in a floating state. The calculated DOF of the full and superelement models are listed in Fig. 48. Anti-pitch supports are named AP1 and AP2, and vertical supports are designated VT1 to VT6, as shown in Fig. 49. The loads applied are gravity and longitudinal inertia load.

Nonlinear analyses of the full FE model and residual gap FE model using superelement method are performed. The static and slip friction coefficient applied is 0.2. The convergence criteria applied are EPSP = 1E-3 (error tolerance for load criterion) and EPSW = 1E-5 (error tolerance for work criterion).

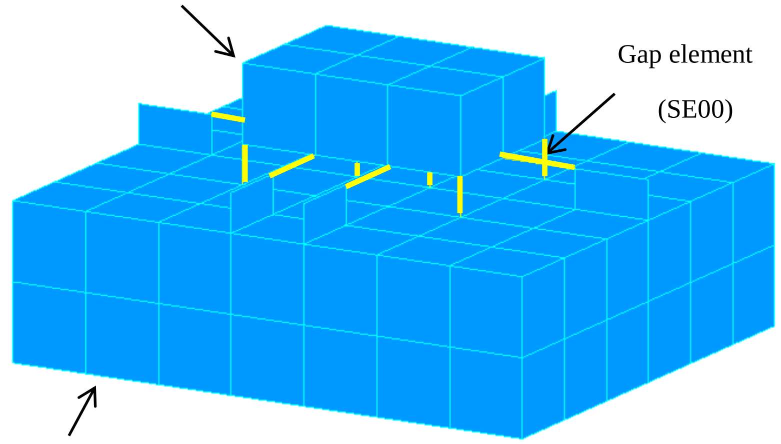

Full FE model degrees of freedom (gap element, lower, and upper steel boxes)		
1,740		
Superelement model degrees of freedom		
Residual (gap element)	Superelement 10 (lower steel box)	Superelement 20 (upper steel box)
144	1,596 (original)	144 (original)
	72 (condensed)	72 (condensed)

Fig. 48. Simple FE model for nonlinear superelement analysis verification.

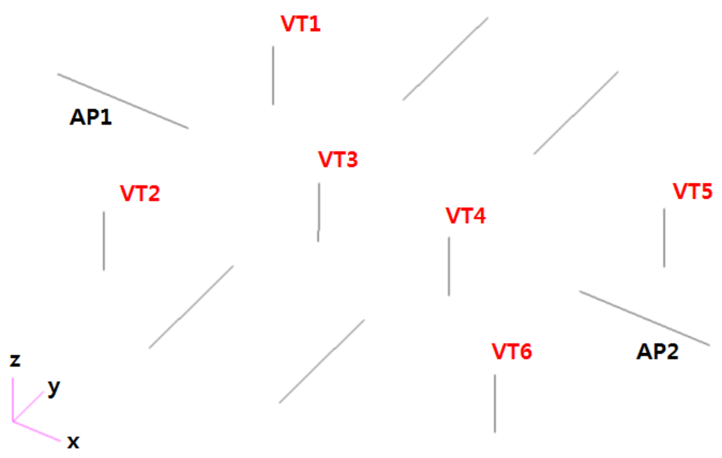

Fig. 49. Notation of gap elements: ant-pitch (AP) and vertical (VT) elements.

Fig. 50 shows that the result of the condensed FE analysis using superelement method coincides with the one from full FE analysis. The direction of contact force is in line with that of the gap element. Friction (I) and (II) forces are in two orthogonal directions of contact force. In this analysis, nonlinear large displacement effects are not considered. Considering the nonlinear large displacement effects, the results can be different according to the rotational displacement level of the upper steel box. It is noted that the proposed procedure is only valid in the case that the relative rotational displacement of the independent object is small.

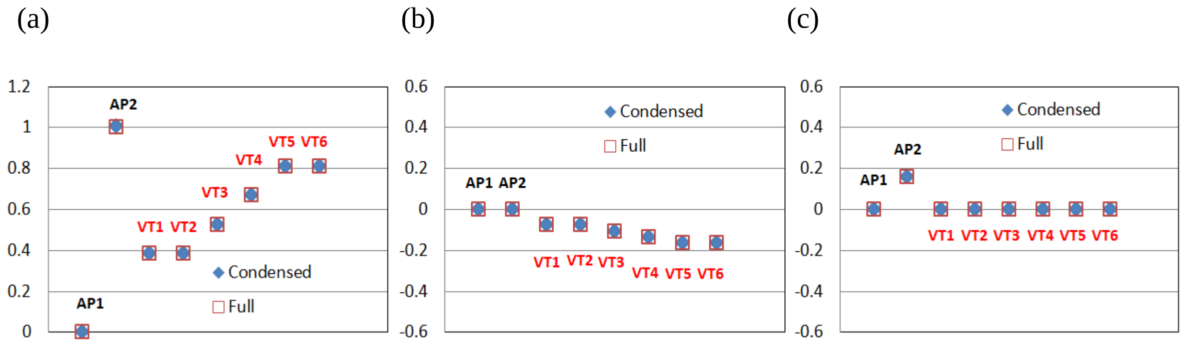

Fig. 50. Normalized contact and friction force comparison between full FE model and condensed FE model using the proposed superelement method (static and slip friction coefficient = 0.2, convergence criteria: EPSP = 1E−3 and EPSW = 1E−5); (a) contact force, (b) friction(i) force, and (c) friction(ii) force.

APPLICATION I: FLNG INDEPENDENT CARGO TANK

Membrane type CCS (Cargo Containment System) for LNG (Liquefied Natural Gas) storage is widely used in LNG carriers and FLNG (Floating Liquefied Natural Gas) projects. The sloshing impact pressure is one of most critical design loads for the CCS, and many structural issues induced by the sloshing still remain to the present. To reduce sloshing related issues, another type of CCS which names as independent type B prismatic tank system is being tried for application to FLNG in a FEED (Front-End Engineering and Design) project. From a structural safety point of view, independent tank supports are critical areas because they are load-carrying members; so the reliable evaluation of the structural strength of the tank supports is required.

Classification Societies [45-48] have proposed applicable evaluation procedures in consideration of the use of friction coefficients with nonlinear contact behaviors of interface areas of the supports. Fig. 51(a) shows the example of cargo tank supports for vertical and anti-roll. The vertical and anti-pitch supports are generally arranged on inner bottom of the hull, and anti-roll supports are arranged along the tank centerline at the top and bottom of the hull. Contact and friction forces act on interface areas between the tank and hull where the tank contacts the supports, as shown in Figs. 51(b) and 51(c). In this support configuration, the characteristics of the frictional behavior of their contact, including the initial gap on supports and static dead loads, result in very complex effects on the support structures.

(a)

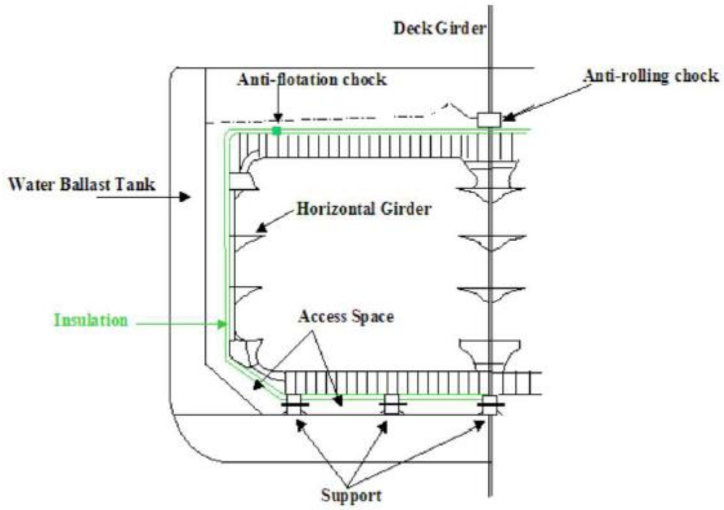

(b)

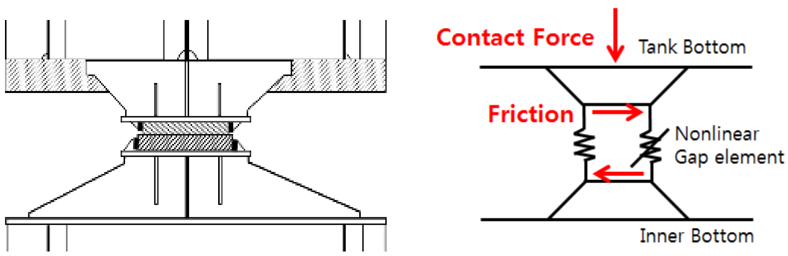

(c)

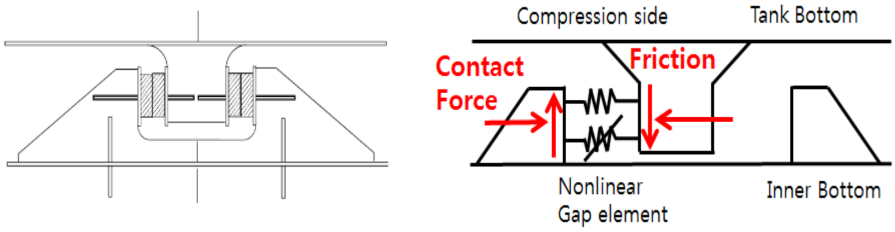

Fig. 51. Example of independent cargo tank supports [47]: (a) the mid ship section, (b) the vertical support model and (c) the anti-roll and anti-pitch support models.

In this study, a two-row independent tank type FLNG is considered for evaluation of tank supports. From the hydrodynamic analysis, the hydrodynamic pressure and inertia load RAOs (Response Amplitude Operators) are generated. Fig. 52 shows the generated hydrodynamic pressure RAO on the internal tank and external surface at a certain wave frequency. For the hydrodynamic load generation, a representative sea state of the Pierson-Moskowitz wave spectrum (significant wave height of 5 m and peak period of 10.5 s) is selected, which corresponds to a 100-year return period maximum level in Southeast-Asia gas fields. The irregular hydrodynamic pressure and inertia loads are generated by superposition of regular load RAOs, at all-time instants during 300 s, with intervals of 0.5 s only for the applicability check of the proposed method.

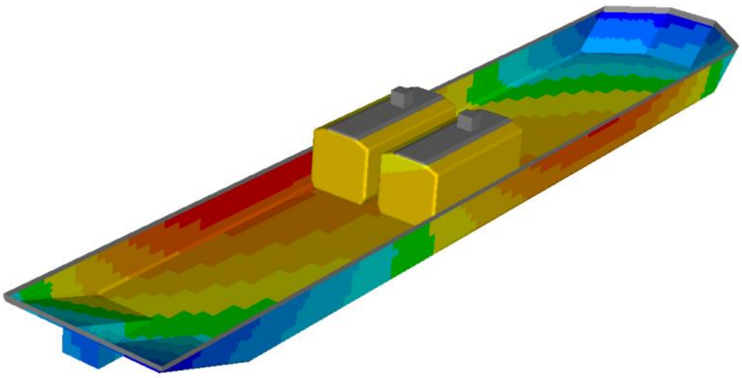

Fig. 52. Hydrodynamic and internal tank pressure RAO (LNG tank fully-loaded condition, quartering sea, ω= 0.398).

Table 3. Stiffness matrix sizes (degrees of freedom) of full and superelement models for FLNG independent cargo tank.

Full FE model degrees of freedom (gap element, LNG tank, and hull)		
2,729,646		
Superelement model degrees of freedom		
Residual (gap element)	Superelement 10 (starboard LNG tank)	Superelement 20 (hull)
1,728	94,014 (original)	2,635,632 (original)
	864 (condensed)	864 (condensed)

The DOF in the stiffness matrix of the starboard tank are condensed to the DOF of the gap elements on the tank side, which is denoted as superelement No. 10. The other adjacent hull structure is condensed to the DOF of the gap elements on the hull side, which are denoted as superelement No. 20. The loads generated are condensed to the DOF of both end nodes of the gap elements in the same manner used for the stiffness matrix. The solving of the residual gap elements is performed with condensed stiffness matrices and local loads. The calculated DOF of the full and superelement models are listed in Table 3; those of the full matrix are about 2.7 million. On the other hand, after applying the condensation technique, the matrix size is dramatically reduced to 864.

The static and slip friction coefficient applied is 0.2, and the stiffness of gap elements are appropriately estimated to represent the stiffness of the inserted wood and local steel support structure. It is noted that the values applied for the coefficients and stiffness are selected as appropriate for the feasibility check of the proposed procedure.

Figs. 53 and 54 show the critical support locations where the highest contact forces occur. All the critical support locations are at corners, in the case that the stiffness of all the supports are the same. In an actual design, stiffness optimization is required according to the location of each support. Figs. 55 to 58 show the normal contact force distributions, which are the maximum values during 300 s of simulation.

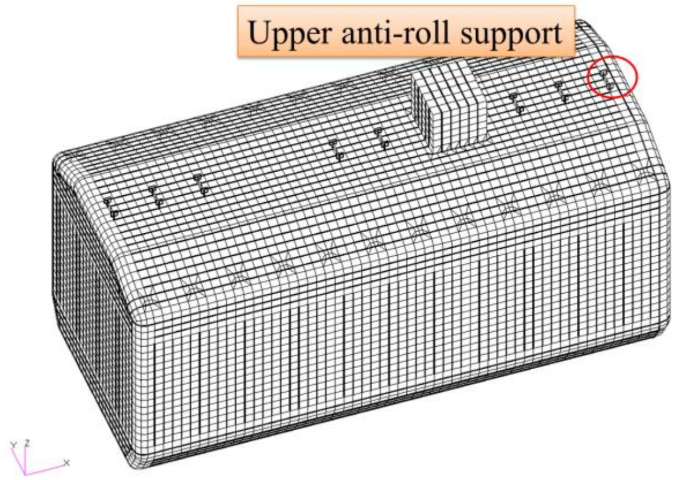

Fig. 53. Considered anti-roll support location in a starboard side tank.

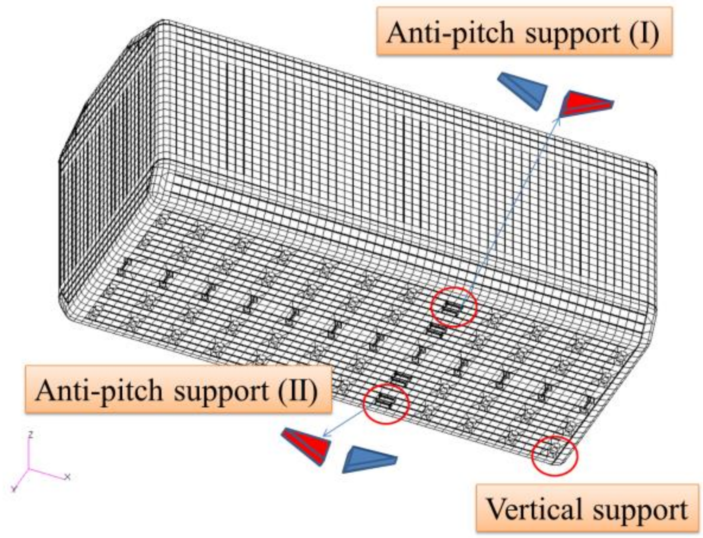

Fig. 54. Considered anti-pitch and vertical support locations in a starboard side tank.

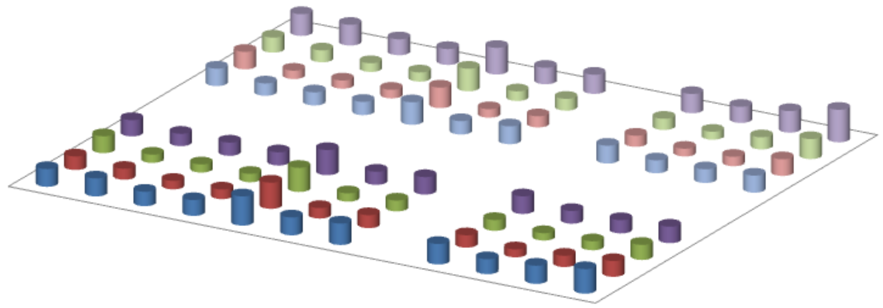

Fig. 55 Maximum vertical contact forces on vertical support (static and slip friction coefficient = 0.2, convergence criteria: EPSP = 1E−3 and EPSW = 1E−5).

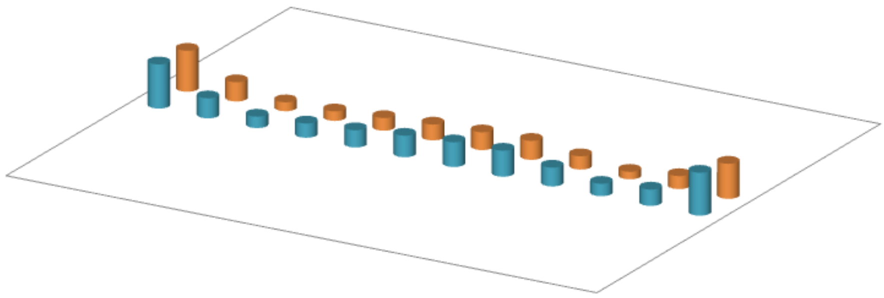

Fig. 56. Maximum transverse contact forces on lower anti-roll support (static and slip friction coefficient = 0.2, convergence criteria: EPSP = 1E−3 and EPSW = 1E−5).

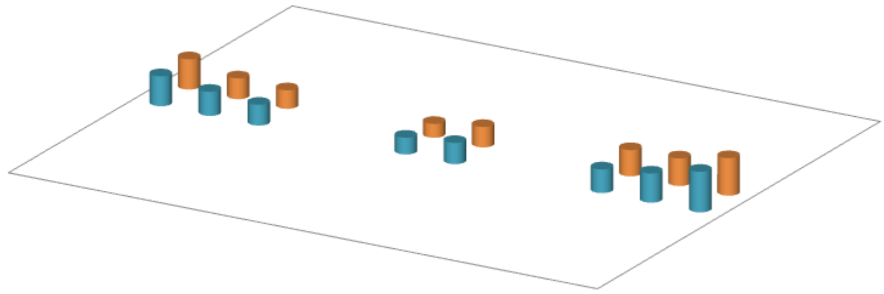

Fig. 57. Maximum transverse contact forces on upper anti-roll support (static and slip friction coefficient = 0.2, convergence criteria: EPSP = 1E−3 and EPSW = 1E−5)

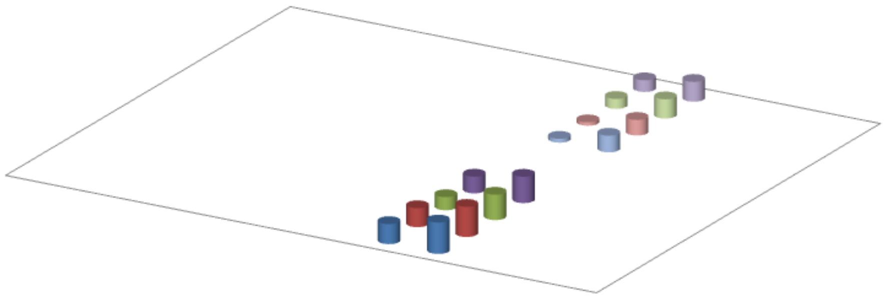

Fig. 58. Maximum longitudinal contact forces on anti-pitch support (static and slip friction coefficient = 0.2, Convergence criteria: EPSP = 1E−3 and EPSW = 1E−5).

The effects of the sensitivity of friction coefficient values between zero and 0.2 on the resultant contact forces are compared. Table 4 shows the top three maximum values among the specified support locations in Figs. 53 and 54, during 300 s of simulation. The contact forces assuming friction (coefficient = 0.2) are smaller than when there is no friction, and the ratios are from 89.77 to 98.80 % for vertical and upper anti-roll support. In case of anti-pitch support, the two supports considered show different tendencies. Anti-pitch support (II) shows very large differences compared to anti-pitch support (I). The maximum contact forces with friction are smaller than the ones with no friction, and the ratios are very low (21.69 to 26.75%) for anti-pitch support (II). The reason is that adjacent vertical supports in the lower hull non-symmetrically resist longitudinal inertia loads as substantial friction, when friction is considered. It is found that adequate friction has to be considered in the nonlinear analysis to obtain reliable contact forces on the anti-pitch supports.

Table 4. Contact forces and their ratios on tank supports: friction sensitivity check for friction coefficients of zero and 0.2.

Friction coefficient	Vertical support			Upper anti-roll support		
	1st Max	2nd Max	3rd Max	1st Max	2nd Max	3rd Max
Zero	1.0000	0.9390	0.8957	1.0000	0.8624	0.7567
0.2	0.9869	0.9220	0.8850	0.9407	0.7842	0.6792
0.2 / Zero	98.69%	98.19%	98.80%	94.07%	90.93%	89.77%
Friction coefficient	Anti-pitch support (I)			Anti-pitch support (II)		
	1st Max	2nd Max	3rd Max	1st Max	2nd Max	3rd Max
Zero	1.0000	0.8325	0.6903	1.0000	0.8647	0.7855
0.2	1.0258	0.9892	0.8229	0.2675	0.1745	0.1704
0.2 / Zero	102.58%	118.83%	119.20%	26.75%	20.19%	21.69%

Note
1) Force is normalized by each 1st maximum value for friction coefficient of zero
2) Convergence criteria: EPSP = 1E−3 and EPSW = 1E−5

APPLICATION II: OFFSHORE DRY TRANSPORTATION

Recently, large offshore structures are frequently transported while loaded on transportation barges (i.e., dry transportation). Compared with wet towing, the load applied to the cargo structure is smaller because it does not directly encounter wave loads. In terms of transportation cost, it is advantageous because the transportation period is relatively short due to faster towing speed, compared to wet towing. To secure the cargo structure during dry transportation, sea-fastening designs should be considered. Conventionally, an offshore jacket or topside platform structure is often dry-transported. The design of sea-fastening can be conducted by hand calculation or spread sheet because of the simple point contacts between the framed cargo structure and the barge. However, in recent years, plated structures such as FPU (floating production unit), cylindrical FPSO (floating production storage and offloading), and Spar hull are also being dry-transported. Because of the surface contact between the plated cargo structure and the transportation barge, the friction between them should definitely be considered in the sea-fastening design. Friction force depends on the global and local structural deformation of the contact areas. The mutual contact and frictional behaviors of a complex plated structure cannot be determined using simple calculations, but can be evaluated by performing nonlinear FE analysis.

An offshore dry transportation analysis is performed as a second application in this section. Fig. 59 shows the FE model of dry transportation. The model includs a cargo structure, wedge-type large auxiliary structures, cribbing wood, and the transportation barge. Fig. 60 shows the detailed view of the gap elements, longitudinal and transverse stoppers for two representative areas. The analysis consists of two similar load cases that include static gravity, hydrodynamic inertia load, and external pressures. Fig. 61 shows the deformed shape of full-ship nonlinear FE analysis, considering horizontal contact behavior with gap elements, for a specific load case. The cargo is overhung in the longitudinal direction. It is expected that longitudinal friction is considerable from the deformed shape; however, the vertical cribbing wood is not expected to be slip, and was linearly modeled. This is because the applied horizontal inertia load of the overall cargo is less than the overall horizontal friction in this study.

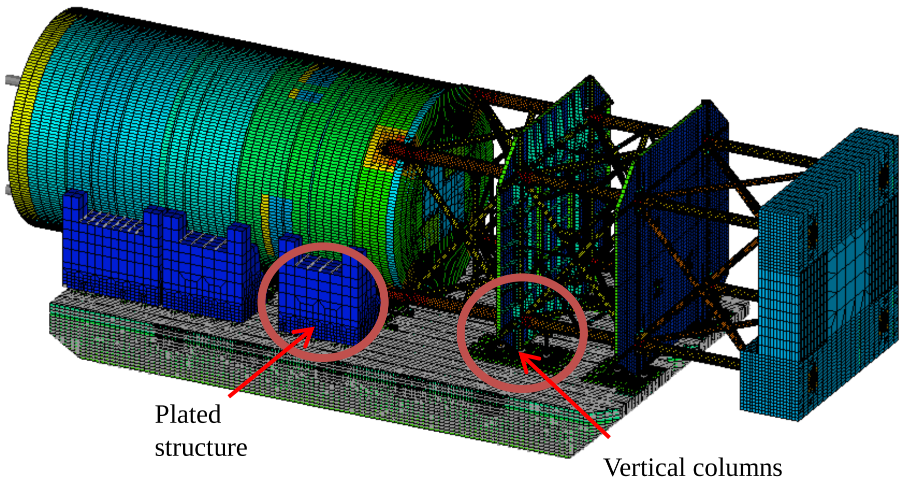

Fig. 59. Overall FE model of dry transportation.

(a)

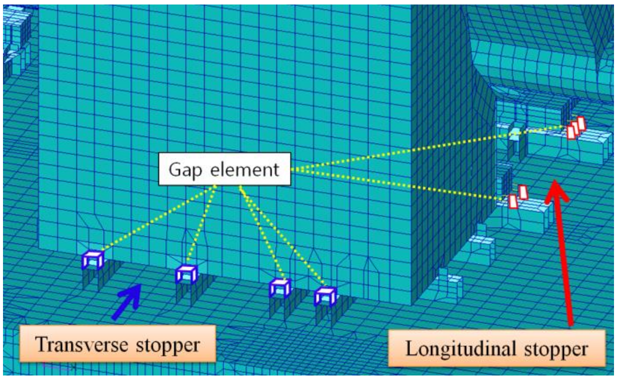

(b)

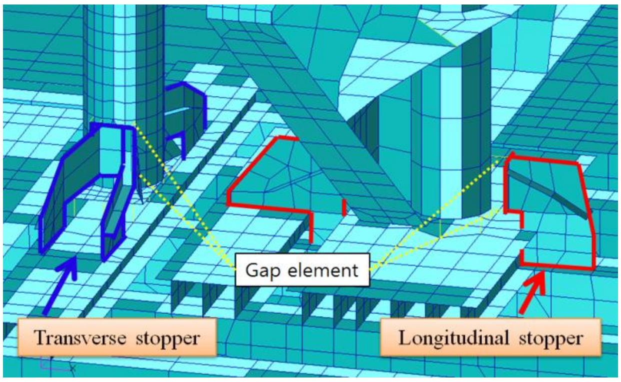

Fig.60. Detailed view of sea-fastening stopper and gap elements between cargo and transportation barge: (a) plated structure and (b) vertical columns.

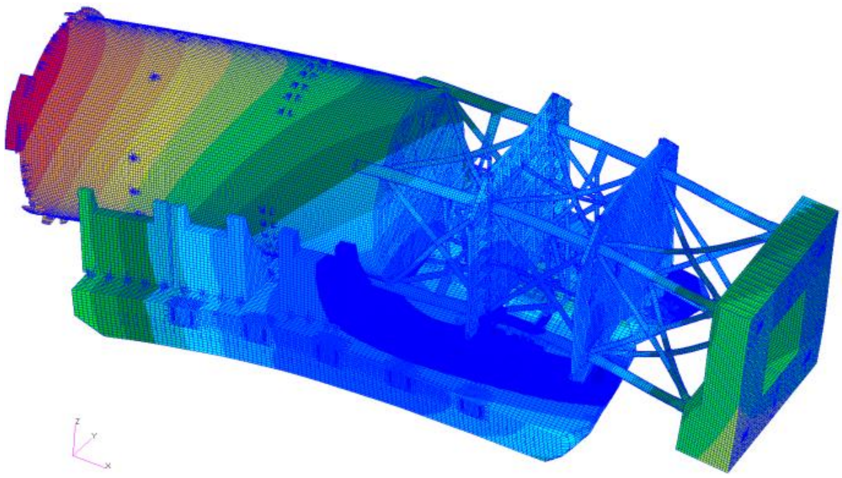

Fig.61. Deformed shape of dry transportation model for load case 2.

The superelement analysis is performed in the same manner as for the FLNG independent tank support. Gap elements on the horizontal stoppers are assigned residual DOF and all the other elements of cargo, auxiliary, and barge structures are considered to remove DOF. The sizes of the matrices considered (for DOF) of a full FE model and reduced model, are shown in Table 5.

Table 5. Stiffness matrix sizes (degrees of freedom) of full and superelement models for dry transportation.

<table>
<tr><th colspan="2">Full FE model
(gap element, cargo, and barge)</th></tr>
<tr><td colspan="2">3,067,356</td></tr>
<tr><td colspan="2">Superelement model</td></tr>
<tr><td>Residual
(gap element)</td><td>Superelement 10
(cargo and barge)</td></tr>
<tr><td rowspan="2">1,968</td><td>3,067,356 (original)</td></tr>
<tr><td>1,968 (condensed)</td></tr>
</table>

The validity of the proposed superelement analysis is checked as shown in Table 6. The static and slip friction coefficient applied is 0.2, and the stiffness of gap elements are appropriately estimated to represent the stiffness of the local steel stopper structure. The maximum contact forces are compared with the ones from full FE analysis for two load cases. The largest difference in the contact forces is just 2.63E-6, i.e., nearly negligible, at a longitudinal stopper. A comparison of computing time is shown in Table 7. The processor of the computer used was a GenuineIntel / 1699 MHz. The full FE analysis of 3.1 million of DOF for the two load cases studied, required 13.67 h. However, the superelement analysis for 1,968 DOF requires only 43 s. Prior to this, pre-processing time of 7.25 hours is required for stiffness and load condensation. If a large number of load cases are considered to obtain load responses against fatigue load time history, the efficiency of the proposed calculation approach will be very high compared to full FE analysis.

Table 6. Comparison of maximum contact forces of full and superelement analysis for dry transportation.

Load Case	Location	Full FE *	Superelement *	Difference ratio
1	Longitudinal stopper	1.0	1.0	0
	Transverse stopper	1.0	1.00000263	2.63E-6
2	Longitudinal stopper	1.0	1.0	0
	Transverse stopper	1.0	1.0	0

Note
1) * Contact force is normalized by each full FE analysis result
2) Static and slip friction coefficient = 0.2
3) Convergence criteria: EPSP=1E-3 and EPSW=1E-5

Table 7. Comparison of computing time of full and superelement nonlinear analysis for dry transportation.

Full FE	Superelement	
Iterative solving	Static condensation	Iterative solving
13.67 hours	7.25 hours	43 seconds

Note
1) System: GENUINEINTEL / 1699MHZ / RAM 62GB
2) Platform: INTEL LINUX 2.6.16.60-0.21
3) Static and slip friction coefficient = 0.2
4) Convergence criteria: EPSP=1E-3 and EPSW=1E-5

The accuracy and computing cost of the proposed superelement analysis method were investigated for use in time consuming analysis. By applying the model reduction method, we confirmed that the contact behavior and the friction effect were well-reflected.

In the FLNG independent cargo tank support analysis case, the sensitivity of the friction effect of supports was investigated. If friction was considered (friction coefficient = 0.2), the maximum contact forces decreased to about one-quarter or one-fifth of the ones for no friction case, for a certain anti-pitch support. The friction at the contact interface seriously affected the magnitude of contact force according to the support location. Therefore, adequate friction had to be considered to obtain reliable contact forces on the independent tank supports.

In the case of contact force, accuracy was guaranteed with 2.63E-6 of error ratio, which was observed in the dry transportation load cases considered. Superelement analysis could reliably be considered to reflect both global and local behaviors. The full FE analysis considered millions of DOF while superelement analysis considered only thousands of DOF. In terms of calculation efficiency, full ship FE analysis required 13.67 h and superelement analysis required only 43 s, aside from the static condensation work.

In the nonlinear large displacement problem, the accuracy of nonlinear contact results might be reduced because the condensed stiffness matrix was not updated along with the variation of stiffness induced by geometric nonlinearity. The result was valid for the calculation of small displacement problems.

Many load cases needed to be considered during structural design. Occasionally, full ship FE analyses were required to evaluate the global structural strength. When repeated analyses were required due to design changes during actual offshore project design development, nonlinear full ship analysis was not applicable. From this study, however, it was found that the proposed superelement analysis with static condensation was quite applicable for a particular nonlinear contact problem, and had the advantage of short calculation time.

5.2 Comparisons with reduced domain analyses

In this section, the structural stability is evaluated by the reduced model analysis for the two examples in Chapter 4, and compared with the results of the full domain analysis.

5.2.1 Horizontally stiffened cylindrical structure with radial bulkheads

We evaluate the structural stability by applying the model reduction method for the local stringer part considered in section 4.3. Two cases are evaluated for different ranges of nonlinear analysis. The one is the stringer region of interest, and the other is the extended range of the stringer with adjacent bulkheads in order to improve the accuracy of the analysis result. The stiffness of all other areas except the selected area is condensed. The model reduction method uses both the stiffness of the part of interest and the condensed stiffness of the other part.

The structural stability is also evaluated by applying linear increment of initial prescribed displacement, which is commonly applied in previous studies [35, 36]. The prescribed displacement analysis method uses only a stiffness of the part of interest. In this way, the results of the model reduction and prescribed displacement cases are compared with the full domain analysis in this section.

As shown in Fig. 62, the nonlinear analysis is performed only for the stringer region of interest with the model reduction of the other region. In addition, the analysis is performed by incrementing prescribed displacement at the initial reference load application. Fig. 63 shows the extended nonlinear analysis domain with the extended model reduction.

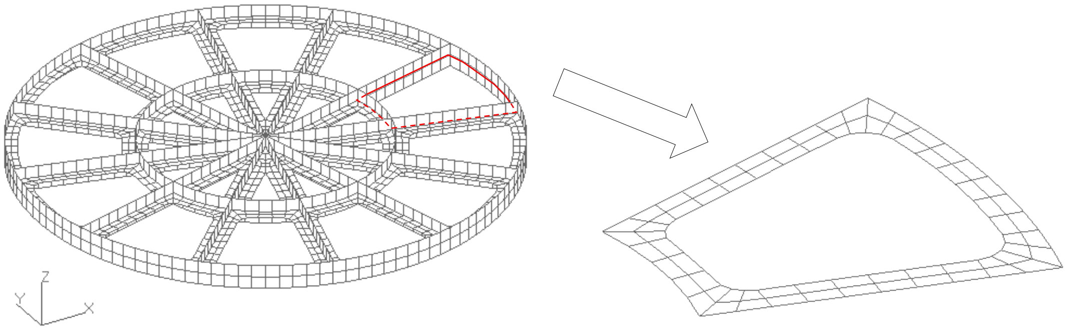

Fig. 62. Nonlinear analysis domain of a stringer of a horizontally stiffened cylindrical structure with radial bulkheads for model reduction and prescribed displacement analysis.

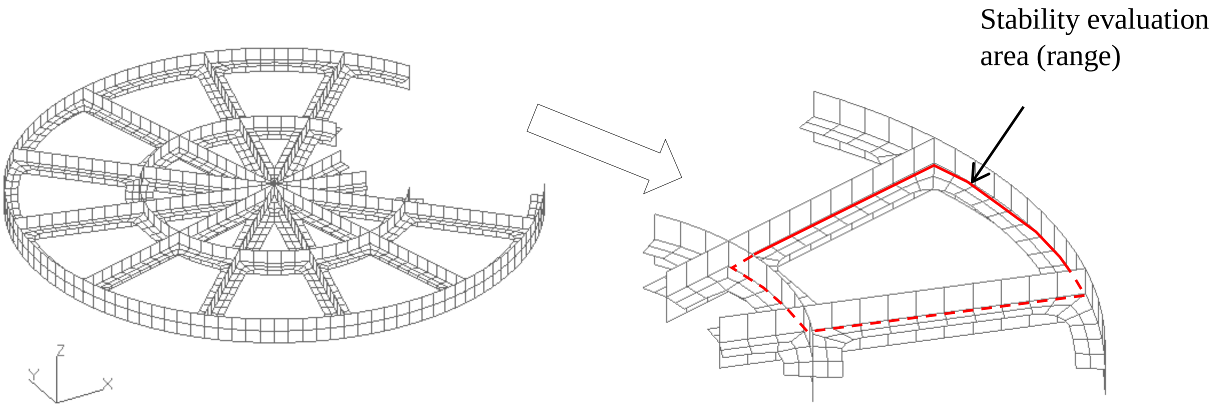

Fig. 63. Nonlinear analysis domain of the extended stringer of a horizontally stiffened cylindrical structure with radial bulkheads for extended model reduction.

The second variations of the local strain energies for model reduction, extended model reduction and prescribed displacement cases are plotted in Figs. 64 to 66. The stability limit is determined by the sign of the second variation of the local strain energy. Fig. 67 shows local load ratio - displacement index curve for full model analysis, model reduction analysis and prescribed displacement analysis by the approximated load method. Figs. 68 to 70 show the local load component plots for the critical load and approximated load at critical step of local structures for model reduction, extended model reduction and prescribed displacement cases. The local safety factors are listed in Table 8 and Fig. 71. Considering the result of full model analysis as a reference value, the error of model reduction result is calculated as 8%, but in the case of extended model reduction, it is reduced to -3%. The error of prescribed displacement analysis result is calculated as 16%.

Fig. 72 shows local load component plots for the critical load and approximated load at critical step for all analyses. Table 9 and Fig. 73 show the standard errors of the local load distributions compared to the one of the full model analysis. The smallest value is 42 kN which is the standard error of the extended model reduction result at maximum local load ratio. In other words, it can be said that the local load distribution of the extended model reduction case is most similar to full model analysis. The prescribed displacement analysis shows large error value as 195 kN. When we consider the computing cost, the extended model reduction case is the best way to represent the local load distribution among the reduced domain analysis cases.

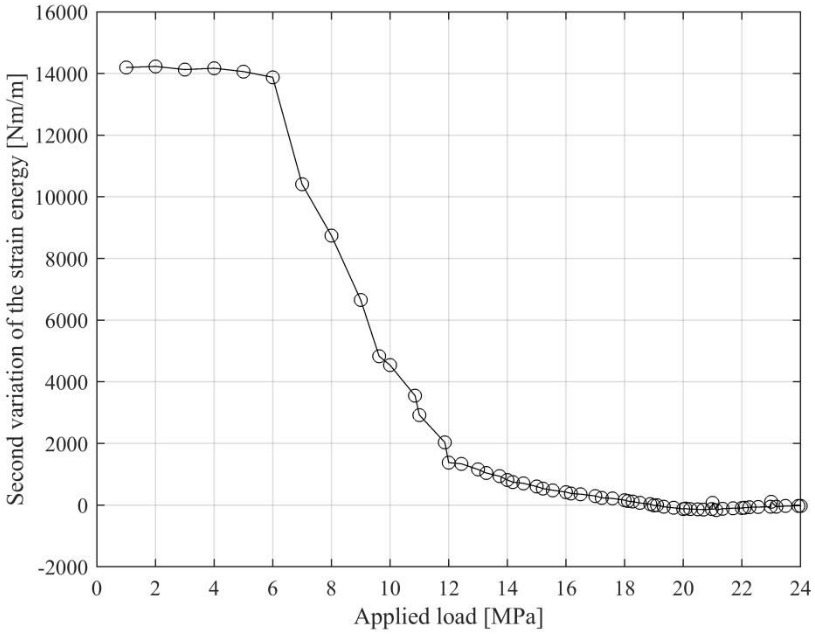

Fig. 64. Second variation of strain energy in local domain of a horizontally stiffened cylindrical structure with radial bulkheads for model reduction case.

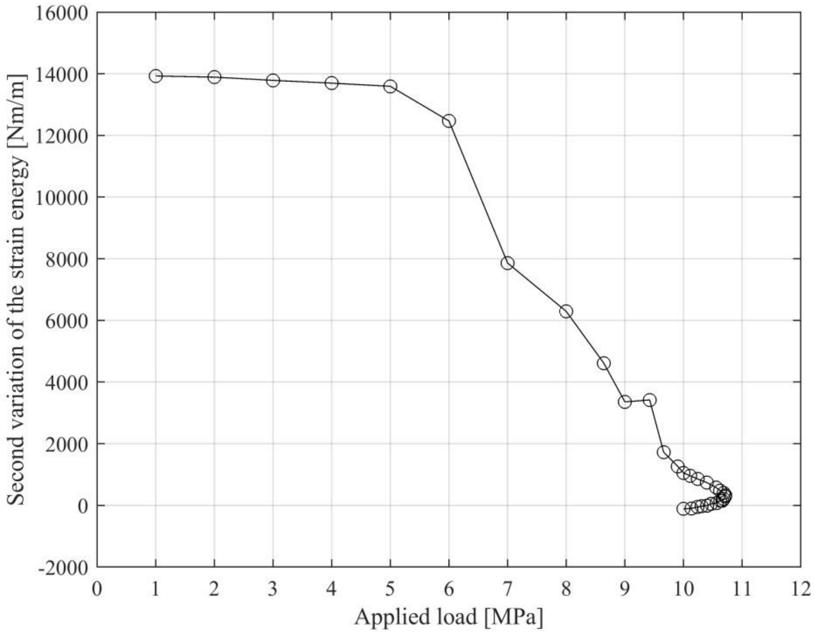

Fig. 65. Second variation of strain energy in local domain of a horizontally stiffened cylindrical structure with radial bulkheads for extended model reduction case.

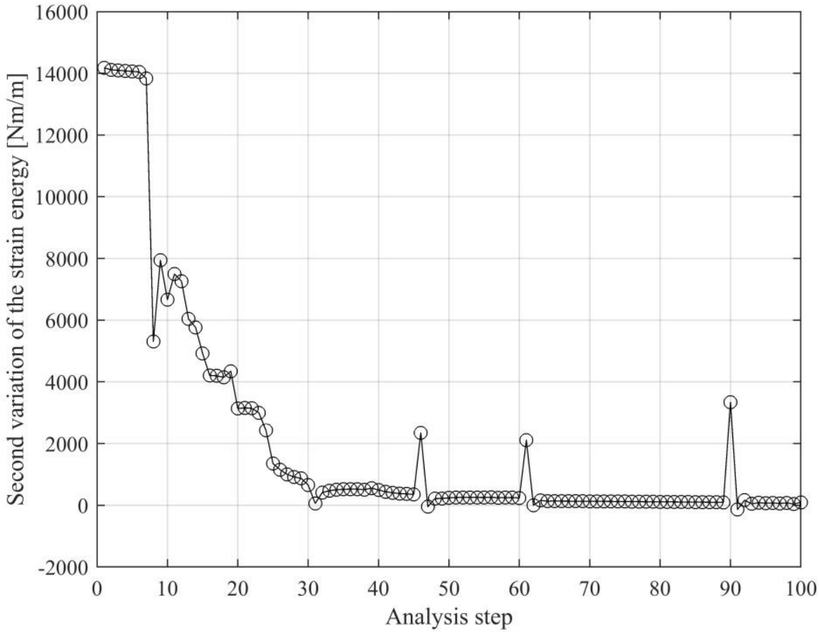

Fig. 66. Second variation of strain energy in local domain of a horizontally stiffened cylindrical structure with radial bulkheads for prescribed displacement case.

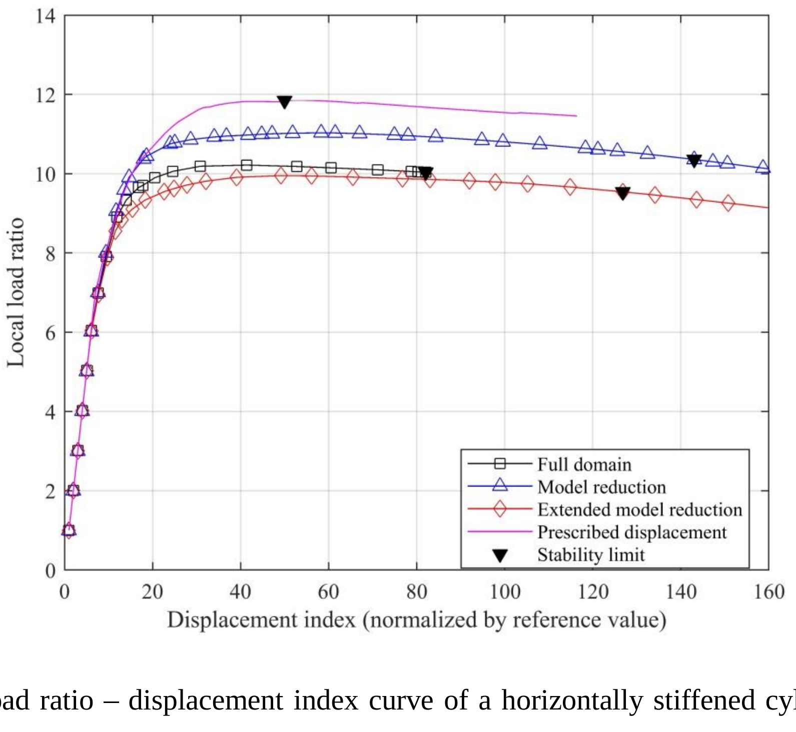

Fig. 67. Local load ratio – displacement index curve of a horizontally stiffened cylindrical structure with radial bulkheads for all analysis cases.

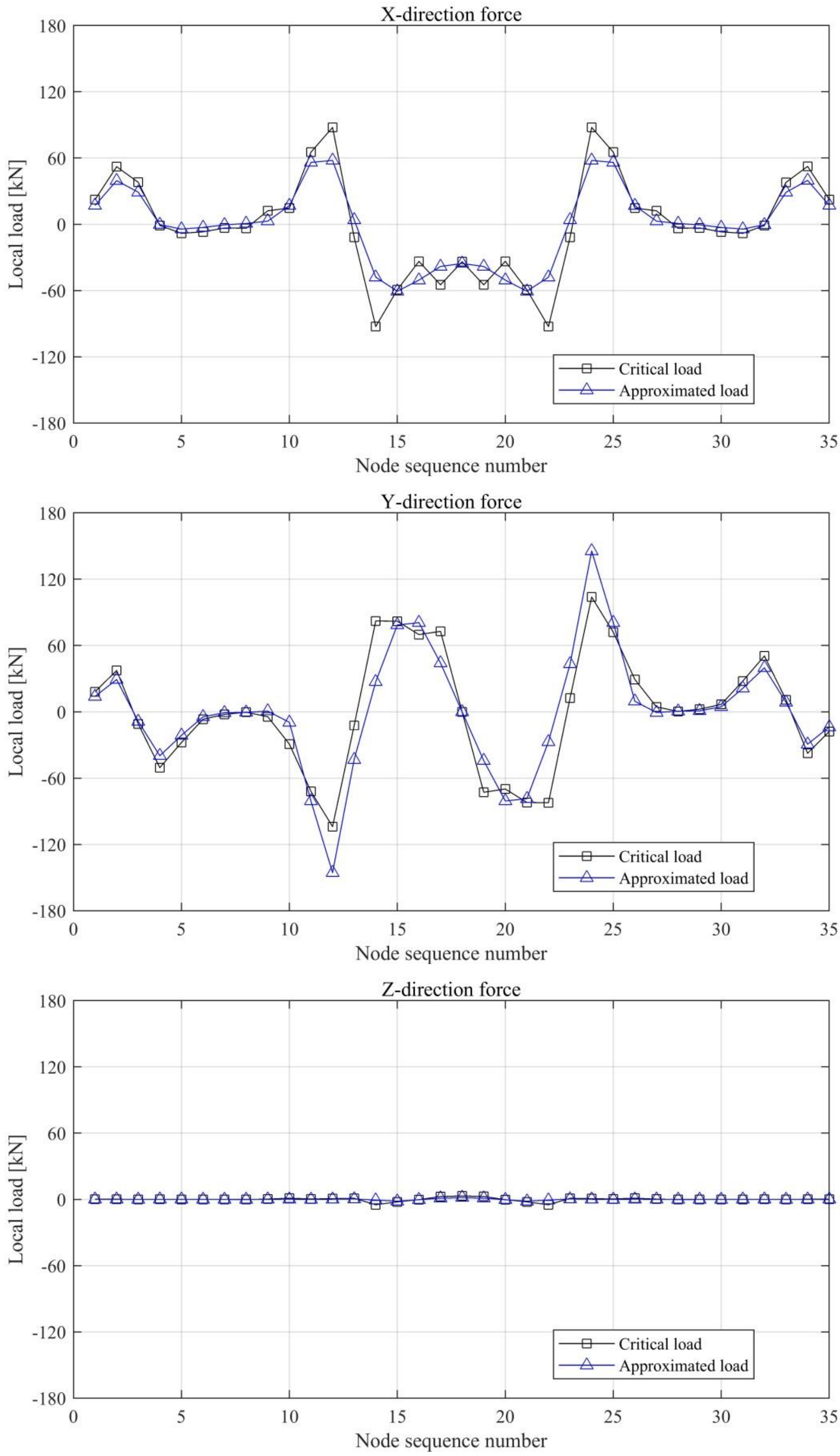

Fig. 68. Local load component plots for the critical load and approximated load at critical step of a horizontally stiffened cylindrical structure with radial bulkheads for model reduction case.

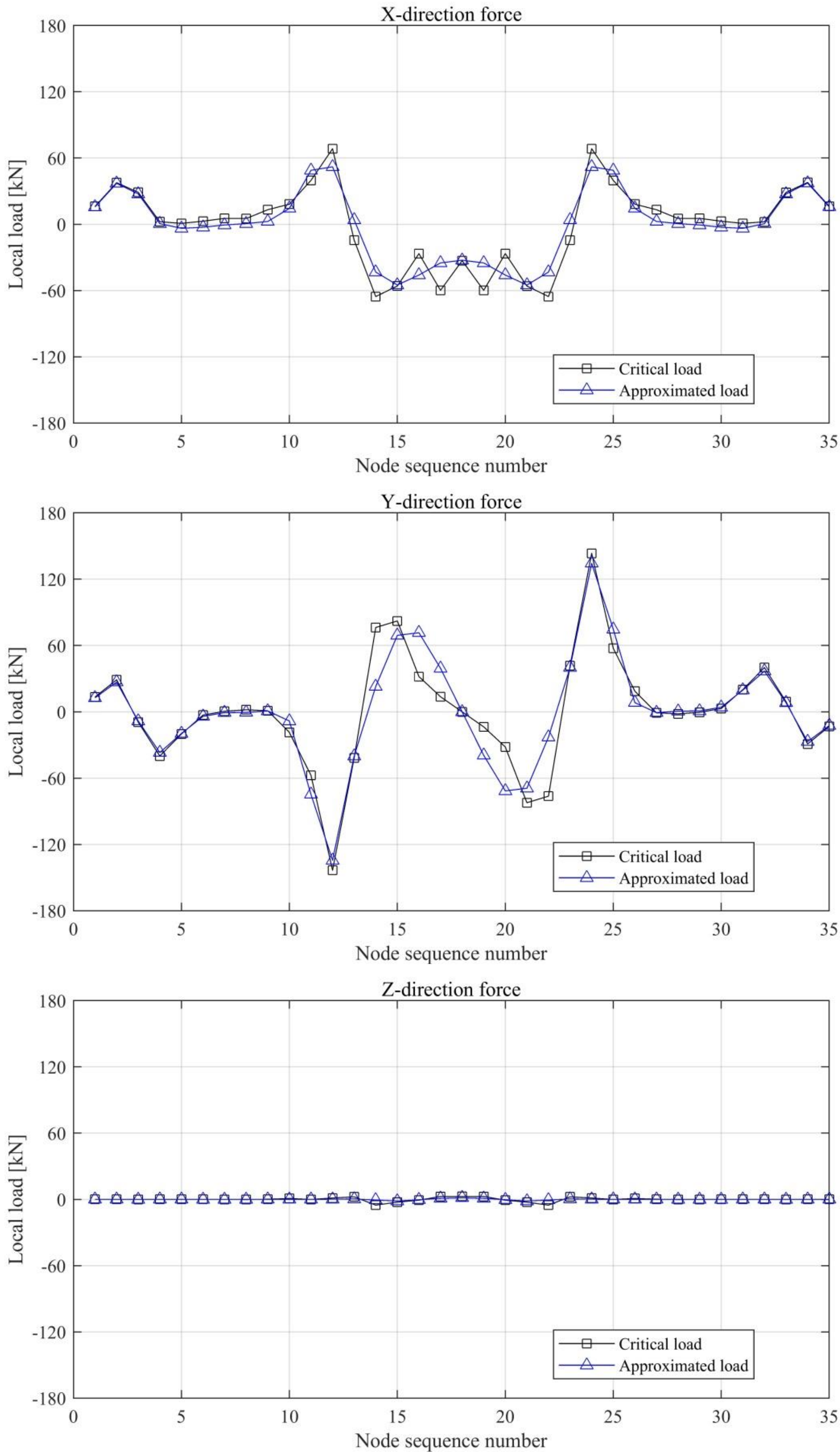

Fig. 69. Local load component plots for the critical load and approximated load at critical step of a horizontally stiffened cylindrical structure with radial bulkheads for extended model reduction case.

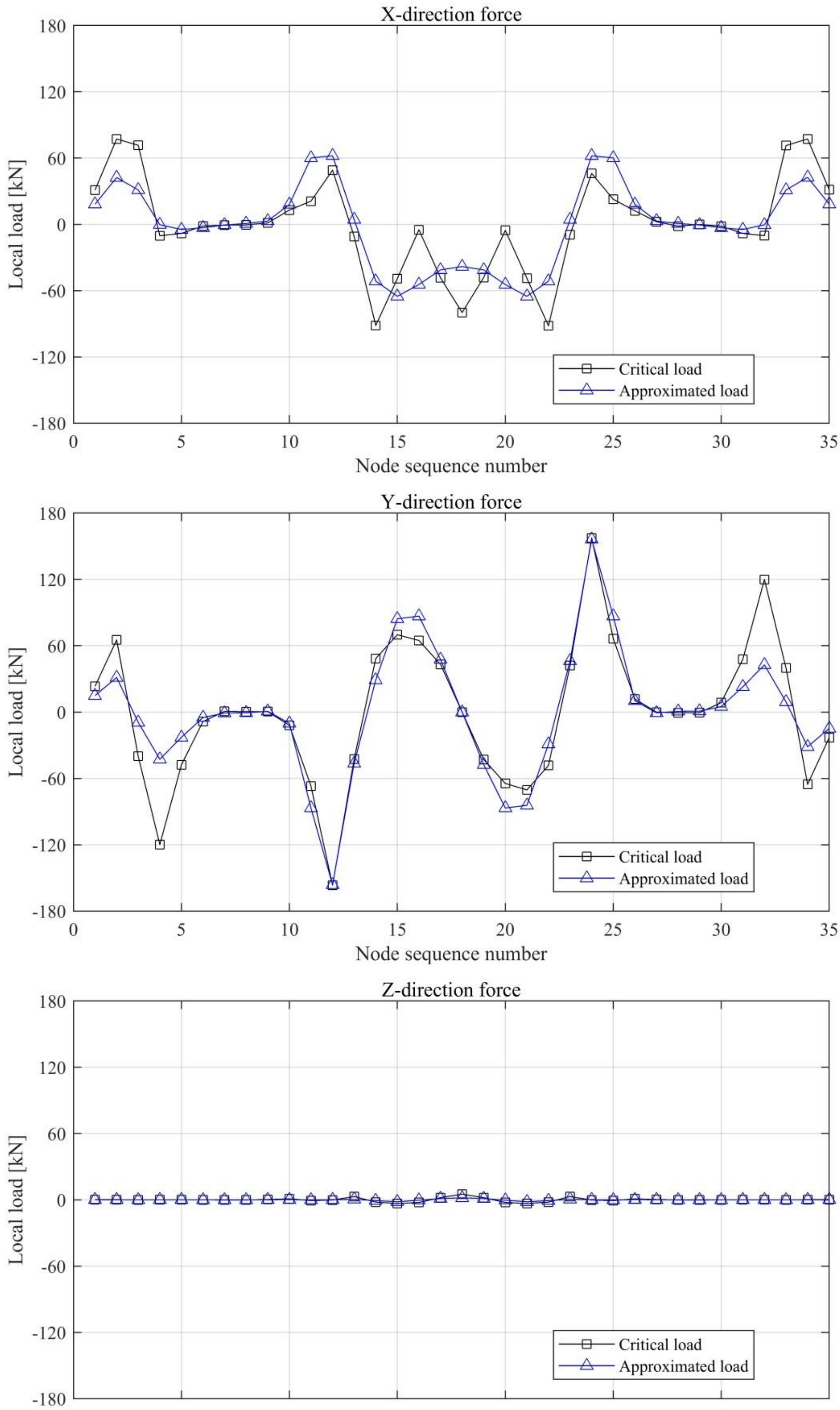

Fig. 70. Local load component plots for the critical load and approximated load at critical step of a horizontally stiffened cylindrical structure with radial bulkheads for prescribed displacement case.

Table 8. Local safety factors (LSF) of a horizontally stiffened cylindrical structure with radial bulkheads for all analysis cases.

	Full domain	Model reduction	Extended model reduction	Prescribed displacement
LSF	10.22	11.03	9.95	11.84
Normalized LSF	1.00	1.08	0.97	1.16

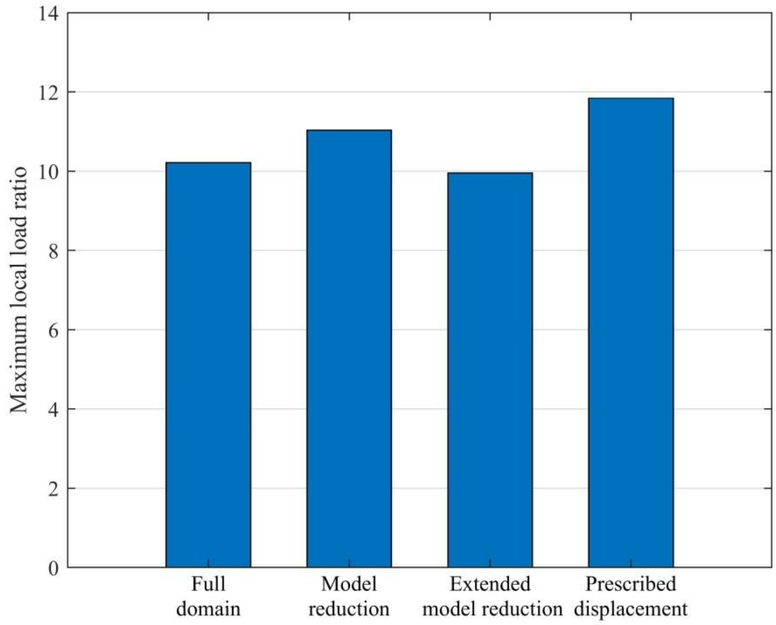

Fig. 71. Local safety factors of a horizontally stiffened cylindrical structure with radial bulkheads for all analysis cases.

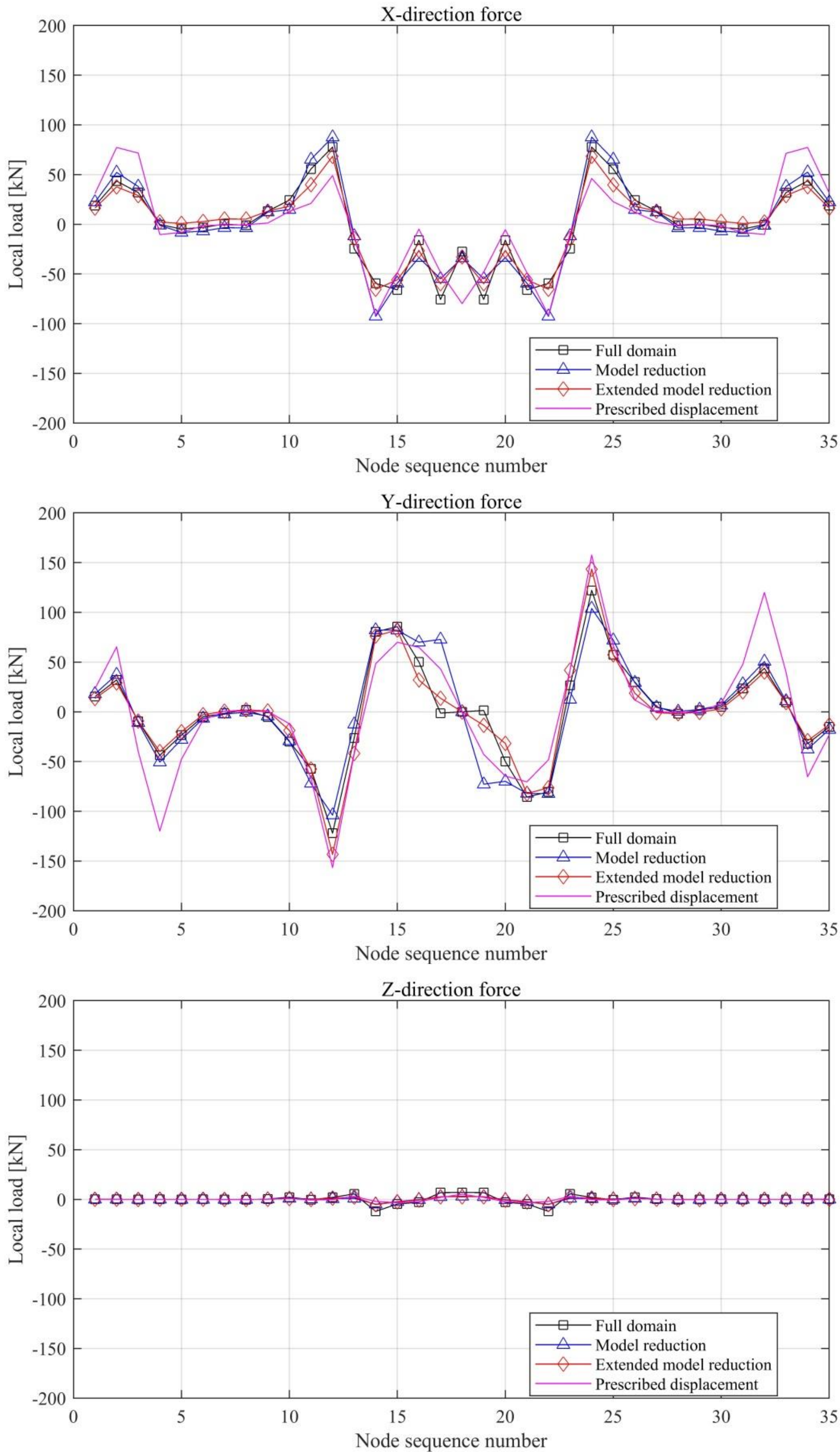

Fig. 72. Local load component plots for the critical load and approximated load at critical step of a horizontally stiffened cylindrical structure with radial bulkheads for all analysis cases.

Table 9. Standard errors of critical local load of reduced domain analyses compared to full domain analysis for a horizontally stiffened cylindrical structure with radial bulkheads (unit: kN).

	Model reduction	Extended model reduction	Prescribed displacement
Standard error of local load *	120	42	195

* Standard error is defined as $\sqrt{\left(\mathbf{f}_i - \mathbf{f}_{i(ref)}\right)\cdot\left(\mathbf{f}_i - \mathbf{f}_{i(ref)}\right)}$, where $\mathbf{f}_i$ is i-th local load vector and $\mathbf{f}_{i(ref)}$ is i-th local load vector in full domain analysis as the reference value.

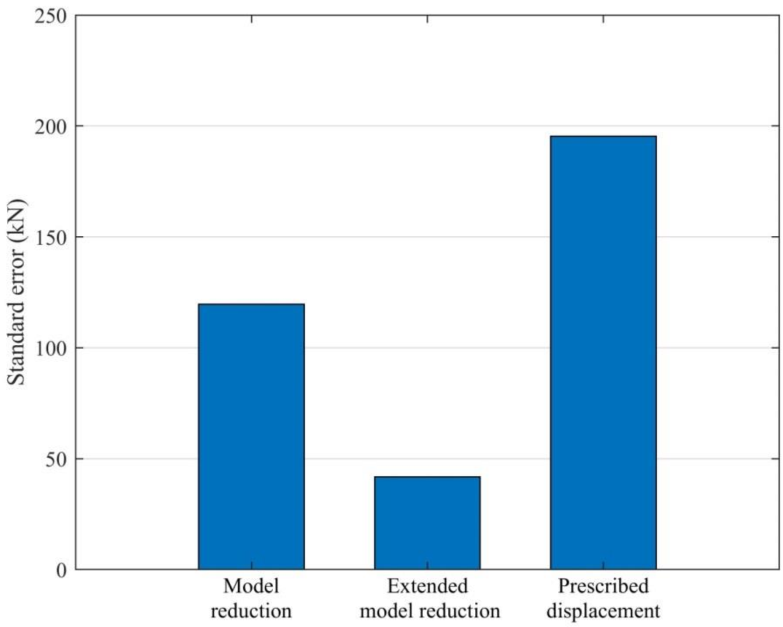

Fig. 73 Standard errors of critical local load of reduced domain analyses compared to critical full domain analysis of a horizontally stiffened cylindrical structure with radial bulkheads. Standard error is defined as $\sqrt{\left(\mathbf{f}_i - \mathbf{f}_{i(ref)}\right)\cdot\left(\mathbf{f}_i - \mathbf{f}_{i(ref)}\right)}$, where $\mathbf{f}_i$ is i-th local load vector and $\mathbf{f}_{i(ref)}$ is i-th local load vector in full domain analysis as the reference value.

5.2.2 Bracket girder in the column-pontoon connection structure of tension leg platform

We evaluate the structural stability by applying the model reduction method for the local bracket girder part considered in section 4.4. As shown in Fig. 74, the nonlinear analysis is performed only for the bracket girder region of interest. Two analyses cases are performed, which are the model reduction of the remaining regions and the prescribed displacement increment based on the reference displacement. Fig. 75 shows the extended the nonlinear analysis domain for the extended model reduction.

Figs. 76 to 78 show the second variation of the strain energy for model reduction, extended model reduction and prescribed displacement cases. Fig. 79 shows local load ratio - displacement index curve for full model analysis, model reduction analysis and prescribed displacement analysis. Figs. 80 to 82 show the local load component plots for the critical load and approximated load at critical step of local structures for model reduction, extended model reduction and prescribed displacement cases. The local safety factor values by the approximated load method are listed in Table 10 and Fig. 83. Considering the result of full model analysis as a reference value, the error of model reduction result is calculated as 12%, but in the case of extended model reduction, it is reduced to -6% error. The error of prescribed displacement analysis result is 4%, which is the lowest. However, there is an unrealistic result that it becomes stable in the next step immediately after the first instability of the local structure occurs at the prescribed displacement analysis case as shown in Fig. 78. We can see that the prescribed displacement analysis case may give a somewhat unstable result and its critical local load ratio is calculated to be quite low compared to the maximum local load ratio in Figs. 79 and 83. Therefore, the extended model reduction case gives a rather reliable result among the reduced analysis cases.

Fig. 84 shows local load component plots for the critical load and approximated load at critical step for all analyses. Table 11 and Fig. 85 show the standard errors of the local load distributions compared to the one of the full model analysis. The smallest value is 231 kN which is the standard error of the extended model reduction result at maximum local load ratio. In other words, it can be said that the local load distribution of the extended model reduction case is most similar to full model analysis. The prescribed displacement analysis shows large error value as 394 kN. Similarly in this example, the extended model reduction case is the best way to represent the local load distributions among the reduced domain analysis cases.

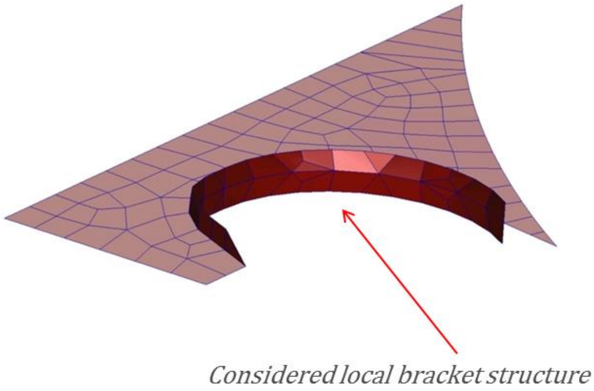

Fig. 74. Nonlinear analysis domain of a bracket girder in the column-pontoon connection structure of tension leg platform for model reduction and prescribed displacement.

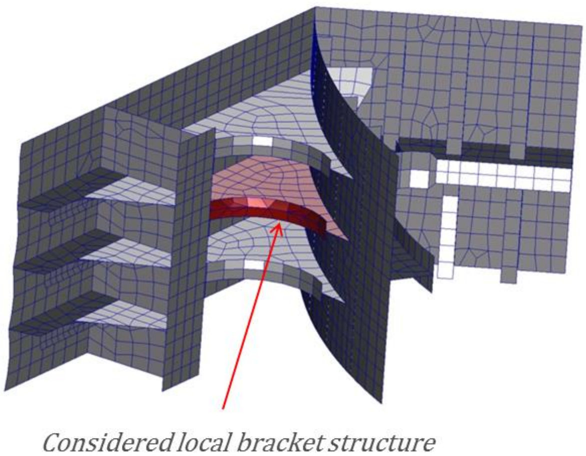

Fig. 75. Nonlinear analysis domain of the extended bracket girder structure in the column-pontoon connection structure of tension leg platform for extended model reduction.

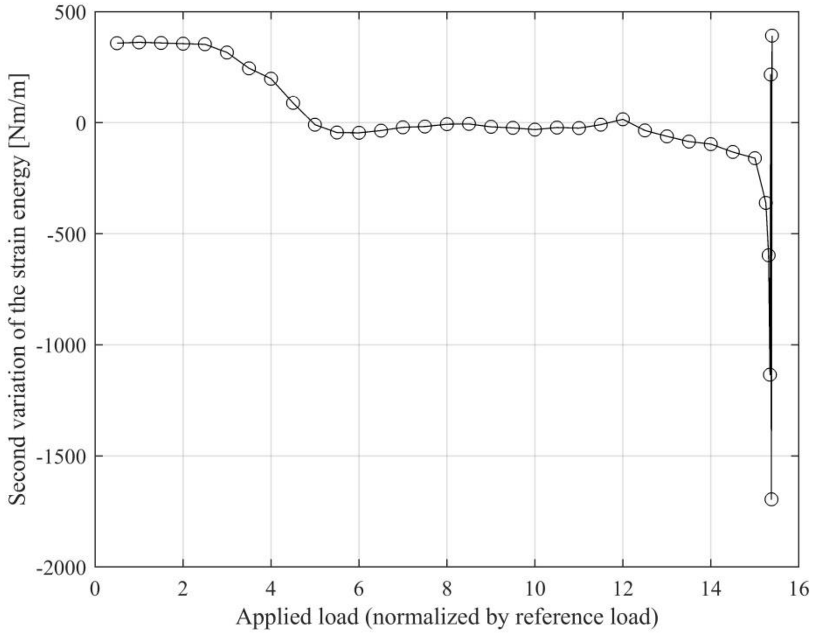

Fig. 76. Second variation of strain energy in local domain of a bracket girder in the column-pontoon connection structure of tension leg platform for model reduction case.

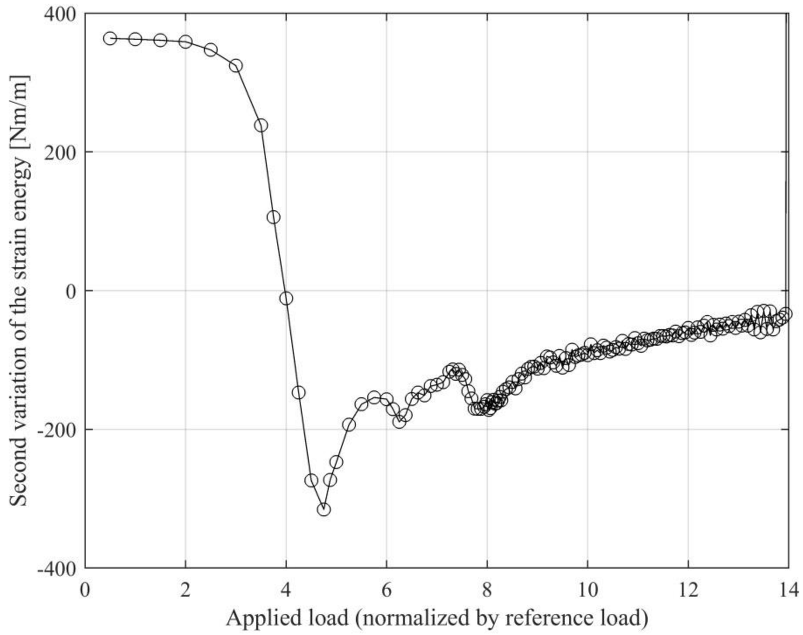

Fig. 77. Second variation of strain energy in local domain of a bracket girder in the column-pontoon connection structure of tension leg platform for extended model reduction case.

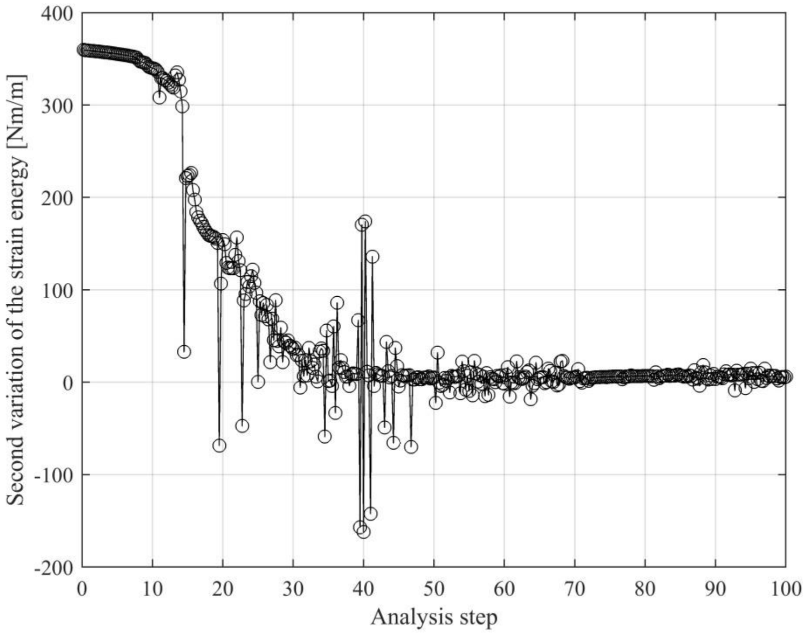

Fig. 78. Second variation of strain energy in local domain of a bracket girder in the column-pontoon connection structure of tension leg platform for prescribed displacement case.

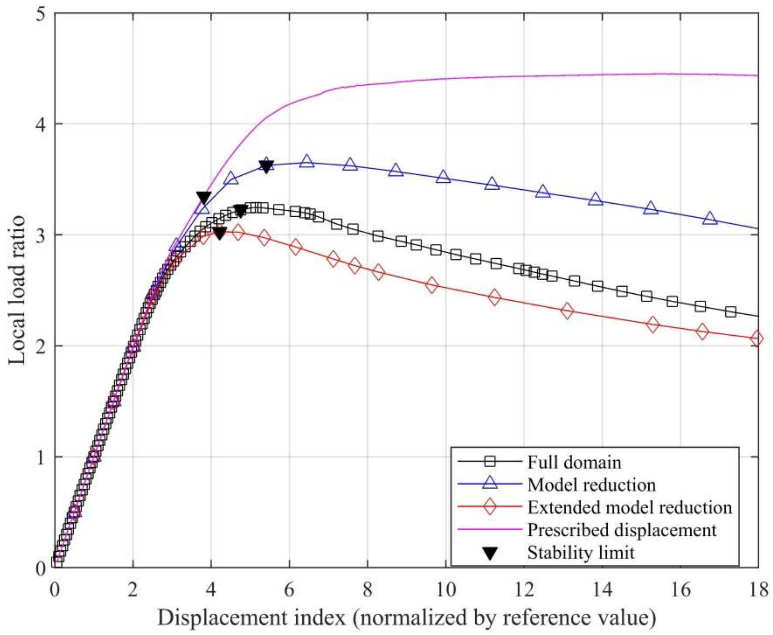

Fig. 79. Local load ratio – displacement index curve of a bracket girder in the column-pontoon connection structure of tension leg platform for all analysis cases.

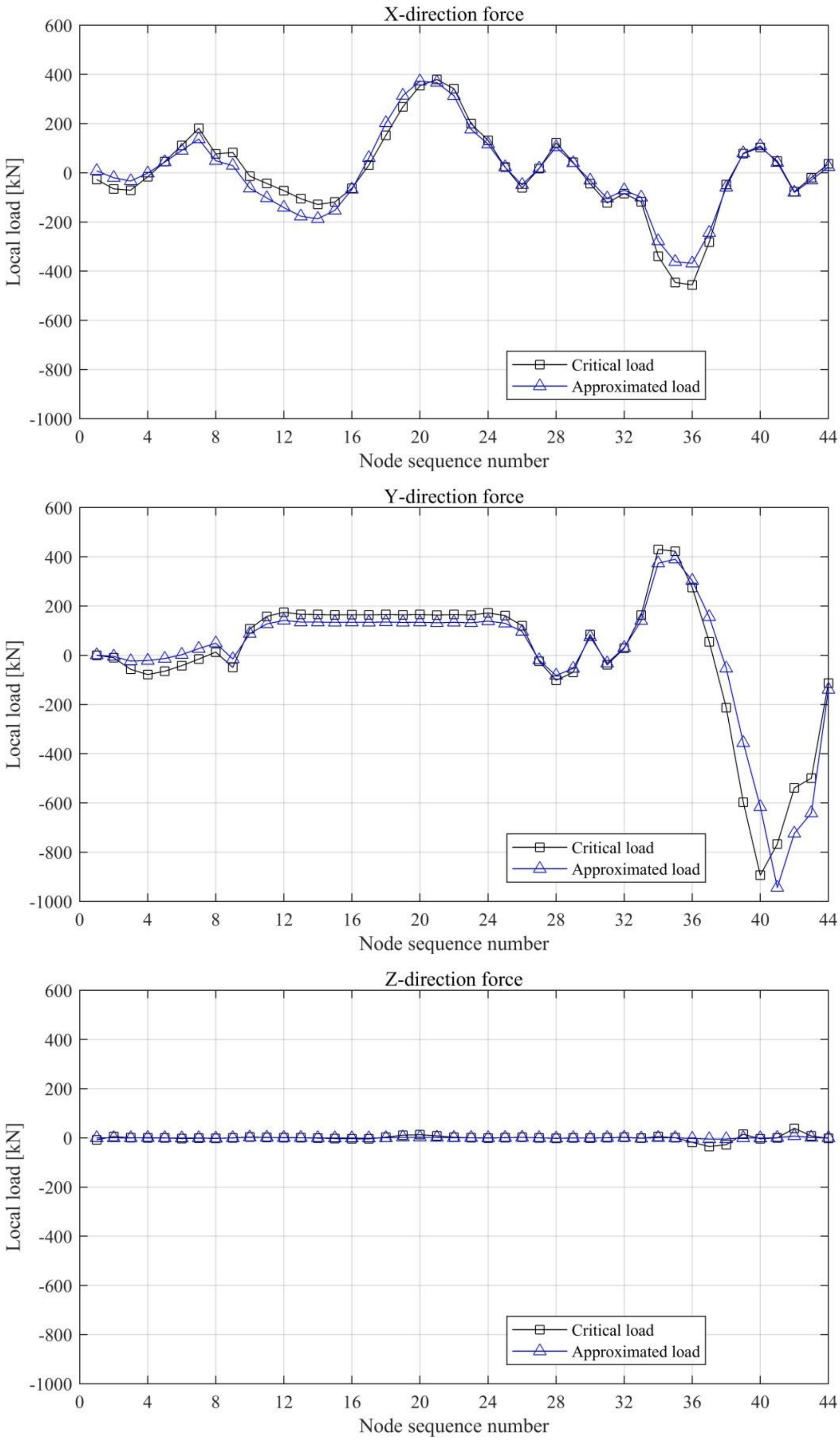

Fig. 80. Local load component plots for the critical load and approximated load at critical step of a bracket girder in the column-pontoon connection structure of tension leg platform for model reduction case.

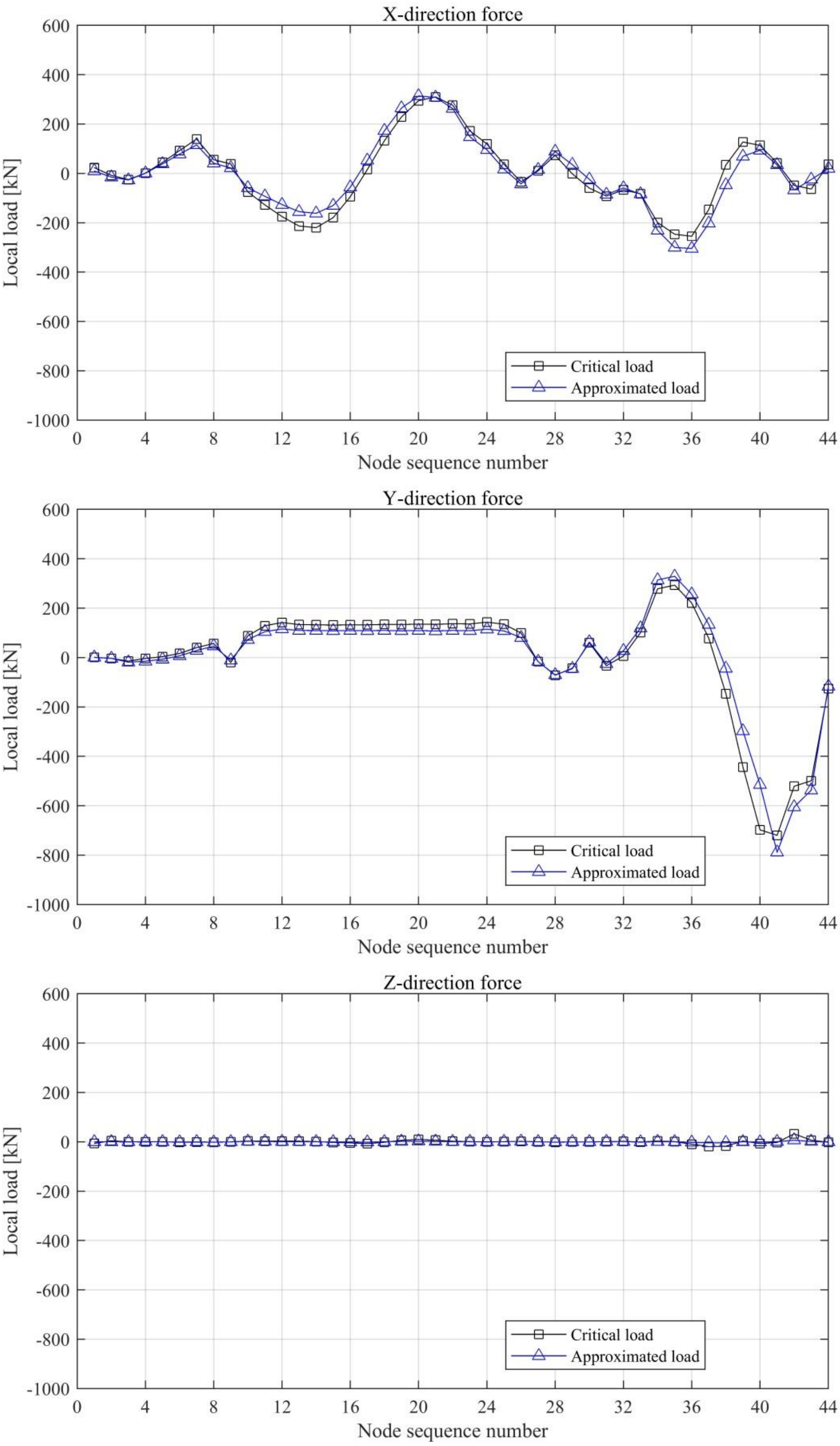

Fig. 81. Local load component plots for the critical load and approximated load at critical step of a bracket girder in the column-pontoon connection structure of tension leg platform for extended model reduction case.

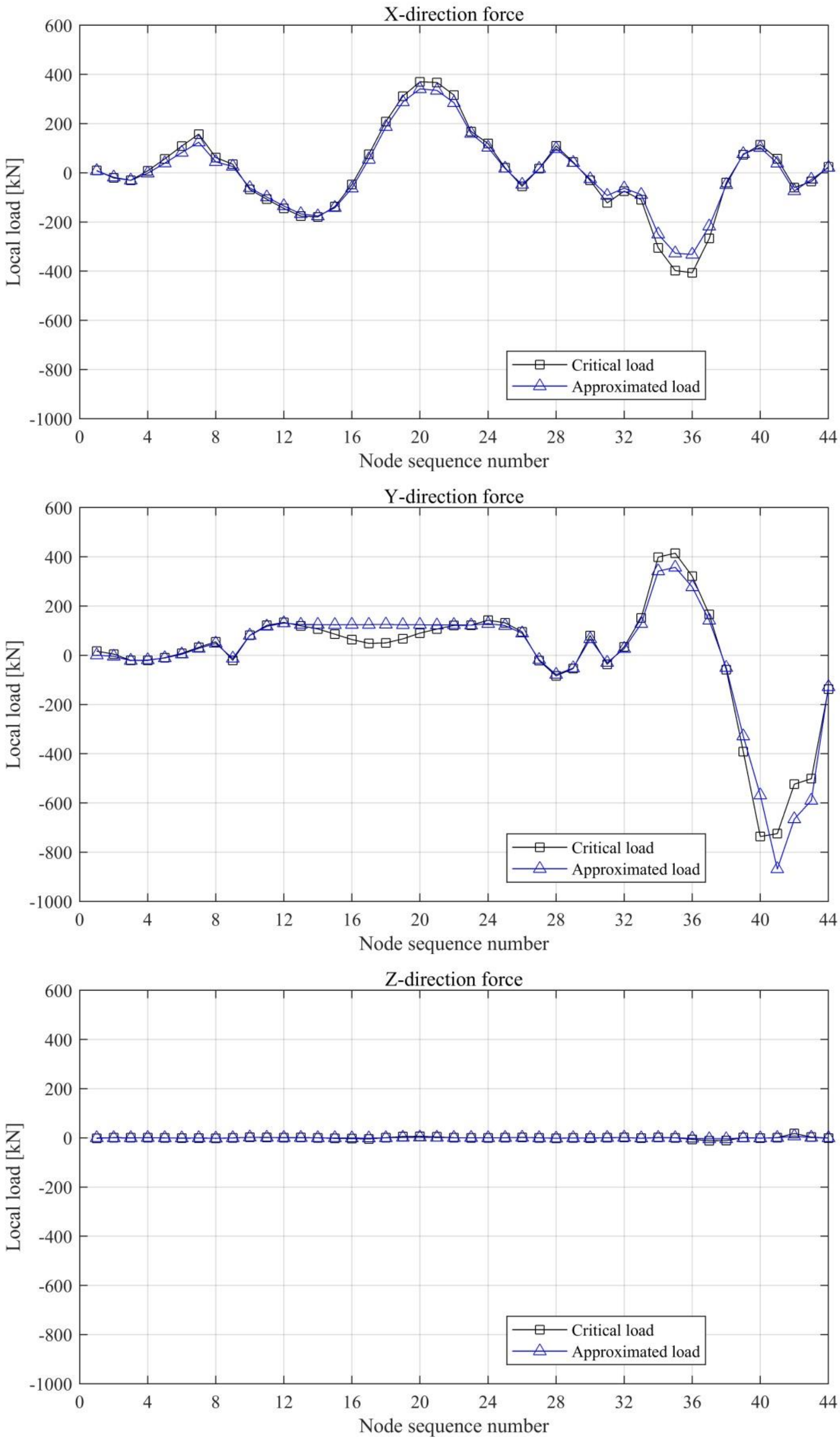

Fig. 82. Local load component plots for the critical load and approximated load at critical step of a bracket girder in the column-pontoon connection structure of tension leg platform for prescribed displacement case.

Table 10. Local safety factors (LSF) of a bracket girder in the column-pontoon connection structure of tension leg platform for all analysis cases.

	Full domain	Model reduction	Extended model reduction	Prescribed displacement
Maximum local load ratio	3.25	3.65	3.03	4.33
Normalized max. local load ratio	1.00	1.13	0.93	1.33
LSF	3.22	3.63	3.03	3.35
Normalized LSF	1.00	1.12	0.94	1.04

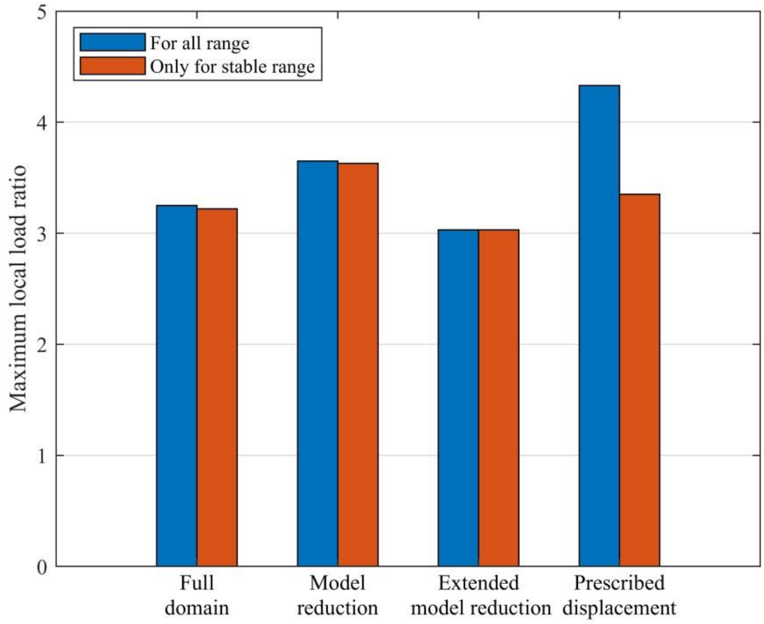

Fig. 83. Maximum local load ratios of a bracket girder in the column-pontoon connection structure of tension leg platform for all analysis cases.

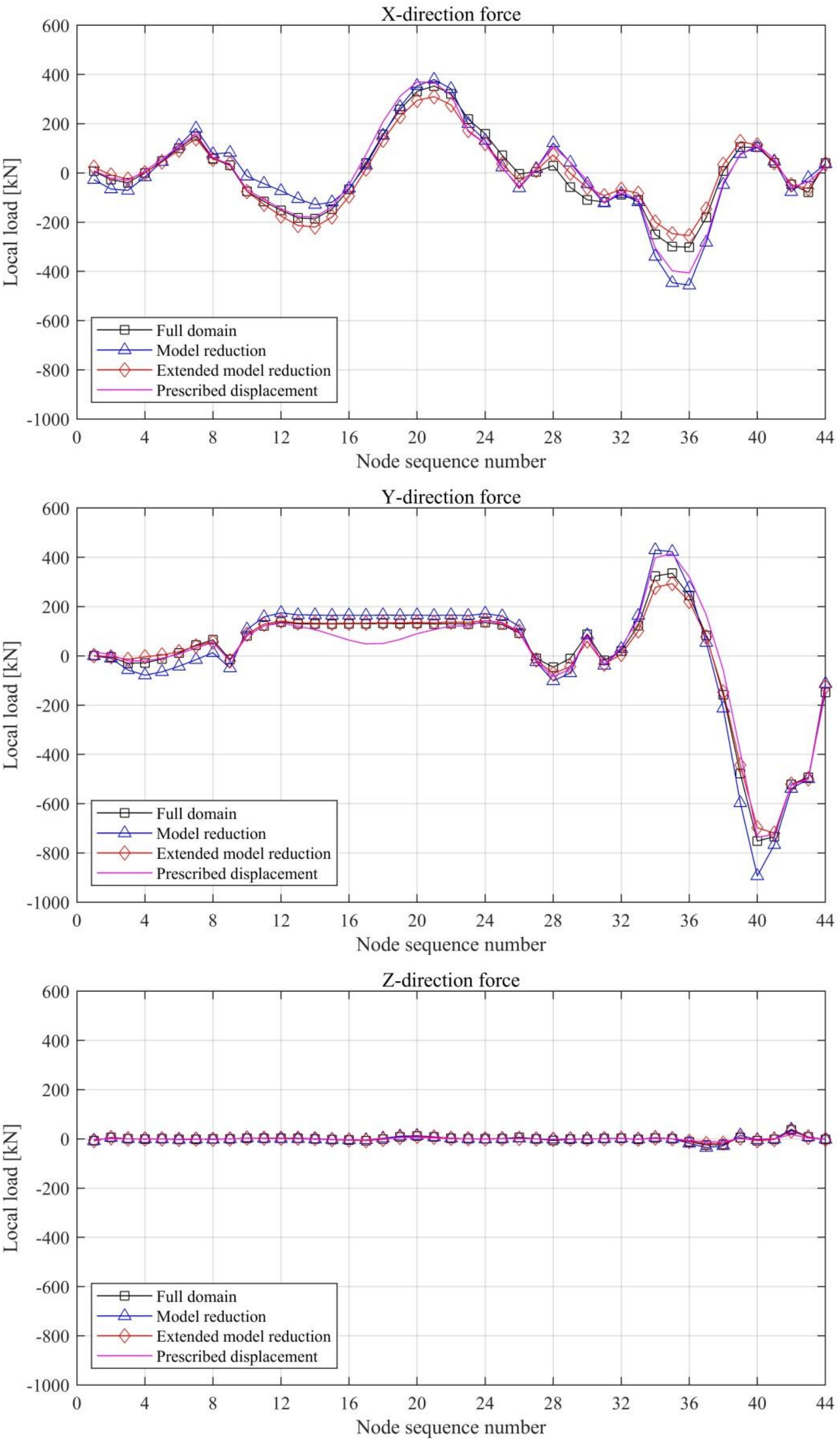

Fig. 84. Local load component plots for the critical load and approximated load at critical step of a bracket girder in the column-pontoon connection structure of tension leg platform for all analysis cases.

Table 11. Standard errors of critical local load of reduced domain analyses compared to full domain analysis for a bracket girder in the column-pontoon connection structure of tension leg platform (unit: kN).

	Model reduction	Extended model reduction	Prescribed displacement
Standard error of local load*	493	231	394

* Standard error is defined as $\sqrt{\left(\mathbf{f}_i - \mathbf{f}_{i(ref)}\right)\cdot\left(\mathbf{f}_i - \mathbf{f}_{i(ref)}\right)}$, where $\mathbf{f}_i$ is *i*-th local load vector and $\mathbf{f}_{i(ref)}$ is *i*-th local load vector in full domain analysis as the reference value.

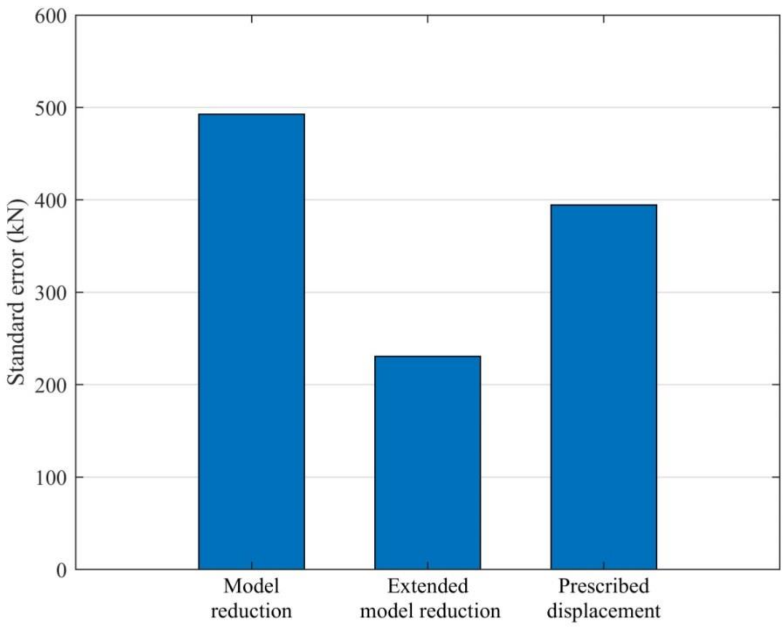

Fig. 85 Standard errors of critical local load of reduced domain analyses compared to critical full domain analysis of a bracket girder in the column-pontoon connection structure of tension leg platform. Standard error is defined as $\sqrt{\left(\mathbf{f}_i - \mathbf{f}_{i(ref)}\right)\cdot\left(\mathbf{f}_i - \mathbf{f}_{i(ref)}\right)}$, where $\mathbf{f}_i$ is *i*-th local load vector and $\mathbf{f}_{i(ref)}$ is *i*-th local load vector in full domain analysis as the reference value.

5.3 Computational efficiency improvement

In this section, we check the computing efficiency. If we are interested only in the local structure, it is very economical to perform nonlinear analysis only for the effective local domain rather than calculating the nonlinear behavior of the global structure.

The required computing time is measured for each evaluation method by the model reduction and the prescribed displacement. The evaluation method by the model reduction takes time in the static condensation process. The extended model reduction case provides the most reliable result among the reduced domain analyses as shown in Table 11 because the standard error of the extended model reduction case is smallest. Also, the time required for the analysis of the local region is reduced to 11.9% (=240/2,023) compared to the full domain as shown in Table 12 and Fig. 86.

Table 12. Computing costs of evaluation domains for a bracket girder in the column-pontoon connection structure of tension leg platform for all analysis cases.

Item		Full domain	Model reduction	Extended model reduction	Prescribed displacement
Number of nodes	Residual model	37,809	159	2,423	159
	Condensed interface		44	263	
Time (seconds)	Condensation		16	54	
	Iterative run	2,023	9	186	16
	Total	2,023	25	240	16

System: GenuineIntel / 2600 MHz / RAM 251GB

Platform: Intel linux 3.10.0-693.el7.x86_64

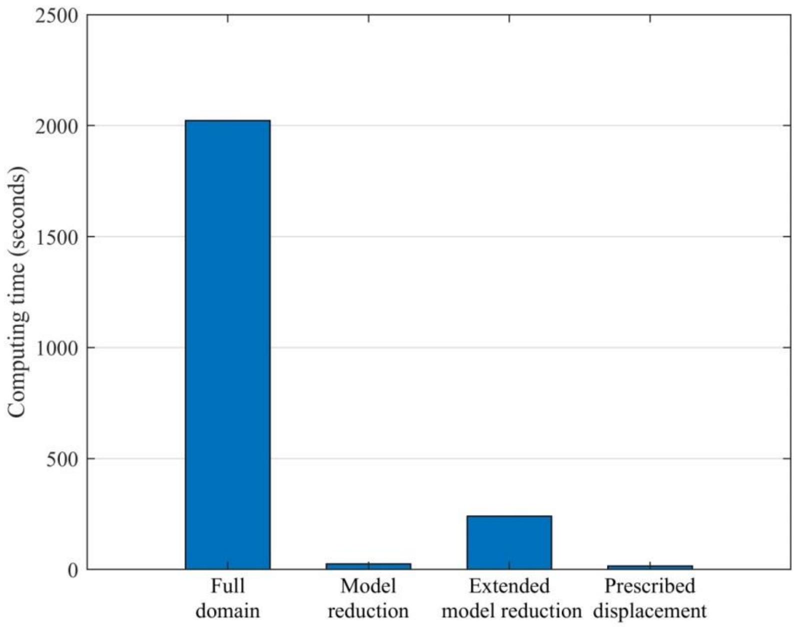

Fig. 86. Total computing time comparison for a bracket girder in the column-pontoon connection structure of tension leg platform for all analysis cases.

Chapter 6. Concluding remarks

In this thesis, a structural stability evaluation method for local structures was developed by investigating the second variation of the local strain energy. The method could be practically used to various arbitrarily shapes of slender local structures for ship and offshore structures by engineers in industries without much effort. The practical effectiveness of this method was demonstrated through numerical examples.

In the proposed method, complicated interactions between local and global structures were fully considered through global nonlinear FE analysis. The instability of the local structure was explicitly identified even if the overall structural integrity was maintained. The local resistance capacity could be precisely quantified by the local safety factor. When the target local structure lost stability, the corresponding magnitude of the external force acting on the global structure could be calculated. Also, where local buckling occurred in the global structure, i.e., locally damaged area, was easily identified.

A method of calculating the safety factor of any arbitrary shape of the local structure was originally proposed. The local load of the local structure was approximated by the least-squares fitting method to quantify the structural safety factor. This approach was very effective for any arbitrarily geometric shape of the local structure. Quantifying single scalar loads, by averaging or integrating the load distribution of local structures, could not be applied to arbitrary shapes, but this method was not limited to being used for any shape.

In the industry, reducing the time required to evaluate structural stability is one of the most important factors in structural design. For large FE models, the analysis time could be reduced economically through the model reduction method. The nonlinear iterative solving was performed only for the local structure in the method. The reliability and computational efficiency were investigated and it was found that the extended model reduction method was the best solution when the nonlinear analysis with a full FE model could not be performed due to the limited time.

In future studies, this practical evaluation method can be applied to demonstrate strength proofs of irregularly reinforced structures and weakened plate openings that are not predefined in design formulas. In addition, the residual strength and damaged area can be identified to determine the reinforcement of local structures after structural damages from grounding or collision accidents.

Bibliography

[1] https://en.wikipedia.org/wiki/I-35W_Mississippi_River_bridge

[2] Chakrabarti, S. (2005), Handbook of Offshore Engineering. Elsevier, Kidlington, U.K.

[3] DNVGL (2015), DNVGL-CG-0128. Class Guideline: Buckling; DNVGL.

[4] DNVGL (2018), DNVGL-RU-SHIP Pt.3 Ch.8. Rules for Classification: Buckling; DNVGL.

[5] BV (2018), Rule Note NI 615 DT R02 E. Buckling Assessment of Plated Structures; Bureau Veritas, Paris, France.

[6] AISC (2016), ANSI/AISC 360-16. An American National Standard: Specification for Structural Steel Buildings; American Institute of Steel Construction, Chicago, U.S.A.

[7] API (2014), RP 2A-WSD. Recommended Practice for Planning, Designing and Constructing Fixed Offshore Platforms- Working Stress Design; American Petroleum Institute, Washington, U.S.A.

[8] DNVGL (2017), DNVGL-RP-C202. Recommended Practice: Buckling Strength of Shells; DNVGL.

[9] DNV (2010), DNV-RP-C201. Recommended Practice: Buckling Strength of Plated Structures; Det Norske Veritas.

[10] ABS (2018), Guide for Buckling and Ultimate Strength Assessment for Offshore Structures; American Bureau of Shipping, New York, U.S.A.

[11] Yao, T. and Fujikubo, M. (2016), Buckling and Ultimate Strength of Ship and Ship-Like Floating Structures. Elsevier Inc., New York, U.S.A.

[12] Paik, J.K. (2018), Ultimate Limit State Analysis and Design of Plated Structures, 2nd Edition. Jon Wiley & Sons, Chichester, U.K.

[13] Wang, C.M. and Liew, K.M. (1994), “Buckling of triangular plates under uniform compression”, Eng.Struct., 16(1), 43–50.

[14] Xiang, Y., Wang, C.M., Kitipornchai, S. and Liew, K.M. (1994), “Buckling of triangular Mindlin plates under isotropic in-plane compression”, ActaMech., 102(1–4), 123–135.

[15] Jaunky, N., Knight, N.F. and Ambur, D.R. (1995), “Buckling analysis of general triangular anisotropic plates using polynomials”, AIAA J., 33(12), 9387–2654.

[16] Xiang, Y. (2002), “Buckling of triangular plates with elastic edge constraints”, ActaMech., 156(1–2), 63–77.

[17] Aung, T.M. (2006), “Plastic Buckling of Mindlin Plates”, PhD Dissertation. National University of Singapore, Singapore.

[18] Lee, S.E., Thayamballi, A.K. and Paik, J.K. (2015), “Ultimate strength of steel brackets in ship structures”, Ocean Eng. 101, 182–200.

[19] Tham, L.G. and Szeto, H.Y. (1990), “Buckling analysis of arbitrarily shaped plates by spline finite strip method”, Computers & Structures, 36(4), 729-735.

[20] Wang, C.M., Xiang, Y., Kitipornchai, S. and Liew, K.M. (1994). “Buckling solutions for Mindlin plates of various shapes”, Eng. Struct., 16(2), 119–127.

[21] Jaunky, N., Knight, N.F. and Ambur, D.R. (1995), “Buckling of arbitrary quadrilateral anisotropic plates”, AIAA J., 33(5), 938-944.

[22] Saadatpour, M.M., Azhari, M. and Bradford, M.A. (1998), “Buckling of arbitrary quadrilateral plates with intermediate supports using the Galerkin method”, Computer Methods in Applied Mechanics and Engineering, 164(3–4), 297-306.

[23] Wu, L. and Feng, W. (2003), “Differential cubature method for buckling analysis of arbitrary quadrilateral thick plates”, Struct. Eng. Mech., 16(3), 259-273.

[24] Jamshidi, S. and Fallah, N. (2019), “Buckling analysis of arbitrary point-supported plates using new hp-cloud shape functions”, Struct. Eng. Mech., 70(6), 711-722.

[25] Brubak, L., Hellesland, J. and Steen, E. (2007), “Semi-analytical buckling strength analysis of plates with arbitrary stiffener arrangements”, Journal of Constructional Steel Research, 63(4), 532-543.

[26] Brubak, L. and Hellesland, J. (2007b), “Approximate buckling strength analysis of arbitrarily stiffened, stepped plates”, Engineering Structures, 29(9), 2321-2333.

[27] Kim, H.S., Park, Y.M., Kim, B.J. and Kim, K. (2018), “Numerical investigation of buckling strength of longitudinally stiffened web of plate girders subjected to bending”, Struct. Eng. Mech., 65(2), 141-154.

[28] Kim, H.S., Park, Y.M., Kim, K. and Choi, B.H. (2019), “Web bend-buckling strength of plate girders with two longitudinal web stiffeners”, Struct. Eng. Mech., 69(4), 383-397.

[29] Muhammad, T. and Singh, A.V. (2005), “The buckling of rectangular plates with opening using a polynomial method”, Struct. Eng. Mech., 21(2), 151-168.

[30] Komur, M.A. and Sonmez, M. (2008), “Elastic buckling of perforated plates subjected to linearly varying in-plane loading”, Struct. Eng. Mech., 28(3), 353-356.

[31] Kim, U.N., Choe, I.H. and Paik, J.K. (2009), “Buckling and ultimate strength of perforated plate panels subject to axial compression: experimental and numerical investigations with design formulations”, Ships and Offshore Structures, 4(4), 337-361.

[32] Kim, J.H., Jeon, J.H., Park, J.S., Seo, H.D., Ahn, H.J. and Lee, J.M. (2015), “Effect of reinforcement on buckling and ultimate strength of perforated plates”, International Journal of Mechanical Sciences, 92, 194-205.

[33] Saad-Eldeen, S., Garbatov, Y.C. and Soares, G. (2016), “Experimental strength assessment of thin steel plates with a central elongated circular opening”, Journal of Constructional Steel Research, 118, 135-144.

[34] Mohammadzadeh, B., Choi, E. and Kim, W.J. (2018), “Comprehensive investigation of buckling behavior of plates considering effects of holes”, Struct. Eng. Mech., 68(2), 261-275.

[35] DNVGL (2016), DNVGL-RP-C208. Recommended Practice: Determination of Structural Capacity by Non-linear Finite Element Analysis Methods; DNVGL.

[36] Zi, G., Kim, H.H., Ahn, J.Y. and Oh, M.H. (2017), "Evaluation of buckling strength of non-structured plates by using the deformation energy", Journal of the Korea Institute for Structural Maintenance and Inspection, 21(3), 102-113.

[37] MSC Software (2014), MSC Nastran 2014 Quick Reference Guide. MSC Software, Newport Beach, U.S.A.

[38] Bazant, Z.P. and Cedolin, L. (1991), Stability of Structures: Elastic, Inelastic, Fracture, and Damage Theories. Oxford University Press, New York, U.S.A.

[39] Kim, D.K., Poh, B.Y., Lee, J.R. and Paik, J.K. (2018), "Ultimate strength of initially deflected plate under longitudinal compression: Part I = An advanced empirical formulation", Struct. Eng. Mech., 68(2), 247-259.

[40] Lei, Y., Chen, S., Wang, L. and Xu, H. (2018), "Global strength analysis of a monocolumn FPSO", The 28th International Ocean and Polar Engineering Conference. 10-15 June, Sapporo, Japan.

[41] Blarez, E. (2018), "OTC-28406-MS. Moho Nord, A Complex Integrated Project", Offshore Technology Conference. 20-23 March, Kuala Lumpur, Malaysia.

[42] Qu, Z.Q. (2004), Model Order Reduction Techniques: with Applications in Finite Element Analysis. Springer-Verlag, London, U.K.

[43] Guyan, R. (1965), "Reduction of stiffness and mass matrices", AIAA J., 3(2), 380-380.

[44] Boo, S.H. and Oh, M.H. (2017), "Automated static condensation method for the local analysis of large finite element models", Struct. Eng. Mech., 61(6), 807-816.

[45] ABS (2012), Guide for Building and Classing: Floating Offshore Liquefied Gas Terminals; American Bureau of Shipping, New York, U.S.A.

[46] BV (2015), Rule Note NR 622: Structural Assessment of Independent Tanks and Supports for Asphalt Carriers; Bureau Veritas, Paris, France.

[47] DNV (2013), Classification Notes 31.12. Strength Analysis of Liquefied Gas Carriers with Independent Type B Prismatic Tanks; Det Norske Veritas.

[48] LR (2012), Guidance Notes for Liquefied Gas Carriers Adopting IMO Type B Independent Tanks Primarily Constructed of Plane Surfaces; Lloyd's Register, London, U.K.